THE WAKSMAN FOUNDATION OF JAPAN INC.

Honorary President

Prince Takahito Mikasa

Honorary Counselor

Shozo Yokogawa, Counselor, Yokogawa Electric Corp.

Board of Directors

Chairman : Ichiro Kitasato, Chairman of the Board, Meiji Seika Kaisha, Ltd.

Shogo Sasaki, Prof. Emeritus, Keio Univ.

Kazuhisa Saito, Prof. Emeritus, Keio Univ.

Teruhiko Beppu, Prof. Emeritus, Tokyo Univ.

Takao Saruta, Prof. Emeritus, Keio Univ.

Takeshi Ishikawa, Director, 150th Anniversary Commemorative Project Office of Keio

Shigeo Koyasu, Prof., Keio Univ. Sch. Med.

Kazumine Kobari, Prof. Emeritus, Ryukyu Univ.

Shogo Kuwahara, Prof. Emeritus, Toho Univ.

Rinji Kawana, Prof. Emeritus, Iwate Med. Univ.

Tadakatsu Shimamura, Prof., Showa Univ. Sch. Med.

Managing Director : Takeji Nishikawa, Prof. Emeritus, Keio Univ.

Comptroller : Kannosuke Nakamura, Counselor, Kyowa Hakko Kogyo, Co., Ltd.

Yoshiharu Wakiyama, Senior Adviser, Kaken Pharmaceutical, Co., Ltd.

Councilors

Kimio Uyeno, Honorary Chairman, Chugai Pharmaceutical, Co., Ltd.

Susumu Sato, Chairman, Sato Pharmaceutical, Co., Ltd.

Yuji Naito, Chairman, Eisai Pharmaceutical, Co., Ltd.

Ryoichi Mori, Prof. Emeritus, Kyushu Univ.

Masaki Kitajima, Prof., Keio Univ. Sch. Med.

Yuichiro Anzai, President, Keio Univ.

Keizo Takemi, Member, The House of Councilors

Kiyoshi Morita, President, Daiichi Pharmaceutical, Co., Ltd.

Tetsuo Takato, President, Sankyo, Co., Ltd.

Akira Uehara, President, Taisho Pharmaceutical, Co., Ltd.

Koichi Yamanishi,Director General, National Institute of Biomedical Innovation

Masamichi Fujii, Prof. Emeritus, St. Marianna Univ.

Osamu Sato, Prof. Emeritus, Tokai Univ.

Sachiko Goto, Prof. Emeritus, Toho Univ.

Yoshihiro Miwa, President, Kowa, Co., Ltd.

2005

Edited and Published by

THE WAKSMAN FOUNDATION OF JAPAN INC.

30-8 Daikyo-cho, Shinjuku-ku,
Tokyo 160-0015, Japan
http : //www.waksman.or.jp/
E-mail office@waksman.or.jp

Printed by

FUKOKU PRINTING CO., LTD.

Tokyo, Japan

PREFACE (2000)

Since the Waksman Foundation published its first cinqueannual report in 1962, annual report followed regularly until 1986 without changing its style, i.e. yellow cover in B5 size. The royalties of patent of streptomycin expired in 1970 and the Foundation was forced to change the way of running. Fortunately, it manages to continue its activity by supporting the research activities of Japanese investigators and by encouraging them to take part in an international meeting and also by hosting scientific meetings with professional societies. The total number of support counts 628 research projects and costs approximately 4,500,000 U.S. dollars. The Foundation is administered by the Board of Directors consisting of 5-9 representatives of professional societies and Prince Takahito Mikasa as the honorary President.

At our recent business meeting it was decided unanimously to publish the reports of the researchers who recieved research grant from the Foundation for the past 15 years to commemorate the year 2000. To meet with the current style of a scientific journal the Foundation has adopted an international size and totally renewed the cover as you are aware of. From the new millennium on it is expected that the report from the awardees of the research grants will be distributed regularly each year.

Shozo Yokogawa
Chairman, Board of Directors,
The Waksman Foundation of Japan, Inc.

Preface to the First Report (1962)

It is indeed a privilege to take this opportunity to write a few words of introduction to the first report of the Waksman Foundation of Japan Inc., covering five years of its activities and comprising the results of the work of the first two years of research carried out by various scholars in Japan in the fields of microbiology and medical science, supported by this Foundation.

In 1952, I accepted the invitation from Keio University and the Kitasato Institute, to deliver the centennial lecture in honor of the great Japanese bacteriologist, Shibasaburo Kitasato. Before departing for Japan, I proposed to the trustees of the Rutgers Research and Educational Foundation which owned the patents on streptomycin, to share the royalties under the patent in Japan, for the support of research in microbiology and allied fields in that country. The trustees heartily approved my recommendation that I make such announcement to that effect.

Soon upon my arrival in Japan (December 17, 1952), I invited a group of eminent microbiologists, biochemists, and clinical investigators to meet with me in order to discuss the plan. Everyone present was very enthusiastic about the proposal. It was decided that a proper committee be selected to work out the plan of a Foundation under which the royalties were to be received and distributed for the support of Japanese investigators working in different universities in Japan and elsewhere, in the fields of microbiology and medical research. The committee recommended that a Board of Directors be selected and the proposed Foundation be named THE WAKSMAN FOUNDATION OF JAPAN INCORPORATION.

The Rutgers Research and Educational Foundation approved at once the above recommendations and issued a statement, signed by Dr. Lewis Webster Jones, President of the Foundation, to the effect that

"The Rutgers Research and Educational Foundation desires to emphasize that its principal concern is the advancement of scientific knowledge in the public interest and that it confidently expects that the Waksman Foundation for Microbiology and Medical Research in Japan will be similarly motivated, thereby serving the peoples of both countries."

This announcement was received with enthusiasm both by the scientific world and the popular press in Japan and in the United States. It took several years before the Waksman Foundation of Japan Inc. was properly organized, and before applications were received and approved. In 1958, I had the privilege of participating in the first official meetings of the Board of Directors of the Japanese Foundation and to greet personally the first group of scholars to whom grants had been made.

In summarizing these brief remarks in connection with the first cinqueannual report of the Waksman Foundation of Japan Inc., I would like to enphasize that this example of collaboration between universities and scientists of the United States and Japan may serve to encourage collaboration between scientific workers throughout the world towards a better understanding between men and women and towards a happier and healthier human race, so that all the nations on this earth can live in peace and that man may finally "break

his swords and build out of them plowshares" for the betterment of mankind as a whole.

Selman A. Waksman
Professor Emeritus
Rutgers-State University N. J., U. S. A.

The "Waksman Foundation of Japan Inc." was established in 1957 with the spirit of humanity by Dr. S.A. Waksman, Professor of Microbiology, Rutgers University, U.S.A. The Foundation's operations are possible only because Dr. S.A. Waksman and the Rutgers Research and Educational Foundation donated patent royalties he received from the production in Japan of the discovery, Streptomycin.

Because of these royalties, each year many Japanese scholars and research workers in the fields of Microbiology and medical science are encouraged and find it possible to continue their work. Especially, in accordance with Dr. Waksman's suggestion, the funds are distributed to scholars in local and economically hampered schools and laboratories and to those developing research workers who are endeavoring to expand in their fields. This thought of Dr. Waksman's is most appreciated, as it matches our Oriental phylosophy, and results in the search for a jewel among ordinary stones, which is the highest work of the science-leader.

Some five years have now passed since the start of this Foundation, and many persons have received aid through this period.

The reports which are presented herein cover the first and second group of research workers who received financial assistance from the Foundation.

Toshio Katow, M. D.
Executive Director

Contents

—— Report of Researches in 2004 ——

Genetics and Physiology of Ribosomal Mutations That Activate Antibiotic Production; Further Development of Ribosome Engineering

Kozo Ochi

National Food Research Institute, 2-1-12, Kannondai, Tsukuba, Ibaraki 305-8642, Japan

Introduction

Improvement of the antibiotic productivity of commercially available microbiotic strains is an important field in microbiology, since wild-type strains isolated from nature usually produce only a low level (1 ～ 100μg/ml) of antibiotics. A great deal of effort and resources has therefore been committed to search for improving the productivity of antibiotic-producing strains to meet commercial requirements. Current methods of improving the productivity of industrial microorganisms range from the classical "random" approach to highly rational methods, for example metabolic engineering. Although classical methods are still effective even without using genomic information or genetic tools to obtain highly productive strains, these methods are always time- and resource- consumptive (20, 24). Thus, it is crucially important to make the cell's ability exert fully for antibiotic production.

Since we found a dramatic activation of antibiotic production by a certain ribosomal mutation (a mutation in *rpsL* gene encoding the ribosomal protein S12) (18), we thought of an idea that bacterial gene expression may be changed dramatically by modulating the ribosomal proteins or rRNA, eventually leading to activation of inactive (silent) genes. Thus, our ultimate aim was to construct "Ribosome Engineering" for a rational approach to make fully elicit the bacterial abilities. In bacteria, ribosome plays a special role for their own gene expression by synthesis of ppGpp. One of the most important adaptation systems for bacteria is the stringent response, which leads to the repression of stable RNA synthesis in response to nutrient limitation (2). The stringent response depends on the transient increase of hyperphosphorylated guanosine nucleotide ppGpp, which are synthesized from GDP and ATP by the *relA* gene product (ppGpp synthetase) in response to binding of uncharged tRNA to the ribosomal A site. Since bacterial secondary metabolism is often triggered by ppGpp when cells entered into stationary phase, it is important to take stringent response into consideration in activation or enhanement of the bacterial secondary metabolism. In this review, we first describe the outline of our Ribosome Engineering and its applicability, especially focusing on strain improvement for antibiotic overproduction in *Streptomyces*. Subsequently, we describe our current study on fusidic acid-resistant (*fus*) and thiostrepton-resistant (*tsp*) mutations, which can elicit cell's ability to produce greater amount of antibiotics.

1. Antibiotic Overproduction by *rpsL* (Ribosomal Protein S12) Mutations

Activation of actinorhodin production.

Members of the genus *Streptomyces* produce a wide variety of secondary metabolites that include about half of the known microbial antibiotics. Advances in understanding the regulation of secondary metabolism in this genus have come from the study of antibiotic production in *Streptomyces coelicolor* A3(2) and its close relative *Streptomyces lividans* 66. *S. coelicol-*

or produces at least four antibiotics, including the blue-pigmented polyketide antibiotic actinorhodin (Act). *S. lividans* normally does not produce Act, although the strain has complete set of Act biosynthetic genes. Act production in this organism can be activated by introduction of certain regulatory genes or cultivation under specific conditions.

A strain of *S. lividans*, TK24, has been found to produce large amount of Act under the normal culture condition (18) (Fig.1). Genetic analyses revealed that a streptomycin-resistant mutation *str-6* in TK24 is responsible for activation of Act synthesis and that *str-6* is a point mutation in the *rpsL* gene encoding ribosomal protein S12, changing Lys-88 of the protein to Glu (K88E mutation). It was also shown that introduction of streptomycin-resistant mutations improves Act production in wild-type *S. coelicolor* (5) (Fig.1), and circumvents the detrimental effects on Act production in certain developmental mutants (*relA*, *relC* and *brgA*) of *S. coeliolor* (13, 14, 18). These streptomycin-resistant mutations result in the alteration of the Lys-88 to Glu (K88E) or Arg (K88R) and Arg-86 to His (R86H) in the *rpsL* gene. In addition to these streptomycin-resistant *rpsL* mutations, a paromomycin-resistant *rpsL* mutation (P91S) also can activate Act production in *S. coelicolor* (15). These findings indicate that the antibiotic production (secondary metabolism) in streptomycetes is significantly controlled by the translational machinery "ribosome".

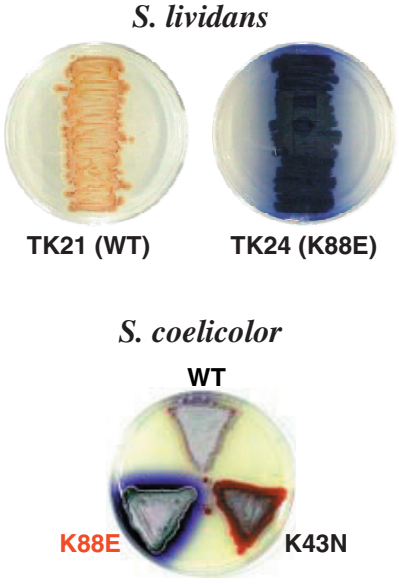

Fig. 1. Activation of antibiotic production by *rpsL* (encoding ribosomal protein S12) mutations in *Streptomyces lividans* 66 and *Streptomyces coelicolor* A3(2). Blue color represents an antibiotic, actinorhodin. K88E means a mutation at lysine-88 altering to glutamate.

Much progress has been made in elucidating the organization of antibiotic biosynthesis gene clusters in several *Streptomyces* species, and a number of pathway-specific regulatory genes that are required for the activation of their cognate biosynthetic genes have been identified (22). In the Act biosynthetic gene cluster, *act*II-ORF4 plays such a pathway-specific regulatory role, and the expression level of this gene directly determines the productivity of Act (1). Western blot analysis using anti-ActII-ORF4 antibody showed that expression of ActII-ORF4 protein was strongly enhanced in the Act-high-producing *rpsL* mutant strains (8). Furthermore, RT-PCR experiment revealed that the increase of this regulatory protein is attributed to the enhanced expression of *act*II-ORF4 mRNA. Thus, certain *rpsL* mutations enhance expression of *act*II-ORF4 gene, leading to massive production of Act.

Mechanism of activation.

The ribosomal protein S12, a component of 30S subunit in bacteria, is best characterized with respect to a role in the selection efficiency of cognate tRNAs for an accuracy enhancement. Most of the mutation in S12 protein associated with streptomycin resistance lead to an error-restrictive phenotype, due to changes in the kinetic properties of the tRNA-ribosome interaction (10). As mentioned above, antibiotic production by bacteria, including *Streptomyces* spp., is activated or enhanced by introducing certain mutation into the *rpsL* gene (encoding the ribosomal protein S12) that confer streptomycin resistance (7, 17, 19). Recently, we found that K88E (which corresponds to position 87 in *Escherichia coli* S12 protein) *rpsL* mutant of *S. coelicolor* A3(2), with an enhanced Act production, exhibits an aberrant protein synthesis activity. To clarify the presence or absence of the causal relationship between

this aberrant protein synthesis activity and the observed antibiotic overproduction, we have uncovered characteristic properties of the *S. coelicolor* K88E mutant in synthesis of protein *in vivo* and *in vitro* (16). The results demonstrated that 1) the K88E mutation, like classic S12 mutations (K42N and K42T) in *E. coli*, confers a restrictive phenotype in addition to resistance to streptomycin, 2) the K88E mutant exhibits a high level of protein synthesis activity *in vivo* at the late growth phase as determined by the incorporation of labeled leucine, 3) the K88E mutant ribosomes from the late stationary phase cells have a high capacity for translating both synthetic polynucleotide [poly(U)] and natural mRNA, 4) S150 solution from K88E mutant cells grown to late stationary phase supports a higher level of protein synthesis activity *in vitro*, and 5) the K88E mutant ribosomes are structurally more stable under stress conditions, such as amino acid starvation and low concentration of magnesium. Thus, we concluded that the increased stability of the 70S complex and level of specified translation-associated factor(s) are responsible for the aberrant activation of protein synthesis in the *S. coelicolor* K88E mutant (Fig.2). This observation is in agreement with our recent findings that the *E. coli* K87E mutant also show an aberrant protein synthesis activity at late growth phase (6). Our findings lead to the suggestion that a change from Lys to Glu at position 87 (according to the *E. coli* numbering) in S12 protein renders cells potentially more active for protein synthesis under the starvation conditions as represented by the late growth phase. Such a characteristic would be highly advantageous for the production of proteins from newly transcribed genes (such as those involved in antibiotic production) at the late growth phase. Thus, the aberrant protein synthesis found in the *S. coelicolor* K88E *rpsL* mutant could be the cause, at least in major part, of remarkably activated antibiotic production in this mutant strain.

The *rpsL* mutations found so far in *S. coelicolor* A3(2) and *S. lividans* 66 are K43N, K43R, K43T, K88E, K88R, and P91S. Of these, only two mutations

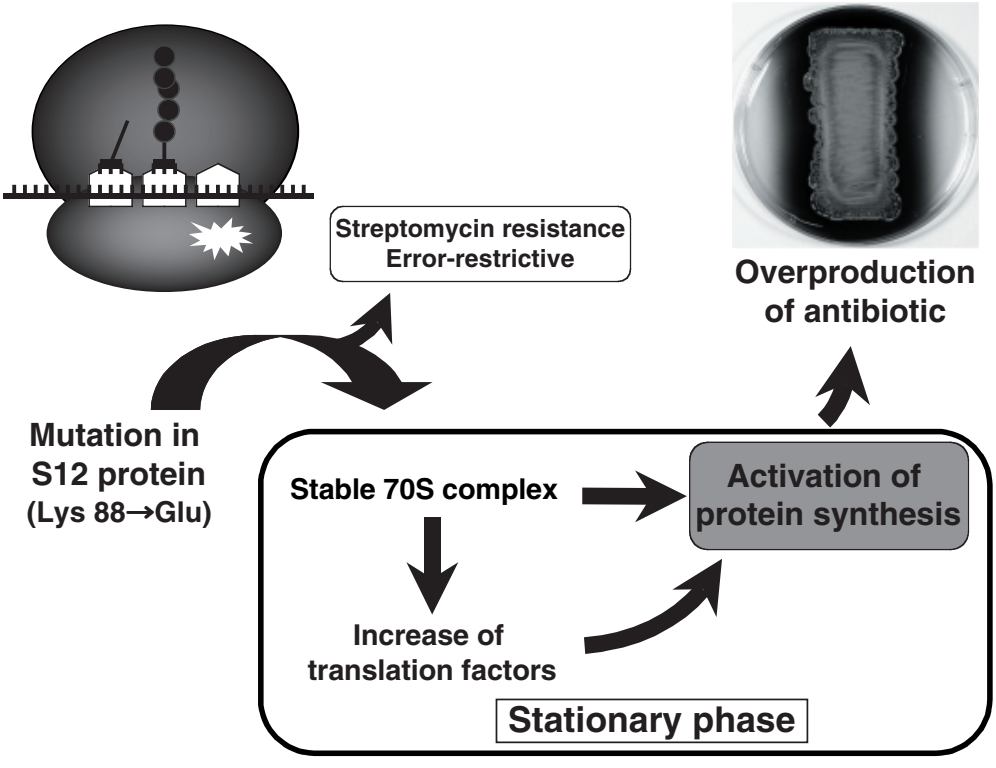

Fig. 2. Outline of mechanism by which mutation in S12 protein activates antibiotic production.

(K88E and P91S) effectively activated antibiotic production. It thus appears that certain mutations around Lys-88 region may distinctively affect antibiotic production and that isolation of such mutants could be effective for developing the antibiotic-overproducing strains. However, since most of those mutations are not likely to confer resistance to streptomycin, it would be impossible to identify such mutations by virtue of their ability to resist to the drug. To circumvent this difficulty, we used site-directed mutagenesis to create seven novel *rpsL* mutations (R86L, V87K, K88G, D89R, L90K, G92D, and R94G), and introduced these mutant genes into wild-type *S. lividans* cells by using a single-copy-number plasmid (17). Of these mutations, two (L90K and R94G) activated a red-pigmented antibiotic (undecylprodigiosin) production by *S. lividans* much more potently than streptomycin-resistant K88E mutation. Neither L90K nor R94G mutation conferred an increase in the level of resistance to streptomycin and paromomycin, indicating non-availability of these mutant alleles among the resistant isolates. Since the experimental system chosen in this study to evaluate the new *rpsL* mutations involves expression of the mutant S12 protein using a plasmid and does not require any special technique for replacing the wild-type *rpsL* gene on the chromosome with the created mutant genes, this approach could be applicable to a variety of strains (even if any genetic information are not available) for improvement of antibiotic productivity.

2. Antibiotic Overproduction by *rpoB* (RNA Polymerase) Mutations

Antibiotic biosynthesis pathways and their genetic regulatory cascade are one of the most attractive field in *Streptomyces* genetics and important in considering strain improvement. Onsets of the morphological differentiation and the secondary metabolism, including antibiotic production, are supposed to be coupled and influenced by a variety of physiological and environmental factors (4). Antibiotic production in streptomycetes is generally growth phase-dependent. Thus, the signal molecule for growth rate control, ppGpp, is suggested to play a central role in triggering the onset of antibiotic production in *Streptomyces*. Namely, the ribosomes play an essential role for adjusting gene expression level by synthesizing ppGpp in response to nutrient limitation. Following positive correlation between ppGpp and antibiotic biosynthesis, disruption of the ppGpp synthetase gene, *relA*, or deletion mutation (designated as *relC*) in ribosomal L11 protein gene has been shown to lead to a deficiency in ppGpp accumulation after amino acid depletion (so-called "relaxed" phenotype) accompanied by impairment in antibiotic production (3, 12). The expression levels of many genes are regulated by ppGpp, either positively or negatively. Many genetic studies in *E. coli* suggested that RNA polymerase (RNAP) is the target for ppGpp regulation. Genetic analysis reveals that 4 major functional domains exist in RNAP β-subunit. The ppGpp-sensitivity domain is close to another important domain of RNAP β-subunit, the rifampicin (Rif) -binding domain (9). The crystal structure clearly revealed that Rif-cluster I is involved in the *E. coli* RNAP active center. Therefore, it is reasonable to consider that certain mutation in the Rif-binding domain could affect the activity of RNAP and then may affect the function of the adjacent ppGpp-binding domain.

We postulated that the impaired ability to produce antibiotic due to the *relA* or *relC* mutation may be circumvented by introducing certain Rif-resistant (*rif*) mutations into the RNAP β-subunit. This hypothesis is based on a notion that the mutated RNAPs may behave like "stringent" RNAP without ppGpp binding. The results from *rel* mutants of *S. coelicolor* A3(2) and *S. lividans* strongly supported this hypothesis (11, 23). All the Rif-resistant isolates from the *rel* mutants regained the ability to produce the colored antibiotic actinorhodin, and various types of point mutation were mapped in the so-called Rif-cluster I in the *rpoB* gene that encodes the RNAP β-subunit. More impressively, gene expression analysis revealed that the restoration of actinorhodin production in the *rel rif* double mutant strains is accompanied by increased expression of the pathway-specific regulatory gene *act*II-ORF4, which normally decreased in the *rel* mutants. Accompanying the restoration of antibiotic production, the *rel rif* mutants also exhibited a lower rate of RNA synthesis compared to the parental strain when grown in a nutri-

tionally rich medium. Since the dependence of *S. coelicolor* A3(2) on ppGpp to initiate antibiotic production can be apparently bypassed by certain mutations in the RNAP, the mutant RNAP may function by mimicking the ppGpp-bound form. This proposal can be supported by the fact that the mutant RNAP behaved like "stringent" RNAP with respect to RNA synthesis, as demonstrated using cells growing in a nutritionally rich medium.

3. Combined Drug-Resistant Mutations

Introduction of combined drug-resistant mutations was found to be quite effective to increase the productivity of antibiotics in a hierarchical order (8). The increased productivity of actinorhodin by sequential introduction of *str*, *gen*, and *rif* in *S. coelicolor* A3(2) is shown in Fig3A. Mutants with enhanced (1.6- to 3-fold-higher) actinorhodin production were detected at a high frequency (5 to 10%) among isolates resistant to streptomycin (*str*), gentamicin (*gen*), or rifampin (*rif*), which developed spontaneously on agar plates containing one of the three drugs. Construction of double mutants (*str gen* and *str rif*) by introducing gentamicin or rifampin resistance into an *str* mutant resulted in further increased (1.7- to 2.5-fold-higher) actinorhodin productivity. Likewise, triple mutants (*str gen rif*) thus constructed were found to have an even greater ability for producing the antibiotic, eventually generating a mutant being able to produce 48 times more actinorhodin than the wild-type strain. Although analysis of *str* mutants revealed that a point mutation occurred within the *rpsL* gene, mutation points in *gen* mutants still remain unknown. These single, double, and triple mutants displayed a remarkable increase in the production of ActII-ORF4, a pathway-specific regulatory protein, in hierarchical order (8). The superior ability of the triple mutants was demonstrated by physiological analyses under various culture conditions. Thus, we can continuously increase the production of antibiotic in a stepwise manner by inducing combined drug-resistant mutation. Although much progress has been made in improving antibiotic producers, our method is characterized by the host cell's amenability (generation of spontaneous drug-resistant mutation) and the applicability to a number of microorganisms. It should also be emphasized that combined resistant mutations (triple mutations) demonstrated no significant impairment in growth or sporulation. Antibiotic production is in general subjected to the suppressive effects caused by an excess of nutrients such as carbon, nitrogen, and phosphate sources. In particular, ammonium and phosphate both appear to be major regulators of antibiotic production and their control systems may be interrelated in some way. Consistent with this notion, actinorhodin production in wild-type and mutant strains is more or less dependent on the medium, displaying more production in R4 medium

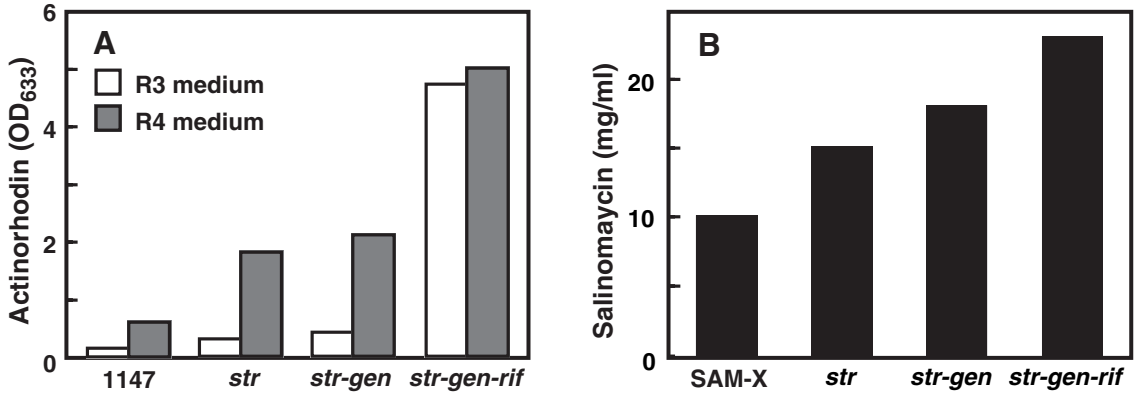

Fig. 3. Hierarchical increase of antibiotic production by introducing combined drug-resistance mutations in *Streptomyces coelicolor* wild-type strain 1147 (A) and *Streptomyces albus* industrial strain SAM-X (B), which produces a high amount (10 mg/ml) of salinomycin.

(containing less yeast extract and phosphate) than in R3 medium. The triple (*str gen rif*) mutants constructed revealed less sensitivity to such suppressive effects (Fig.3A).

Unlike wild-type strains stated above, improvement of antibiotic productivity of industrial strains is, in general, much more difficult as productivity has already been raised by various genetic and physiological approaches. Nevertheless, demonstration of efficacy of drug-resistant mutation in industrial strains is intriguing, because the improvement of industrial strains are linked directly with economic aspects. Working with a *Streptomyces albus* strain that had previously been bred to produce industrial amounts (10 mg/ml) of salinomycin, the efficacy of introducing drug-resistant mutations for further improvement of the antibiotic productivity has been demonstrated (19). Mutants with enhanced salinomycin production were detected at a high incidence (7 to 12%) among isolates of spontaneously resistant to streptomycin, gentamicin, or rifampicin. Finally, we successfully demonstrated improvement of the salinomycin productivity of the industrial strain by 2.3-fold by introducing a triple mutation (Fig.3B). The *str* mutant was shown to have a point mutation within the *rpsL* gene (encoding ribosomal protein S12). Likewise, the *rif* mutant possessed a mutation in the *rpoB* gene (encoding the RNA polymerase β subunit). Combined drug-resistant mutations (triple mutation) caused no impairment of growth and sporulation. Rather, the ability to produce aerial mycelium and spores was, in fact, enhanced.

Strikingly, *str* mutant with increased salinomycin production revealed high translation activity at the stationary phase as determined with the *in vitro* translation assay system (19) (Fig. 4). This high translation activity could be a reason why the *str* mutant is capable of producing a greater amount of salinomycin. The aberrant protein synthesis ability of the *str* mutant resulted presumably from a more stable ribosome structure, as demonstrated in the presence of a low Mg^{2+} concentration. Antibiotic production, including salinomycin production, usually commences at the late growth phase (i. e., transition phase or stationary phase). Therefore, the enhanced ability of protein synthesis at late growth phase would promote the initiation processes (i. e. formation of positive regulatory proteins for antibiotic gene expression) or biosynthetic processes (or both).

4. Further Development of Ribosome Engineering

We recently found that certain mutations conferring resistance to fusidic acid and thiostrepton, in addition to streptomycin and gentamicin, also activate antibiotic producing ability of *S. coelicolor*. The frequency of mutants that show the increased antibiot-

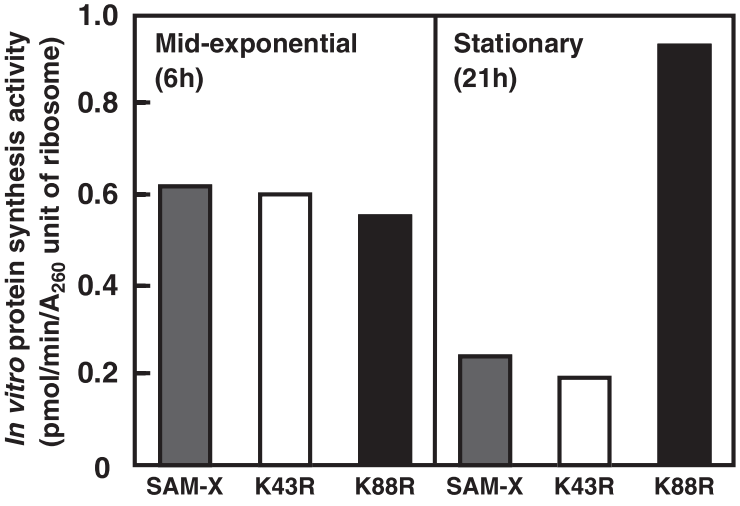

Fig. 4. *In vitro* translation activities of ribosomes prepared from *S. albus* cells at various growth phase. Translation activities were determined with poly(U)-directed cell-free translation system.

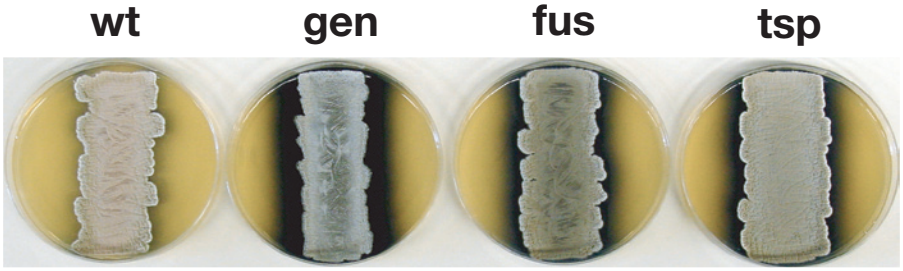

Fig. 5. Activation of antibiotic production by gentamicin-resistant (*gen*), fusidic acid-resistant (*fus*), or thiostrepton-resistant (*tsp*) mutation. Strains were incubated for 5 days on GYM agar medium. Blue color represents the antibiotic, actinorhodin.

Table 1. Locations of mutations in the *fusA* gene of *S. coelicolor* A3(2) and their effects on antibiotic production

Strain	Mutation in *fusA* gene	Amino acid exchange	Fusidic acid resistance level (μg/ml)	Antibiotic production (OD_{640})
1147	Wild-type	–	<100	0.10
7	ND	ND	200	2.67
28	1021G → C	Val341 → Leu	300	1.61
125	281C → G	Tyr94 → Ser	300	0.15
128	1421T → G	Leu474 → Arg	300	0.06

ic production was as high as 5%. The representative *fus* and *tsp* mutants are shown in Fig. 5. Fusidic acid and thiostrepton are antibiotics, which inhibit bacterial protein synthesis by binding to ribosomal components. The fusidic acid-resistant (*fus*) mutations are known to come frequently from a mutation of *fusA* gene (coding for the elongation factor G). As expected, the *S. coelicolor fus* mutants were found to have a point mutation in *fusA* gene (Table 1), except for mutant No. 7 which had no mutation in *fusA* gene. As shown in Fig. 6, mutant No. 28 (V341L) produced much greater amount of actinorhodin in both agar plate culture and liquid culture, while mutants No. 125 (T94S) and No. 128 (L474R) produced the antibiotic to the level of the wild-type strain 1147. To investigate whether or not the V341L mutation was indeed responsible for the observed increase in antibiotic production, we performed gene replacement experiments, as summarized in Fig. 7. Since recombinants with Fus^R (but not Fus^S) displayed a markedly increased antibiotic productivity, we concluded that the *fusA* mutation is responsible for the observed antibiotic over production. The ribosomes of *str* mutant cells having an increased ability to produce antibiotics show an increased stability of 70S particle

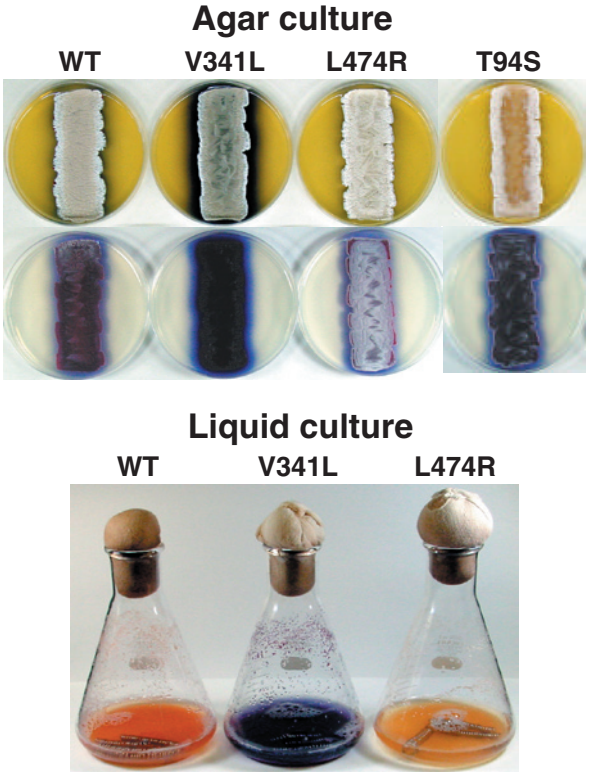

Fig. 6. Effects of various *fus* (encoding the elongation factor G) mutations on antibiotic production in solid and liquid culture.

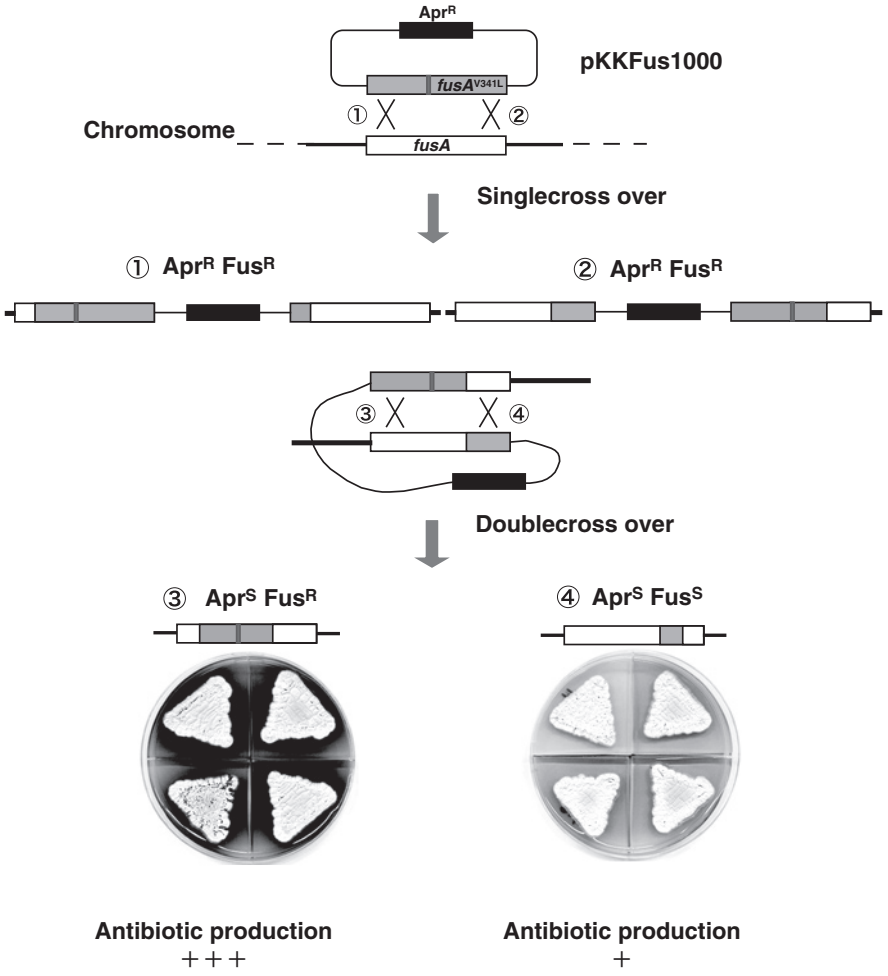

Fig. 7. A scheme for gene replacement of wild-type allele with mutant allele.

under the condition of low Mg^{2+} concentration. The *fus* mutant No. 28 (V341L), however, did not show such a stability, as examined in the presence of 0.8 mM Mg^{2+} (Fig. 8). Therefore, it is conceivable that the *fus* mutant No. 28 exerted its ability by the mechanism which differs from that of *str* mutants. Although the mechanism by which the *fus* mutant exerts the ability of antibiotic overproduction is at present entirely unknown, it is highly likely that the *fus* mutant somehow gained the ability to enhance protein synthesis at late growth phase.

The thiostrepton-resistant (*tsp*) mutations have been well documented ; the mutations come frequently from a point mutation in *rrn* (coding for rRNAs) or *rplK* (coding for the ribosomal protein L11) genes. However, we found no mutations in *rrn* and *rplK* genes when the genes of four *tsp* mutants (see Table 2) displaying an increased antibiotic producing ability were subjected to DNA sequencing. We therefore attempted to map the *tsp* mutations (tsp-17 and tsp-19) by conjugation, a method often used for genetic mapping in *S. coelicolor*. Eventually, we found that the *tsp-17* (and also *tsp-19*) mutation was located just adjacent to *strA* marker (Fig. 9). Since no *rrm* and *rplK* genes are known to lie in this map region, the present *tsp* mutations conferring the antibiotic overproducing ability are considered to be a novel mutation that was not found so far, and thus should provide a good tool to uncover the mechanism of initiation of antibiotic production.

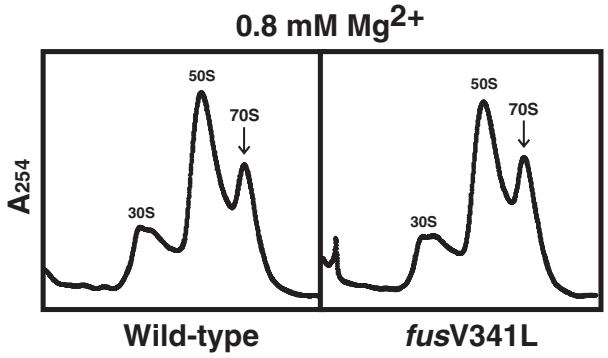

Fig. 8. Sucrose gradient analysis of ribosome fractions. The patterns of dissociation of the 70S complex into 30S and 50S subunits at a low (0.8 mM) concentration of Mg^{2+} were determined using washed ribosomes harvested from cells grown to mid-exponential phase.

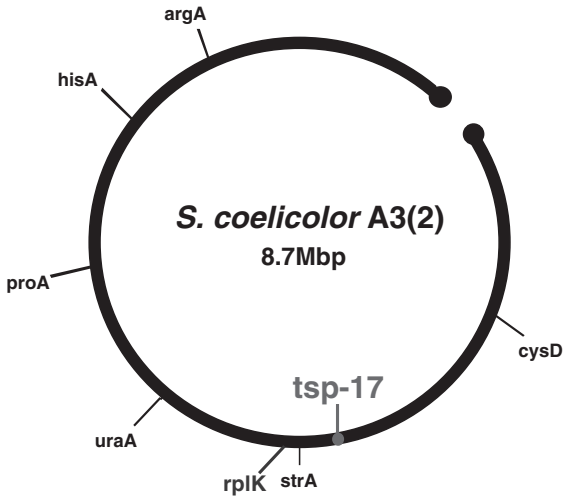

Fig. 9. Proposed position of *tsp-17* mutation in the *S. coelicolor* chromosome.

Table 2. Characterization of *S. coelicolor tsp* mutants

Strain	Resistance level to thiostrepton (μg/ml)	Act production	Red production
Wild-type	1	+	+
No. 6	50	++++	++
No. 17	>100	+++	+
No. 19	30	++++	++++
No. 39	100	+++	++++

Conclusion and Future Prospects

In this review, we demonstrated that cell's function can be altered dramatically by modulating the ribosome with the drug-resistance mutation technique. Our approach is characterized by focusing on ribosomal function at late growth phase (i. e. stationary phase); importance of this phase has been largely overlooked in study of ribosome with only a couple of exceptions [such as a work by Wada et al. (21)]. In summary, our novel breeding approach is based on two different aspects, modulation of the translational apparatus by induction of *str*, *gen*, *fus* and *tsp* mutations, and modulation of the transcriptional apparatus by induction of a *rif* mutation (Fig.10). Modulation of these two mechanisms may function cooperatively to increase antibiotic productivity.

In the study of current topics, we have found several important facts (or phenomena), which might be useful in eliciting cell's ability. These facts, together with the studies mentioned above, encourage us to construct more elegantly designed and more widely-applicable "Ribosome Engineering" in near future.

References

(1) Arias, P., Fernández-Moreno, M. A., and Malpartida, F. (1999). Characterization of the pathway-specific positive transcriptional regulator for actinorhodin biosynthesis in *Streptomyces coelicolor* A3(2) as a DNA-binding protein. *J. Bacteriol.* **181**: 6958−6968.

(2) Cashel, M., Gentry, D.R., Hernandez, V.J., Vinel-

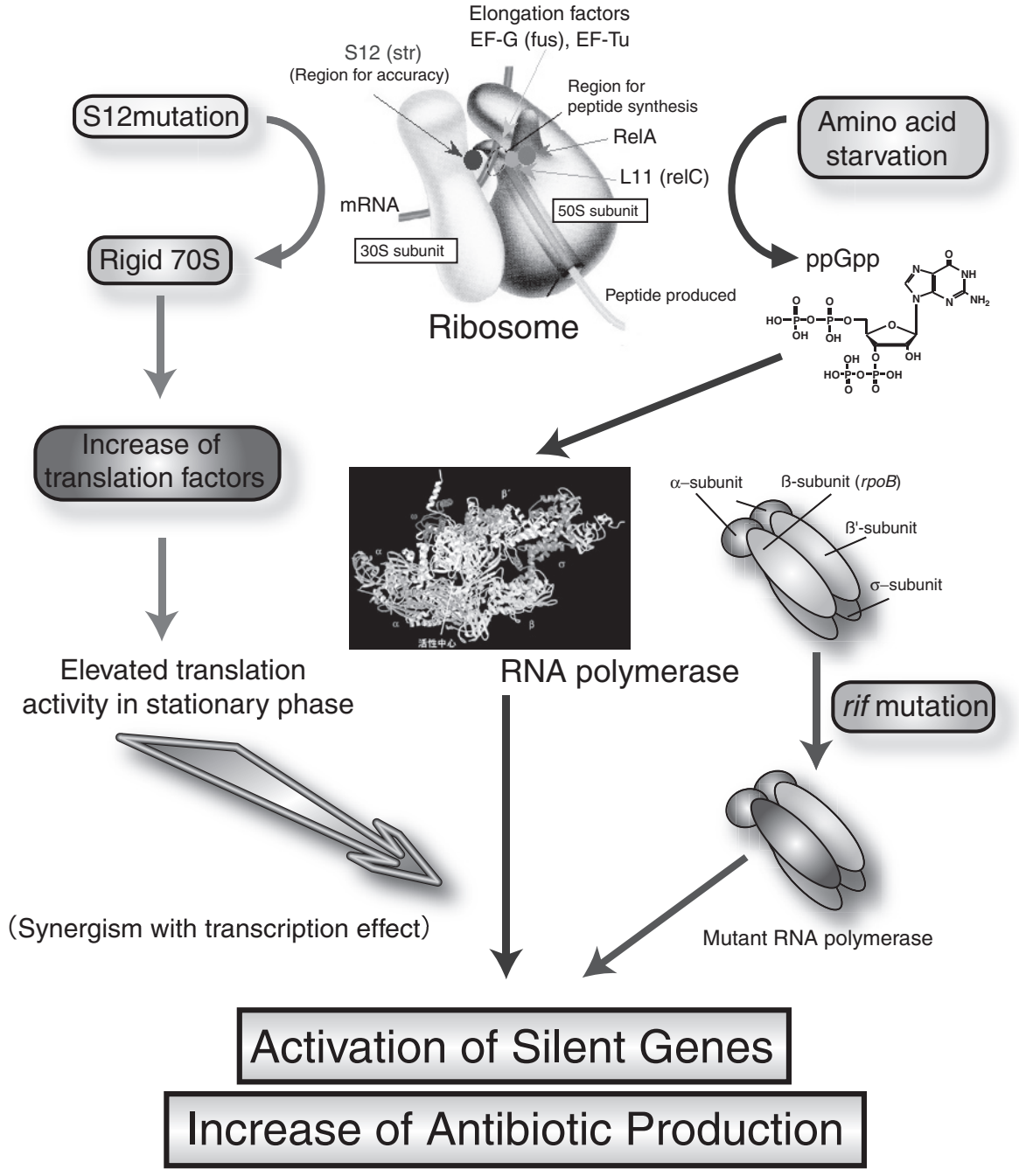

Fig. 10. Scheme of "Ribosome Engineering" to activate cell's ability.

la, D. (1996). The stringent response. *In* Neidhardt FC, Curtiss III R, Ingraham JL, Lin ECC, Low KB, Magasanik B, Reznikoff WS, Riley M, Schaechter M, Umbarger HE (ed.), *Escherichia coli* and *Salmonella typhimurium*: cellular and molecular biology, 2nd ed., vol.1. *American Society for Microbiology*, Washington, D.C., 1458–1496.

(3) Chakraburtty, R., White, J., Takano, E., Bibb, M.J. (1996). Cloning, characterization and disruption of a (p)ppGpp synthetase gene (*relA*) of *Streptomyces coelicolor* A3(2). *Mol. Microbiol*. **19**: 357–368.

(4) Chater, K.F., and Bibb, M.J. (1997). Regulation of

bacterial antibiotic production. *In* H. Kieinkauf and H. von Dohren (ed.). Biotechnology, vol. 7, Products of secondary metabolism. VCH, Weinheim, Germany, 57−105.

(5) Hesketh, A. and Ochi, K. (1997). A novel method for improving *Streptomyces coelicolor* A3(2) for production of actinorhodin by introduction of *rpsL* (encoding ribosomal protein S12) mutations conferring resistance to streptomycin. *J. Antibiot*. **50**: 532−535.

(6) Hosaka, T., Tamehiro, N., Chumpolkulwong, N., Hori-Takemoto, C., Shirouzu, M., Yokoyama, S. and Ochi, K. (2004). A novel mutation K87E in *Escherichia coli* ribosomal protein S12 causes an aberrant protein synthesis activity. *Mol. Genet. Genomics*. **271**: 317−324.

(7) Hosoya, Y., Okamoto, S., Muramatsu, H., and Ochi, K. (1998). Acquisition of certain streptomycin-resistant (*str*) mutations enhances antibiotic production in bacteria. *Antimicrob. Agents Chemother*. **42**: 2041−2074.

(8) Hu, H. and Ochi, K. (2001). Novel approach for improving the productivity of antibiotic-producing strains by inducing combined resistant mutations. *Appl. Environ. Microbiol*. **67**: 1885−1892.

(9) Ishihama, A., Fujita, N., Igarashi, K., and Ueshima, R. (1990). Structural and functional modulation of *Escherichia coli* RNA polymerase. *In* Felicia Y, Wu H, Cheng WW (ed.), Structure and function of nucleic acids and proteins. Raven Press, New York, 153−159.

(10) Kurland, C.G., Hughes, D., and Ehrenberg, M. (1996). Limitations of translational accuracy. *In* Frederick CN (ed.) *Escherichia coli* and *Salmonella*, Cellular and Molecular Biology. ASM Press, Washington, D. C. 979−1004.

(11) Lai, C., Xu, J., Tozawa, Y., Okamoto-Hosoya, Y., Yao, X., and Ochi, K. (2002). Genetic and physiological characterization of *rpoB* mutations that activate antibiotic production in *Streptomyces lividans*. *Microbiology* **148**: 3365−3373.

(12) Ochi, K. (1990). *Streptomyces relC* mutants with an altered ribosomal protein ST-L11 and genetic analysis of a *Streptomyces griseus relC* mutant. *J. Bacteriol*. **172**: 4008−4016.

(13) Ochi, K., and Hosoya, Y. (1998). Genetic mapping and characterization of novel mutations which suppress the effect of a *relC* mutation on antibiotic production in *Streptomyces coelicolor* A3(2). *J. Antibiot*. **51**: 592−595.

(14) Ochi, K., Zhang, D., Kawamoto, S., and Hesketh, A. (1997). Molecular and functional analysis of the ribosomal L11 and S12 protein genes (*rplK* and *rpsL*) of *Streptomyces coelicolor* A3(2). *Mol. Gen. Genet*. **256**: 488−498.

(15) Okamoto-Hosoya, Y., Sato, T., and Ochi, K. (2000). Resistance to paromomycin is conferred by *rpsL* mutations, accompanied by an enhanced antibiotic production in *Streptomyces coelicolor* A3(2). *J. Antibiot*. **53**: 1424−1427.

(16) Okamoto-Hosoya, Y., Hosaka, T., and Ochi, K. (2003). An aberrant protein synthesis activity is linked with antibiotic overproduction in *rpsL* mutants of *Streptomyces coelicolor* A3(2). *Microbiology* **149**: 3299−3309.

(17) Okamoto-Hosoya, Y., Okamoto, S., and Ochi, K. (2003). Development of antibiotic-overproducing strains by site-directed mutagenesis of the *rpsL* gene in *Streptomyces lividans*. *Appl. Environ. Microbiol*. **69**, 4256−4259.

(18) Shima, J., Hesketh, A., Okamoto, S., Kawamoto, S., and Ochi, K. (1996). Induction of actinorhodin production by *rpsL* (encoding ribosomal protein S12) mutations that confer streptomycin resistance in *Streptomyces lividans* and *Streptomyces coelicolor* A3(2). *J. Bacteriol*. **178**: 7276−7284.

(19) Tamehiro, N., Hosaka, T., Xu, J., Hu, H., Otake, N., and Ochi, K. (2003). Innovative approach for improvement of an antibiotic-overproducing industrial strain of *Streptomyces albus*. *Appl. Environ. Microbiol*. **69**: 6412−6417.

(20) Vinci, V. A. and G. Byng. (1999). Manual of industrial microbiology and biotechnology. ASM Press, Washington, D. C.

(21) Wada, A., Igarashi, K., Yoshimura, S., Aimoto, S., and Ishihama, A. (1995). Ribosome modulation factor: stationary growth phase-specific inhibitor of ribosome functions from *Escherichia coli*. *Biochem. Biophys. Res. Commun*. **214**: 410−417.

(22) Wietzorrek, A. and Bibb, M. (1997). A novel fam-

ily of proteins that regulates antibiotic production in streptomycetes appears to contain an OmpR-like DNA-binding fold. *Mol. Microbiol*. **25**: 1181−1184.

(23) Xu, J., Tozawa, Y., Lai, C., Hayashi. H., and Ochi. K. (2002). A rifampicin resistance mutation in the *rpoB* gene confers ppGpp-independent antibiotic production in *Streptomyces coelicolor* A3(2). *Mol. Genet. Genomics* **268**: 179−189.

(24) Zhang, Y.X., Perry, K., Vinci, V.A., Powell, K., Stemmer, W.P., and del Cardayre, S.B. (2002). Genome shuffling leads to rapid phenotypic improvement in bacteria. *Nature* **415**: 644−6460.

Type III Polyketide Synthases Responsible for Phenolic Lipids Synthesis in *Azotobacter vinelandii*

Nobutaka Funa

Department of Biotechnology, Graduate School of Agriculture and Life Sciences, the University of Tokyo, Bunkyo-ku, Tokyo 113-8657, Japan

Introduction

The genus *Azotobacter*, a gram-negative, nitrogen-fixing soil organism, produces phenolic lipids, which are the mixture of homologs of alkylresorcinols and alkylpyrones with various lengths of side chains (Fig. 1A). Alkylresorcinols are widely distributed among lower and higher plants, fungi, bacteria, and animals, and play several roles, which are concerned with cellular biochemistry and membrane chemistry (1). For example, 5-alkylresorcinols can be easily incorporated into phospholipids, bilayer, and biological membranes, thereby causing considerable changes in their structure and properties (1). 5-alkylresorcinols also act as modulators of oxidation of liposomal membranes and fatty acids (1). When *Azotobacter vinelandii* differentiates to metabolically dormant cysts, the phospholipids in the membranes are replaced by 5-alkylresorcinols (2). This unique membrane matrix may contribute to the physiology and desiccation resistance of the cyst (2). Although no precursor incorporation studies had been reported for this change of the membrane of *A. vinelandii*, the biosynthesis of alkylresorcinol can be best explained by the polyketide pathway.

All three bacterial polyketide synthases (PKSs), like their ancestors, possess a ketosynthase activity that catalyzes the sequential head-to-tail incorporation of acetate building blocks into a growing chain. Type I PKSs are multifunctional enzymes that are organized into modules, each of which harbors a set of distinct catalytic domains (3). Modular type I PKSs assemble polyketides by using each ketosynthase domain once to add many extender substrates onto a "starter substrate", while iterative type I PKSs use a single ketosynthase domain repeatedly for several times of extension. Type II PKSs consist of a "minimal PKS" and auxiliary subunits contain a single set of iteratively used active sites which are carried on separate proteins (4). Type III PKSs are ketosynthases with a homodimeric form, which act iteratively for polyketide chain extension (5). Chalcone synthase (CHS) (Fig. 1B), which catalyzes the condensation of three molecules of malonyl-CoA to *p*-coumaroyl-CoA synthesizing naringenin chalcone and is responsible for flavonoid synthesis in plant, is a member of type III PKSs (5). Stilbene synthase (STS) and coumaroyl triacetic acid synthase (CTAS) share over 70% amino acid sequence identity with CHS, and both type III PKSs catalyze the same iterative condensation to yield tetraketide intermediate identical to the CHS reaction (Fig. 1B). However, the mode of ring folding differs each other among these three type III PKSs. STS cyclizes the tetraketide intermediate via an intramolecular C2 to C7 aldol condensation, rather than the intramolecular C5 oxygen to C1 lactonization which is utilized by CTAS (Fig. 1B). Because the structure of the product of STS only differs from alkylresorcinols by its moiety derived from the starter substrate, we expected that type III PKS(s) might be involved in the formation of alkylresorcinols in *A. vinelandii*. As expected, an operon containing two type III PKSs was identified from the database of genome sequence of *A. vinelandii* and was revealed to be involved in the synthesis of phenolic lipids by the gene inactivation experiment, and therefore we designated this operon *ars* operon (Fig. 2A). By *in vitro*

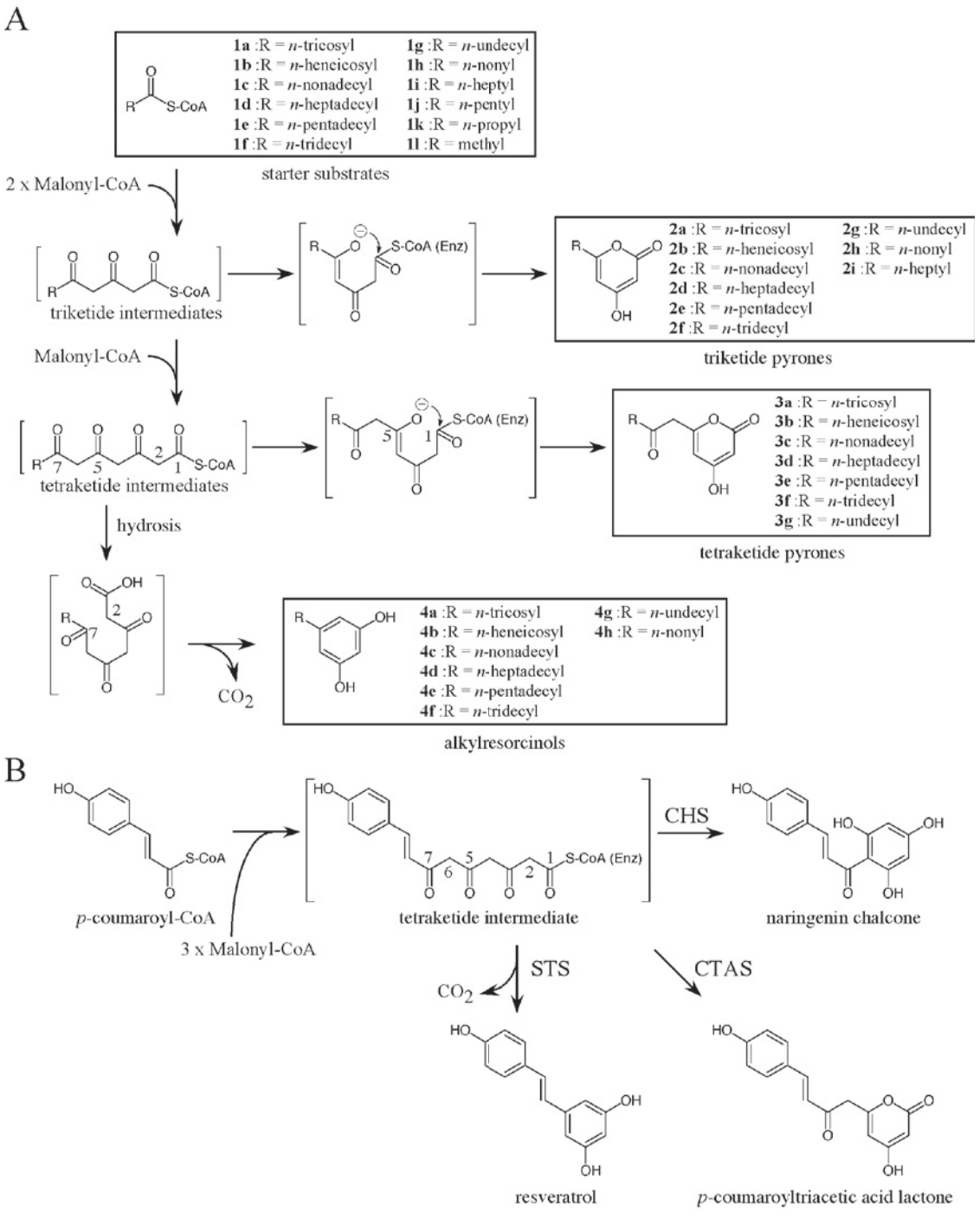

Fig. 1. Reactions catalyzed by type III PKSs. *A*, Alkylresorcinol and alkylpyrone synthesis by ArsB and ArsC. *B*, Reactions of plant type III PKSs. CHS, STS, and CTAS utilize common tetraketide intermediate, which was derived from *p*-coumaroyl-CoA and malonyl-CoA.

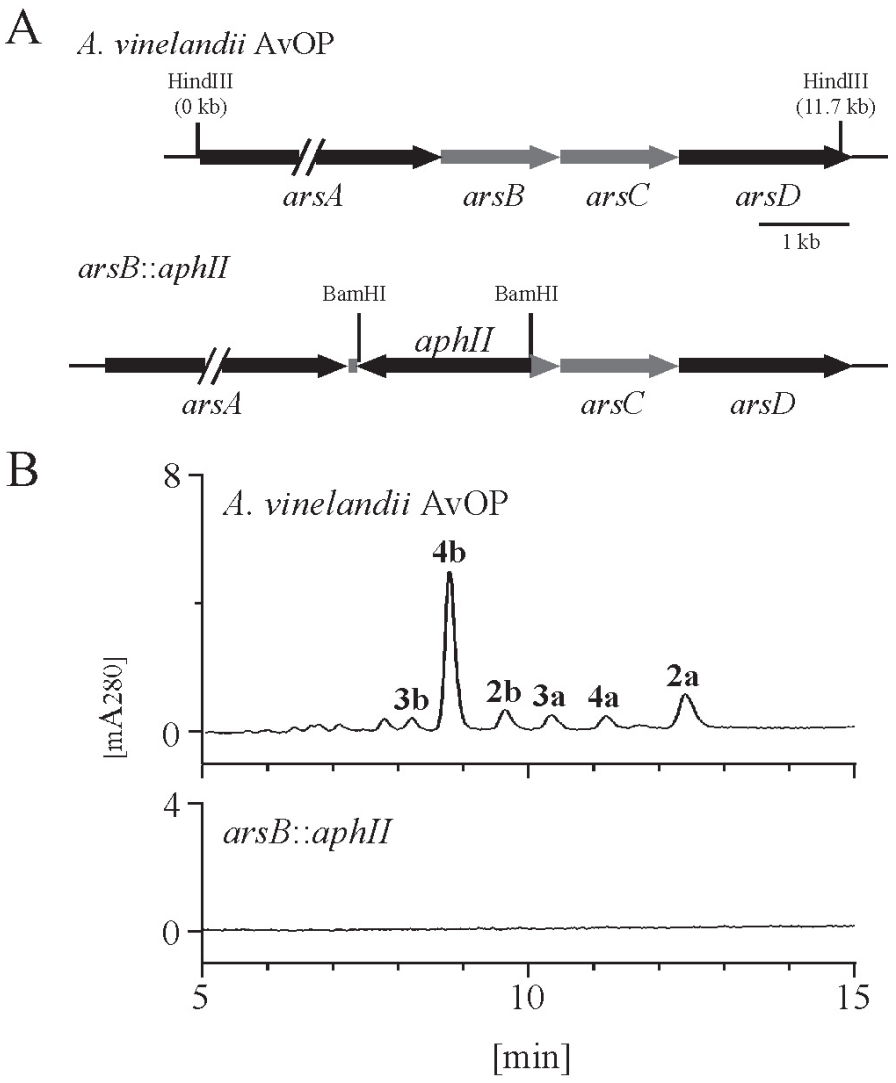

Fig. 2. Requirement of *ars* operon for phenolic lipid synthesis in *A. vinelandii*. *A*, Gene organization of the *A. vinelandii* chromosomal region including the *ars* operon. ArsA (accession number, ZP_00418324) and ArsD (ZP_00418327) are similar to iterative type I PKS. ArsB (ZP_00418325) and ArsC (ZP_00418326) are homologous to type III PKSs. The *arsB::aphII* mutant was constructed by replacing *arsB* sequence with kanamycin resistance gene, *aphII*. *B*, HPLC chromatograms of the extract from cysts of *A. vinlandii* AvOP and *arsB::aphII* mutant.

analysis of these newly identified type III PKSs, we have characterized ArsB and ArsC as alkylresorcinol synthase and alkylpyrone synthase, respectively. This is the first report of the identification of the enzyme responsible for alkylresorcinol synthesis.

Materials and Methods

Bacterial strains, plasmids and media.

A. vinelandii AvOP was obtained from Ray Dixon. *E. coli* JM109 and plasmids pUC19, used for DNA manipulation, were purchased from Takara Biochemicals. pET16b (Novagen) was used for expres-

sion of His-tagged proteins in *E. coli* BL21 (DE3). Media and growth conditions for *E. coli* were described by Maniatis *et al*. (6). *A. vinelandii* was routinely cultured at 30°C on Burk's medium (7) containing 2% glucose for 7 days.

Inactivation of ars operon in A. vinelandii.

The 1.7-kb DNA fragment containing the region from Ser-1993 of ArsA to Thr-13 of ArsB was amplified with primer I: 5'-CGC*AAGCTT*CC**TCG**GCCGGCCTGCCGGTC-3' (the boldface letters correspond to the Ser-1993 codon of ArsA and the italic letters indicate a HindIII site) and primer II: 5'-CGCAAGCTT-*GGATCC***TGT**GAAGCCGGTGAGAACTG-3' (the boldface letters correspond to the Thr-13 codon of ArsB and the italic letters indicate a BamHI site). The amplified fragment was cloned between the HindIII and BamHI sites of pUC19, resulting in pUC19-N-BamHI. The 1.6-kb DNA fragment containing the region from Glu-404 of ArsB to His-120 of ArsD was amplified with primer III: 5'-CGC*GGATCC***GAG**AAAATATGAACGACATG-3' (the boldface letters correspond to the Glu-404 codon of ArsB, the underline indicates the stop codon of ArsB, and the italic letters indicate a BamHI site) and primer IV: 5'-CGC-*GAATTC*GCTTGACCCCGGGGGC**ATG**G-3' (the boldface letters correspond to the His-120 codon of ArsD and the italic letters indicate an EcoRI site). The amplified fragment was cloned between the BamHI and HindIII sites of pUC19, resulting in pUC19-C-BamHI. After confirmation of the correct sequence, the HindIII-BamHI fragment from pUC19-N-BamHI and the BamHI-EcoRI fragment from pUC19-C-BamHI were ligated via the common BamHI site and cloned between the HindIII and EcoRI sites of pUC19. The 1.9-kb BamHI fragment containg *aphII* from Tn*5* was inserted into the BamHI site of the resultant plasmid, resulting in pUC19-⊿ArsB, in which the sequence of encoding from Pro-14 to Leu-403 of ArsB was replaced by the *aphII* sequence. pUC19-⊿ArsB was linearized with DraI, denatured with 0.1 M NaOH, and introduced into *A. vinelandii* AvOP by transformation according to the method of Page and von Tigerstorm (8). The kanamycin resistance transformants were selected and a gene replacement, as a result of double crossover, was confirmed by Southern blot analysis (data not shown).

Isolation and identification of 5-heneicosylresorcinol.

A. vinelandii strain AvOP was inoculated to 2 l × 4 of Burk's medium containing 2% glucose and grown at 30°C for 12 days. The cells were harvested by centrifugation, suspended in a small volume of water, and then extracted with chloroform/methanol (2:1, v/v). After the cell debris was filtrated off, the filtrate was lyophilized to dryness. The crude material was dissolved in chroloform and separated by silica gel chromatography using chroloform as an eluent. The major compound in the fraction was further purified by reversed-phase preparative HPLC [Pegasil C4 (Shenshu Scientific Co.), 10 × 250 mm] eluted with 95% CH_3CN in water containing 0.1% trifluoroacetic acid at a flow rate of 3 ml/min to provide 2 mg of 5-heneicosylresorcinol as a white solid. ^{1}H NMR (500 MHz, $CDCl_3$) δ 6.22 (m, 2H, C4H, C6H), 6.15 (m, 1H, C2H), 2.46 (t, J = 8 Hz, 2H, C1'H), 1.23 (m, 38H, methylene of C2' to C21'), 0.86 (t, J = 7 Hz, 3H, C22' H); ^{13}C NMR (125 MHz, $CDCl_3$) δ 156.5 (C-1, C-3), 146.5 (C-5), 108.0 (C-4, C-6), 100.1 (C-2), 35.8 (C-1'), 31.9 (C-20'), 31.1 (C-2'), 29.7 (C4' to C19'), 29.4 (C3'), 22.7 (C21'), 14.1 (C22'); atmospheric pressure chemical ionization-mass spectrum (APCI-MS): *m/z* 405.3 ($[M + H]^+$ ion observed in a positive ion analysis), *m/z* 403.2, ($[M - H]^-$ ion observed in a negative ion analysis).

Synthesis of behenyl-CoA.

Behenyl-CoA was synthesized by a modification of the procedure reported by Blecher (9). N-hydroxysuccinimide (345 mg, 3 mmol), 1-ethyl-3-(3-dimethylaminopropyl)-carbodiimide (633 mg, 3.3 mmol), and a catalytic amount of 4-dimethylaminopyridine were added to a solution of docosanoic acid (1022 mg, 3 mmol) in 20 ml of dry dichloromethane. The reaction was stirred at ambient temperature for 12 h before being quenched by adding ice. The aqueous layer was extracted with dichloromethane. The dichlo-

romethane extracts were combined, washed with brine, and dried over anhydrous sodium sulfate. Sodium sulfate was removed by filtration and the organic layer was evaporated under reduced pressure. The resulting solid was dissolved in a small amount of chloroform/methanol (2:1, v/v) and chromatographed in silica gel using chloroform/methanol (2:1, v/v) as an eluant to give docosanoic acid succinimide ester (984 mg, 75% yield) as a white solid: ^{1}H NMR (500 MHz, $CDCl_3$) δ 2.82 (br s, 4H, -CH_2-CH_2- moiety of succinimide), 2.58 (t, 2H, J = 7.5 Hz, C2H), 1.72 (dt, 2H, J = 7.5, 8.0 Hz, C3H), 1.38 (m, 2H, C4H), 1.23 (m, 34H, methylene of C5 to C21), 0.86 (t, 3H, J = 7 Hz, C22H).

To a solution of CoASH (20 mg, 23 μmol) in 5 ml water, thioglycolic acid (18.4 mg, 0.2 mmol), followed by sodium bicarbonate (67 mg, 0.8 mmol), was added. To this solution, a solution of docosanoic acid succinimide ester (353 mg, 0.8 mmol) in 5 ml of tetrahydrofuran was added. Tetrahydrofuran was further added till the mixture formed a single phase. The reaction mixture was stirred at 4°C for 16 h under an argon atmosphere. Tetrahydrofuran was evaporated and the resultant aqueous phase was extracted with chloroform to remove the unreacted succinimide ester. Behenyl-CoA in the crude sample was purified by reverse phase preparative HPLC (Pegasil-B C4, Senshu Scientific Co., 10 × 250 mm) using 70% acetonitrile in 25 mM KH_2PO_4 (pH 5.3) as an eluant at a flow rate of 3 ml/min. The collected fractions were lyophilized, and desalted by reverse phase preparative HPLC (Pegasil-B C4, Senshu Scientific Co., 10 × 250 mm) by a linear gradient as follows: acetonitrile 10% for 10 min, 10 to 80% for 20 min, and 80 to 100 % for 15 min at a flow rate of 3 ml/min. The collected fractions were combined and lyophilized to give 13.9 mg of behenyl-CoA as a white solid.

Synthesis of 6-heneicosyl-4-hydroxy-2-pyrone.

1-eicosanal was prepared by PCC oxidation of eicosanol, as described by Schwink and Knochel (10). 4-benzyloxy-6-methyl-2-pyrone was prepared as described previously. To a solution of 4-benzyloxy-6-methyl-2-pyrone (100 mg, 0.462 mmol) in 5 ml of dry tetrahydrofuran at −78°C, 1.0 M hexane solution of LHMDS (554 μl, 0.554 mmol) was added dropwise over 10 min. After 1 h, a solution of 1-eicosanal (274 mg, 0.924 mmol) in 5 ml of dry tetrahydrofuran was further added dropwise over 10 min, and the reaction mixture was stirred at −78°C for 2 h before saturated aqueous NH_4Cl was added. The mixture was extracted with ethyl acetate, and the resultant aqueous phase was further extracted with chloroform. The organic extracts were separately washed with brine before combined, and dried over anhydrous sodium sulfate. Sodium sulfate was removed by filtration and the organic layer was evaporated under reduced pressure. The preparative thin layer chromatography (TLC) developed in chloroform/methanol (40:1, v/v) gave 4-benzyloxy-6-(2'-hydroxyheneicosyl)-2-pyrone (93 mg, 39% yield) as a white solid: ^{1}H NMR (500 MHz, $CDCl_3$) δ 7.36 (m, 5H, BzH), 5.92 (d, J = 2.0 Hz, 1H, C5H), 5.50 (d, J = 2.0, 1H, C3H), 4.99 (s, 2H, CH_2Bz), 4.02 (m, 1H, C2'H), 2.62 (dd, J = 3.5, 14.5 Hz, 1H, C1'H), 2.48 (dd, J = 8.5, 14.5 Hz, 1H, C1'H), 1.48 (m, 2H, C3'), 1.23 (m, methylene of C4' to C20'), 0.86 (t, , J = 7.0 Hz, C21'H).

To a solution of 4-benzyloxy-(2'-hydroxyheneicosyl)-2-pyrone (90 mg, 0.176 mmol) in 4 ml of dichloromethane, 4-dimethylaminopyridine (220 mg, 1.8 mmol) and *p*-toluene sulfonyl chloride (86 mg, 0.45 mmol) were added. After the mixture was stirred at ambient temperature for 2 h, 1,8-diazabicyclo[5.4.0]-7-undecene (306 mg, 2 mmol) was added. After an additional 15 min stirring, the mixture was diluted with dichloromethane. The resultant mixture was washed with 1 M HCl, saturated aqueous $NaHCO_3$, and brine, successively, and dried over anhydrous sodium sulfate. Sodium sulfate was removed by filtration and the organic layer was evaporated under reduced pressure. The preparative TLC developed in chloroform/methanol (40:1, v/v) gave 4-benzyloxy-6-(heneicos-1'-enyl)-2-pyrone (80 mg, 92% yield) as a white solid: ^{1}H NMR (500 MHz, $CDCl_3$) δ 7.37 (m, 5H, BzH), 6.69 (dt, J = 7.0, 15.0 Hz, 1H, C1'H), 5.91 (dt, J = 1.5, 15.0 Hz, 1H, C2'H), 5.79 (d, J = 2.0 Hz, 1H, C5H), 5.50 (d, J = 2.0, 1H, C3H), 5.00 (s, 2H, CH_2Bz), 2.18 (m, 2H, C3'H), 1.41 (m, 2H, C4'H), 1.23 (m, 32H, methylene of C5' to C20'), 0.86 (t, J = 7.0 Hz, C21'H).

The mixture of 4-benzyloxy-6-(heneicos-1'-enyl)-2-pyrone (75 mg, 0.152 mmol) and 10% palladium on carbon (5 mg) in 10 ml of dry tetrahydrofuran was stirred at ambient temperature under 1 atm of H_2 for 2h. After removal of the palladium catalyst by filtration through celite, the filtrate was evaporated under reduced pressure. The preparative TLC developed in chloroform/methanol (40:1, v/v) gave 6-heneicosyl-4-hydroxy-2-pyrone (50 mg, 81% yield) as a white solid: ^{1}H NMR (500 MHz, $CDCl_3/CD_3OD$, 2:1) δ 5.57 (s, 1H, C5H), 2.07 (t, J = 7.0 Hz, 2H, C1'H), 1.33 (m, 2H, C2'H), 0.94 (m, 36H, methylene of C3' to C20'), 0.56 (t, J = 7.0 Hz, C21'H).

Synthesis of 4-hydroxy-6-(2'-oxotricosyl)-2-pyrone.

1-docosanal was prepared by PCC oxidation of docosanol. To a solution of 4-benzyloxy-6-methyl-2-pyrone (100 mg, 0.462 mmol) in 5 ml of dry tetrahydrofuran at −78°C, 1.0 M hexane solution of LHMDS (554 μl, 0.554 mmol) was added dropwise over 10 min. After 1 h, a solution of 1-dococosanal (300 mg, 0.924 mmol) in 5 ml of dry tetrahydrofuran was added dropwise over 10 min, and the reaction mixture was stirred at −78°C for 4 h before saturated aqueous NH_4Cl was added. The mixture was extracted with ethyl acetate, and the resultant aqueous phase was further extracted with chloroform. The organic extracts were separately washed with brine before combined, and dried over anhydrous sodium sulfate. Sodium sulfate was removed by filtration and the organic layer was evaporated under reduced pressure. The preparative TLC developed in chloroform/methanol (40:1, v/v) gave 4-benzyloxy-6-(2'-hydroxytricosyl)-2-pyrone (93 mg, 37% yield) as a white solid: ^{1}H NMR (500 MHz, $CDCl_3$) δ 7.36 (m, 5H, BzH), 5.92 (d, J = 2.0 Hz, 1H, C5H), 5.50 (d, J = 2.0, 1H, C3H), 4.99 (s, 2H, CH_2Bz), 4.01 (m, 1H, C2'H), 2.62 (dd, J = 4.0, 14.5 Hz, 1H, C1'H), 2.48 (dd, J = 9.0, 14.5 Hz, 1H, C1'H), 1.50 (m, 2H, C3'), 1.23 (m, methylene of C4' to C22'), 0.86 (t, , J = 7.0 Hz, C23'H).

To a solution of 4-benzyloxy-(2'-hydroxytricosyl)-2-pyrone (86 mg, 0.159 mmol) in 3 ml of dry dichloromethane, Dess-Martin periodinane (208 mg, 0.489 mmol) was added. The resultant mixture was stirred at 0°C for 24 h under an argon atmosphere before being filtered through a pad of celite, and the filtrate was evaporated under reduced pressure. The preparative TLC developed in chloroform/methanol (40:1, v/v) gave 4-benzyloxy-6-(2'oxotricosyl)-2-pyrone (69 mg, 81% yield) as a white solid: ^{1}H NMR (500 MHz, $CDCl_3$) δ 7.37 (m, 5H, BzH), 5.95 (d, J = 2.5 Hz, 1H, C5H), 5.52 (d, J = 2.5, 1H, C3H), 5.00 (s, 2H, CH_2Bz), 3.50 (s, 2H, C1'H), 2.51 (t, J = 7.5, 2H, C3'H), 1.56 (m, 2H, C4'H), 1.23 (m, 36H, methylene of C5' to C22'), 0.86 (t, J = 7.0 Hz, C23'H).

The mixture of 4-benzyloxy-6-(2'oxotricosyl)-2-pyrone (66 mg, 0.122 mmol) and 10% palladium on carbon (5 mg) in 10 ml of tetrahydrofuran was stirred at ambient temperature under 1 atm of H_2 for 2h. After removal of the palladium catalyst by filtration through celite, the filtrate was evaporated under reduced pressure. The preparative TLC developed in chloroform/methanol (40:1, v/v) gave 4-hydroxy-6-(2'-oxotricosyl)-2-pyrone (47 mg, 86% yield) as a white solid: ^{1}H NMR (500 MHz, $CDCl_3/CD_3OD$, 2:1) δ 5.79 (s, 1H, C5H), 5.18 (s, 1H, C3H), 4.14 (s, 2H, C1'H), 2.36 (t, J = 7.0 Hz, 2H, C3'H), 1.39 (m, 2H, C4'H), 1.07 (m, 36H, methylene of C5' to C22'), 0.69 (t, J = 7.0 Hz, C23'H).

Production and purification of ArsB and ArsC.

The nucleotide sequence (ATCATG) covering the ATG start codon of ArsB was changed to CATATG to create an NdeI site by PCR with primer V: 5'-CGC<u>GAATTC</u>*CATATG*AGCAGTCCCCACAACG-CAGTT-3' (the italic letters indicate nucleotides to be changed; the underline indicates an EcoRI site) and primer VI: 5'-CGC<u>GGATCC</u>ATCGGCCAGGACC-GCGCT-3'(the underline indicates a BamHI site). Similarly, the nucleotide sequence (AATATG) covering the ATG start codon of ArsC was changed to CATATG to create an NdeI site by PCR with primer VII: 5'-CGC<u>GAATTC</u>*CATATG*AACGACATG-GCCCACCCC-3' (the italic letters indicate nucleotides to be changed; the underline indicates an EcoRI site) and primer VIII: 5'-CGC<u>GGATCC</u>CGCTGTTG-GTATCGAATACC-3'(the underline indicates a BamHI site). After amplification by PCR under the stan-

dard conditions, the EcoRI-BamHI fragments, excised from amplified *arsB* and *arsC* fragments, were separately cloned between the EcoRI and BamHI sites of pUC19, resulting in pUC19-ArsB and pUC19-ArsC, respectively. The absence of undesired alterations was checked by nucleotide sequencing. The NdeI-BamHI fragments, excised from pUC19-ArsB and pUC19-ArsC, were separately cloned between the NdeI and BamHI sites of pET16b, resulting in pET16b-ArsB and pET16b-ArsC, respectively. Histidine-tagged ArsB and ArsC were produced by the following methodology. *E. coli* BL21 (DE3), harbouring pET16b-ArsB or pET16b-ArsC, was grown overnight in Luria broth containing 100 μg/ml ampicillin. Cells were harvested by centrifugation and resuspended in 10 mM Tris-HCl (pH 8.0) and 145 mM NaCl. After sonication, cell debris was removed by centrifugation at 15,000 rpm for 20 min and the clear lysate was applied to a column with His-bind metal chelation resin (Novagen). The purification of histidine-tagged protein was carried out according to the manual from the manufacturer except for adding 10% glycerol in each buffer. The purified histidine-tagged protein was dialyzed with 10 mM Tris-HCl (pH8.0), 500 mM NaCl, and 10% glycerol.

PKS assay.

The standard reaction mixture contained 100 μM [2-^{14}C]malonyl-CoA, 100 μM starter CoA ester, 100 mM Tris-HCl (pH 8.0), 61 μg of ArsB or ArsC in a total volume of 100 μl. Reactions were incubated at 30 °C for 30 min before being quenched with 20 μl of 6 M HCl. The products were extracted with ethylacetate, and the ethylacetate layer was evaporated to dryness. The residual material was dissolved in 15 μl of methanol for TLC analysis or LC/APCI-MS analysis. Silica gel 60 WF_{254} TLC plates (MERCK) were developed in benzene/acetone/acetic acid (85:15:1, v/v/v) and the radiolabeled compounds were detected by using BAS-MS imaging plate (Fujifilm). LC/APCI-MS analysis was carried out by using esquire HCT system (Bruker daltonics) equipped with reverse phase HPLC column, Pegasil-B C4 (Senshu Scientific Co., 4.6 × 250 mm), using acetonitrile/water/acetic acid (900:100:1, v/v/v) (solvent A), (800:200:1, v/v/v) (solvent B), or (500:500:1, v/v/v) (solvent C) as an eluant at a flow rate of 1 ml/min. UV spectra were detected on an Agilent 1100 series diode array detector. Spectral data are summarized in Table 1.

Determination of kinetic parameters of ArsB and ArsC.

The reactions, containing 100 mM Tris-HCl (pH 8.0), 200 mM NaCl, 100 μM malonyl-CoA, and 16.1 μg ArsB or 61.4 μg of ArsC, were performed in a total volume of 100 μl. The concentration of behenyl-CoA was varied between 0.5 and 7 μM. After the reaction mixture had been preincubated at 30°C for 5 min, the reactions were initiated by adding the substrate, and were continued for 60 sec for the ArsB or ArsC reaction. The reactions were stopped with 20 μl of 6 M HCl, and the material in the mixture was extracted with ethylacetate. The organic layer was collected and evaporated. The residual material was dissolved in 15 μl of methanol for HPLC analysis. 5-*n*-heneicosylresorcinol, 4-hydroxy-6-(2'-oxotricosyl)-2-pyrone and 6-heneicosyl-4-hydroxy-2-pyrone were used to generate the standard curves for the quantification of the products. Steady-state parameters were determined by the Lineweaver-Burk's plot.

Results and Discussion

Isolation and characterization of phenolic lipids from A. vinelandii AvOP.

Although occurrence of phenolic lipids in several strains of *Azotobacter* and *Pseudomonas* was well studied (11), there were no data concerning the production of phenolic lipids in *A. vinelandii* AvOP. We prepared the lipid extracts from mature cysts of *A. vinelandii* AvOP and analyzed by HPLC (Fig. 2B). The major compound migrated at a retention time of 8.9 was characterized as 5-heneicosylresorcinol [**4b**] by proton and carbon NMR analysis and LC-APCIMS analysis. By observing $[M - H]^-$ ions at LC-APCIMS analysis, the molecular mass of **3b** and **2b** were revealed to be 448 and 406, respectively, suggesting that

Table 1. Mass spectral characteristics, UV spectra, retention times for compounds synthesized by ArsB and/or ArsC

Compound	MS (*m/z*)	MS/MS[a] (*m/z*)	Retention time (min)	Solvent system
6-tricosyl-4-hydroxy-2-pyrone [**2a**]	433.3[M − H]$^-$	389.3	12.4	A
6-heneicosyl-4-hydroxy-2-pyrone [**2b**]	405.1[M − H]$^-$	361.1	9.7	A
4-hydroxy-6-nonadecyl-2-pyrone [**2c**]	377.0[M − H]$^-$	333.0	7.7	A
6-heptadecyl-4-hydroxy-2-pyrone [**2d**]	349.0[M − H]$^-$	305.0	6.4	A
4-hydroxy-6-pentadecyl-2-pyrone [**2e**]	320.9[M − H]$^-$	276.9	8.7[b]	B
4-hydroxy-6-tridecyl-2-pyrone [**2f**]	292.9[M − H]$^-$	248.8	6.7[b]	B
4-hydroxy-6-undecyl-2-pyrone [**2g**]	264.8[M − H]$^-$	220.8	5.4[b]	B
4-hydroxy-6-nonyl-2-pyrone [**2h**]	236.8[M − H]$^-$	192.7	4.5[b]	B
6-heptyl-4-hydroxy-2-pyrone [**2i**]	208.7[M − H]$^-$	164.7	10.2	C
4-hydroxy-6-pentyl-2-pyrone [**2j**]	180.7[M − H]$^-$	136.7	6.2	C
4-hydroxy-6-(2'-oxopentacosyl)-2-pyrone [**3a**]	475.3[M − H]$^-$	431.3	10.4	A
4-hydroxy-6-(2'-oxotricosyl)-2-pyrone [**3b**]	447.2[M − H]$^-$	403.1	8.2	A
4-hydroxy-6-(2'-oxoheneicosyl)-2-pyrone [**3c**]	419.1[M − H]$^-$	375.1	6.7	A
4-hydroxy-6-(2'-oxononadecyl)-2-pyrone [**3d**]	389.2[M − H]$^-$	346.9	5.7	A
4-hydroxy-6-(2'-oxoheptadecyl)-2-pyrone [**3e**]	363.0[M − H]$^-$	318.9	7.7	B
4-hydroxy-6-(2'-oxopentadecyl)-2-pyrone [**3f**]	334.9[M − H]$^-$	290.9	6.0	B
4-hydroxy-6-(2'-oxotridecyl)-2-pyrone [**3g**]	307.0[M − H]$^-$	262.8	4.9	B
5-tricosylresorcinol [**4a**]	431.3[M − H]$^-$	389.1, 387.7	11.2	A
5-heneicosylresorcinol [**4b**]	403.3[M − H]$^-$	361.0, 359.4	8.9	A
5-nonadecylresorcinol [**4c**]	375.1[M − H]$^-$	332.9, 331.4	7.3	A
5-heptadecylresorcinol [**4d**]	347.1[M − H]$^-$	304.9, 303.3	6.0	A
5-pentadecylresorcinol [**4e**]	319.1[M − H]$^-$	n. d. [c]	8.7[b]	B
5-tridecylresorcinol [**4f**]	291.0[M − H]$^-$	n. d.	6.7[b]	B
5-undecylresorcinol [**4g**]	262.9[M − H]$^-$	n. d.	5.4[b]	B
5-nonylresorcinol [**4h**]	235.0[M − H]$^-$	n. d.	4.5[b]	B

[a]Precursor ions are the observed [M − H]$^-$ ions.
[b]Triketide pyrones and resorcinols were unseparatable in this condition.
[c]Not determined.

the **3b** and **2b** were α-pyrones. The structures of **2b** and **3b** were identified as 6-heneicosyl-4-hydroxy-2-pyrone [**2b**] and 4-hydroxy-6-(2'-oxotricosyl)-2-pyrone [**3b**], respectively, by observing comigrations with corresponding authentic standards, which were synthesized chemically (data not shown). Although compounds **2b**, **3b**, and **4b** differ in structure (*i.e.*, **2b**, **3b**, and **4b** are triketide pyrone, tetraketide pyrone, and resorcinol, respectively), they share common features: the side chain derived from *n*-behenyl-CoA [**1b**], which was presumed to be incorporated by PKS as a starter substrate. We characterized **2a**, **3a**, and **4a**, which would be derived from *n*-heneicosyl-CoA [**1a**], by comparing the patterns of the fragmentation observed in LC-APCI tandem mass analysis with those of **2b**, **3b**, and **4b**, respectively. These results suggest

that *A. vinelandii* AvOP produces phenolic lipids as mixtures of alkylresorcinols and alkylpyrones with saturated side chains ranging from C_{21} to C_{23}, as in the case of many other *Azotobacter* species (11).

Identification of a gene operon responsible for the phenolic lipids production in A. vinelandii.

Our BLAST search toward the *A. vinelandii* AvOP protein database using alfalfa CHS(12)sequence as a query revealed that two type III PKSs, sharing 23% (ArsB) and 25% (ArsC) amino acid identity with CHS, exist in the genome (Fig. 2A). Interestingly, *arsB* and *arsC* form an operon, which is composed of a putative iterative type I PKS (*arsA*), two type III PKS homologs (*arsBC*), and a functional unknown protein (*arsD*). ArsD is unique in that it contains a 4'-phosphopantetheinyl transferase domain, which catalyzes the posttranslational modification of acyl carrier protein by the covalent attachment of 4'-phosphopantetheine moiety of coenzyme A to a conserved serine (13), along with the functionally unknown N-terminal domain that is approximately 400 amino acids in length. We disrupted *arsB* by replacing the *arsB* sequence by a kanamycin resistance gene to examine possible involvement of this gene cluster in the phenolic lipids production (Fig. 2A). It seems likely that the *arsB*::*aphII* mutantion was polar on *arsCD* expression. This probably results in the inactivation of the entire gene cluster, since the 4'-phosphopantetheinyl transferase domain of ArsD would be important for the modification of the acyl carrier protein domain of ArsA. As expected, no phenolic lipids production was observed in mutant *arsB*::*aphII* (Fig. 2B), indicating that *ars* operon is responsible for the biosynthesis of phenolic lipids in *A. vinelandii*.

In vitro analysis of ArsB and ArsC reactions.

We were particularly interested in whether ArsB and ArsC are isozymes or not, because ArsB and ArsC share 71% amino acid identity and form an operon. We prepared ArsB and ArsC with His-tag at its N-terminus from *E. coli* expressing type III PKSs using the T7 expression system. Both recombinant type III PKSs migrated at a position of ca. 43 kDa on SDS-PAGE (data not shown). The first assay of ArsB was carried out with *n*-behenyl-CoA [**1b**] as a starter substrate, since the major component of the phenolic lipids of *A. vinelandii* was 5-heneicosylresorcinol [**4b**]. Incubation of *n*-behenyl-CoA [**1b**] along with [2-^{14}C] malonyl-CoA as extender substrate gave single radioactive product, which was identified as 5-heneicosylresorcinol [**4b**] by comparison of LC-APCIMS spectra appeared on the TLC plate (Fig. 3A, lane 12) with those of the product synthesized from non-radiolabeled substrates (data are summarized in Table 1) . Interestingly, the same reaction but with ArsC instead of ArsB gave two radioactive compounds differ from 5-heneicosylresorcinol [**4b**] in R_f values (Fig. 3B, lane 12). The products were identified as 6-heneicosyl-4-hydroxy-2-pyrone [**2b**] and 4-hydroxy-6-(2'-oxotricosyl)-2-pyrone [**3b**] by comparing LC-APCIMS spectra with those of synthetic standards. These results clearly indicate that ArsB and ArsC are type III PKSs with distinct catalytic properties and are responsible for the biosynthesis of alkylresorcinols and alkylpyrones, respectively. We measured the steady state kinetics parameters for **4b**, **2b** and **3b** synthesis by varying the concentration of *n*-behenyl-CoA [**1b**]. Both ArsB and ArsC exhibited saturation kinetics in response to the increasing concentration of *n*-behenyl-CoA [**1b**]. The k_{cat} value of 5-heneicosylresorcinol [**4b**] formation by ArsB was 6.20 ± 0.18 sec^{-1}. The K_m value of ArsB for *n*-behenyl-CoA [**1b**] was 3.99 ± 0.18 μM (an average of the values obtained from three independent experiments). The k_{cat} value of 6-heneicosyl-4-hydroxy-2-pyrone [**2b**] and 4-hydroxy-6-(2'-oxotricosyl)-2-pyrone [**3b**] formation by ArsC were 2.70 ± 0.35 sec^{-1} and 3.67 ± 0.14 sec^{-1}, respectively. The K_m value of ArsC for *n*-behenyl-CoA [**1b**] was 2.03 ± 0.61 μM. Despite both enzymes utilize identical tetraketide intermediate, the mechanism of ring folding is different between ArsB and ArsC: ArsB catalyzes "STS type" intramolecular C2 to C7 aldol condensation to yield 5-heneicosylresorcinol [**4b**], while ArsC catalyzes "CTAS type" intramolecular C5 oxygen to C1 lactonization to yield 4-hydroxy-6-(2'-oxotricosyl)-2-pyrone [**3b**] (Fig. 1A, B). Another difference between the reaction of ArsB and ArsC from *n*-behenyl-CoA

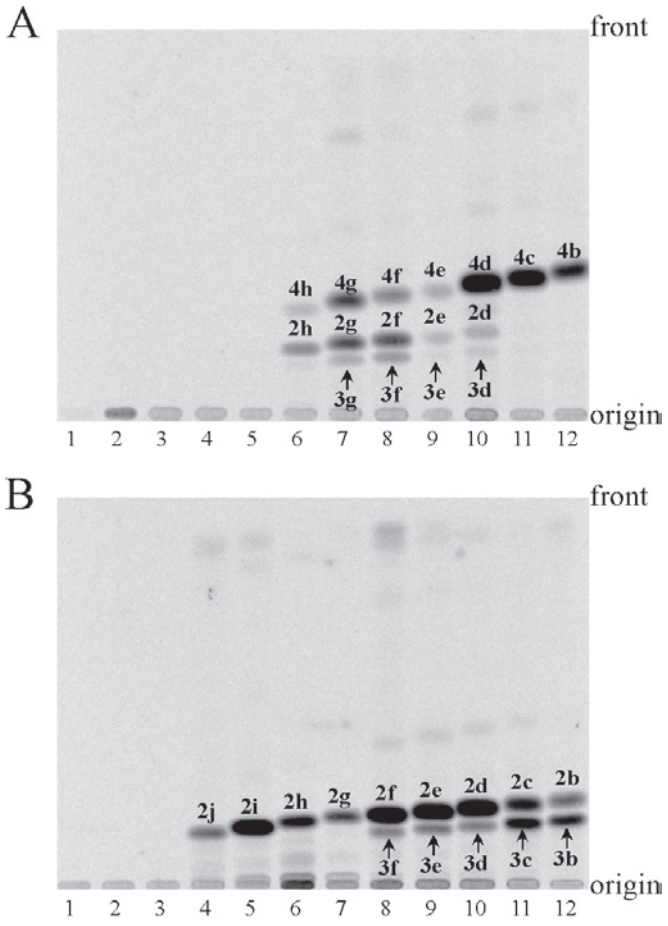

Fig. 3. Radio TLC analysis of products synthesized from various acyl-CoA starter substrates and [2-^{14}C]malonyl-CoA by ArsB and ArsC. *A*, TLC analysis of the products synthesized by ArsB. The starter substrates used are acetyl-CoA [**1l**] (lane 2), butyryl-CoA [**1k**] (lane 3), hexanoyl-CoA [**1j**] (lane 4), octanoyl-CoA [**1i**] (lane 5), decanoyl-CoA [**1h**] (lane 6), lauroyl-CoA [**1g**] (lane 7), myristoyl-CoA [**1f**] (lane 8), palmitoyl-CoA [**1e**] (lane 9), stearoyl-CoA [**1d**] (lane 10), arachidoyl-CoA [**1c**] (lane 11), and behenyl-CoA [**1b**] (lane 12). Lane 1 is a control incubation without a starter substrate. *B*, TLC analysis of the products synthesized by ArsC. The starter substrates used are acetyl-CoA [**1l**] (lane 2), butyryl-CoA [**1k**] (lane 3), hexanoyl-CoA [**1j**] (lane 4), octanoyl-CoA [**1i**] (lane 5), decanoyl-CoA [**1h**] (lane 6), lauroyl-CoA [**1g**] (lane 7), myristoyl-CoA [**1f**] (lane 8), palmitoyl-CoA [**1e**] (lane 9), stearoyl-CoA [**1d**] (lane 10), arachidoyl-CoA [**1c**] (lane 11), and behenyl-CoA [**1b**] (lane 12). Lane 1 is a control incubation without a starter substrate.

[**1b**] is that the size of the product is strictly regulated to tetraketide in ArsB reaction, whereas ArsC produced 6-heneicosyl-4-hydroxy-2-pyrone [**2b**], which was synthesized by lactonization of the triketide intermediate (Fig. 1A). We assume that hydrosis of the thioester, which is linked to CoA or ArsB, takes place before aldol reaction (illustrated in Fig. 1), since we could not detect any alkylresorcinolic acids from the reaction mixture of ArsB by the LC-APCIMS analysis. It is unknown whether decarboxylation is concerted with aldol reaction or occurs during the dehydration/aromatization step after aldol reaction. Similar observations were made on the STS reaction in which stilbene carboxylic acid was not detected (14). Furthermore, supplement of merulinic acid, an alkylresorcinolic acid, to the culture of *A. chroococcum* did not result in the production of the corresponding alkylresorcinol, and therefore enzymatic decarboxylation of alkylresorcinolic acid seems unlikely (1). Recently, a novel mechanism which leads to hydrosis of thioester, in turn re-

sults in "STS type" ring folding, has been proposed for the reaction of STS by solving the crystal structure (14). The difference between ArsB and ArsC could be explained by the absence of the STS-like thioesterase activity in ArsC but not in ArsB.

Substrate specificity of ArsB and ArsC.

Irrespective of plant or bacterial source, Type III PKSs have been shown to have rather promiscuous starter substrate specificity. We checked the reactivities of ArsB and ArsC toward CoA esters of C_2 to C_{22} straight chain fatty acid. The radio TLC (Fig. 3) as well as the LC-APCIMS analyses (summarized in Table 1) of the reaction products revealed the broad starter substrate specificities of ArsB and ArsC. ArsB accepted C_{10} to C_{22} ester, while ArsC exhibited broader substrate specificity than ArsB did. Neither the substrate specificities of the enzymes nor the product profiles of the reactions were affected by the changes in pH over a range of 6 to 9 (data not shown). In contrast, the optimal pH was different among each starter substrates (results not shown). Interestingly, alkylresorcinols were formed in the all reactions of ArsB but not in those of ArsC, suggesting that the mode of ring folding is determined by the functions of enzymes and is independent of the starter substrates incorporated in the polyketide intermediates. Although ArsB and ArsC accepted broad range of starter substrates *in vitro*, the corresponding products were hardly detected or not detected in the mixture of phenolic lipids from *A. vinelandii* (data not shown). This may be due to the production of behenyl-CoA, which is presumably synthesized by the coaction of ArsA and ArsD, resulting in the competition among the CoA esters produced by the primary metabolism (15). Very recently, Sankaranarayanan *et al*. solved the crystal structure of PKS18, a type III PKS from *Mycobacterium tuberculosis*, and discovered a unique tunnel, which extended from the active site to the surface of the protein and accounted for the binding of long chain aliphatic substrates (16). PKS18 displays a broad specificity for C_6 to C_{20} esters to produce tri- and tetraketide pyrones (16), while ArsC accepts C_6 to C_{22} (Fig. 3B). These observations indicate that the reactions catalyzed by these enzymes are essentially the same, although PKS18 and ArsC share only 23% identity in amino acid sequence. It is tempting to speculate that this unique tunnel is also conserved in both ArsB and ArsC.

Conclusion

In conclusion, we have identified two novel type III PKSs, ArsB and ArsC, that are responsible for phenolic lipids synthesis in *A. vinelandii*. From the identical tetraketide intermediate, ArsB catalyzes aldol condensation to form alkylresorcinols, while ArsC synthesizes alkylpyrones by lactonization. By the detailed analysis of *in vitro* reaction of ArsB, we proposed that alkylresorcinols were synthesized from tetraketide intermediate by hydrosis, aldol condensation, decarboxylation, dehydration, and aromatization, which are simultaneously occurs in ArsB, rather than decarboxylation of alkylresorcinolic acid.

Acknowledgments

We would like to thank Ray Dixon for providing us *A. vinelandii* AvOP strain. This work was supported by the Bio Design Program of the Ministry of Agriculture, Forestry, and Fisheries of Japan and by a Grant-in-Aid for Scientific Research on Priority Areas from Monkasho.

References

(1) Kozubek, A. and Tyman, J. H. P. (1999) Resorcinolic lipids, the natural non-isoprenoid phenolic amphiphiles and their biological activity. *Chem. Rev*. **99**: 1−25.

(2) Reusch, R. N. and Sadoff, H. L. (1983) Novel lipid components of the *Azotobacter vinelandii* cyst membrane. *Nature* **302**: 268−270.

(3) Rawlings, J. B. (2001) Type I polyketide biosynthesis in bacteria (Part A−erythromycin biosynthesis). *Nat. Prod. Rep*. **18**: 190−227.

(4) Shen, B. (2000) Biosynthesis of aromatic polyketides. *Top. Curr. Chem*. **209**: 1−51.

(5) Austin, M. B. and Noel, J. P. (2001) The chalcone synthase superfamily of type III polyketide syn-

thases. *Nat. Prod. Rep*. **20**: 79−110.
(6) Maniatis, T., Fritsch, E. F., and Sambrook, J. (1982) *Molecular Cloning: a laboratory manual*, Cold Spring Harbor, NY.
(7) Kennedy, C., Gamal, R., Humphrey, R., Ramos, J., Brigle, K., and Dean, D. (1986) The *nifH*, *nifM* and *nifN* genes of *Azotobacter vinelandii*: characterization of Tn5 mutagenesis and isolation from pLARF1 gene banks. *Mol. Gen. Genet*. **205**: 318−325.
(8) Page, W. J. and von Tigerstrom, M. (1979) Optimal conditions for transformation of *Azotobacter vinelandii*. *J. Bacteriol*. **139**: 1058−1061.
(9) Blecher, M. (1981) Synthesis of long-chain fatty acyl-CoA thioesters using *N*-hydroxysuccinimide esters. *Methods Enzymol*. **72**: 404−408.
(10) Schwink, L., and Knochel, P. (1994) Catalytic asymmetric reductive addition of aldehydes mediated by boron and zinc organometalics. *Tetrahedron Lett*. **35**: 9007−9010.
(11) Kozubek, A., Pietr, S., and Czerwonka, A. (1996) Alkylresorcinols are abundant lipid components in different strains of *Azotobacter chrooccum* and *Psuedomonas* spp. *J. Bacteriol*. **178**: 4027−4030.
(12) Ferrer, J.-L., Jez, J. M., Bowman, M. E., Dixon, R. A., and Noel, J. P. Structure of chalcone synthase and the molecular basis of plant polyketide biosynthesis. *Nat. Struct. Mol. Biol*. **6**: 775−784.
(13) Lambalot, R. H., Gehring, A. M., Flugel, R. S., Zuber, P., La Celle, M., Marahiel, M. A., Reid, R., Khosla, C., and Walsh, C. T. (1996) A new enzyme superfamily−the phosphopantetheinyl transferases. *Chem. Biol*. **3**: 923−936.
(14) Austin, M. B., Bowman, M. E., Ferrer, J.-L., Schröder, J., and Noel, J. P. (2001) An aldol switch discovered in stilbene synthases mediates cyclization specificity of type III polyketide synthases. *Chem. Biol*. **11**: 1179−1194.
(15) Reusch, R. N. and Sadoff, H. L. (1981) Lipid metabolism during encystment of *Azotobacter vinelandii*. *J. Bacteriol.* **145**: 889−895.
(16) Sankaranarayanan, R., Saxena, P., Marathe, U. B., Gokhale, R. S., Shanmugam, V. M. and Rukmini, R. (2004) A novel tunnel in mycobacterial type III polyketide synthase reveals the structural basis for generating diverse metabolites. *Nat. Struct. Mol. Biol*. **11**: 894−900.

Major Outer Membrane Proteins Homologous to OmpA in *Porphyromonas gingivalis*

Fuminobu Yoshimura

Department of Microbiology, School of Dentistry, Aichi-Gakuin University, Nagoya, Aichi 464-8650, Japan

ABSTRACT The major outer membrane proteins Pgm6 (41 kDa) and Pgm7 (40 kDa) of *Porphyromonas gingivalis* ATCC 33277 are encoded by open reading frames *pg0695* and *pg0694*, respectively, which form a single operon. Pgm6/7 have a high degree of similarity to *Escherichia coli* OmpA in the C-terminal region and are predicted to form eight-stranded β-barrels in the N-terminal region. By sodium dodecyl sulfate polyacrylamide gel electrophoresis, Pgm6/7 appear as bands with apparent molecular weights of 40 and 120 kDa, with and without a reducing agent, suggesting a monomer and trimer, respectively. To verify the predicted trimeric structure and function of Pgm6/7, we constructed three mutants with *pg0695*, *pg0694*, or both deleted. The double mutant produced no Pgm6/7. The single-deletion mutants appeared to contain less Pgm7 and Pgm6 and to form homotrimers that migrated slightly faster (115 kDa) and slower (130 kDa), respectively, than wild type Pgm6/7 under non-reducing conditions. N-terminal amino acid sequencing and mass spectrometry analysis of partially-digested Pgm6/7 only detected fragments from Pgm6 and Pgm7. Two-dimensional, diagonal electrophoresis and chemical cross-linking experiments with or without a reducing agent clearly showed that Pgm6/7 mainly form stable heterotrimers via intermolecular disulfide bonds. Furthermore, growth retardation and arrest of the three mutants, and increased permeability of their outer membranes indicated that Pgm6/7 play an important role in outer membrane integrity. Based on results of liposome swelling experiments, these proteins are likely to function as a stabilizer of the cell wall rather than as a major porin in this organism.

Introduction

Porphyromonas gingivalis, a gram-negative, saccharolytic anaerobe, is a major causative agent in the initiation and progression of periodontal disease (1, 2). This organism possesses a variety of virulence factors, including fimbriae, capsular polysaccharide, and hemagglutinins, as well as strong proteolytic enzymes such as Lys- and Arg-gingipains (1-4).

Previously, we identified seven major outer membrane proteins of *P. gingivalis* strain ATCC 33277 (5). Of these proteins, Pgm6 and Pgm7 have been assigned to the immunoreactive 42 kDa antigen PG33 and immunoreactive 43 kDa antigen PG32 of *P. gingivalis* W83, respectively (6, 7). Pgm6/7 share a high degree of similarity to *Escherichia coli* OmpA in the C-terminal region through which they presumably associate with peptidoglycan (8). *E. coli* OmpA forms non-specific diffusion channels that allow the penetration of various solutes (9) and is referred to as "monomeric porin" (10), which plays a structural role in the integrity of the bacterial cell surface (11).

Pgm6/7 appear as a single band on sodium dodecyl sulfate polyacrylamide gel electrophoresis (SDS-PAGE) with apparent molecular weights of 40 and 120 kDa with and without 2-mercaptoethanol (2-ME), respectively (5). This suggests that Pgm6/7 form heterotrimers in the outer membrane although there is no strong evidence that OmpA or OmpA homologs exist as stable oligomers (10).

In this study, we constructed three mutants by de-

leting the open reading frames (*orfs*) *pg0695* and/or *pg0694*, assigned by The Institute for Genomic Research, which encode Pgm6 and Pgm7, respectively, and then verified the heterotrimeric structure and examined the physiological roles of Pgm6/7 in this organism.

Materials and Methods

Bacterial strains, plasmids, and growth conditions.

Bacterial strains and plasmids used in this study are shown in Table 1. All *P. gingivalis* strains were grown in Trypticase soy broth (Becton, Dickinson and Company, Franklin Lakes, NJ) supplemented with 2.5 mg/ml yeast extract, 2.5 μg/ml hemin, 5 μg/ml menadione and 0.1 mg/ml dithiothreitol (DTT) (sTSB) under anaerobic conditions (10% CO_2, 10% H_2 and 80% N_2). In addition, a modified chemically defined medium (CDM) and Dulbecco's modified Eagle medium (DMEM), each supplemented with 3 or 1% bovine serum albumin (BSA), fraction V (BSA [Frac. V], Miles Inc., Kankakee, IL), were used as synthetic media for growth experiments. CDM with 3% BSA was prepared as previously reported (12) except for omission of hemin and menadione. Two BSA preparations, Frac. V and high grade (HG, Product No. A0281, Sigma-Aldrich Co., St. Louis, MO), were used for DMEM. We also used Brucella HK agar (Kyokuto Pharmaceutical Industrial Co., Ltd., Tokyo, Japan) supplemented with 5% laked rabbit blood, 2.5 μg/ml hemin, 5 μg/ml menadione, and 0.1 mg/ml DTT (BHK agar). A Zero Blunt TOPO PCR Cloning Kit, which included the plasmid vector, pCR-Blunt II-TOPO, was purchased from Invitrogen Corporation (Carlsbad, CA), and *E. coli* TOP10 carrying the pCR-Blunt II-

Table 1. Bacterial strain and plasmid list

Strain	Plasmid	Genotype or relevant characteristics	Reference or Source
Porphyromonas gingivalis			
ATCC 33277		Wild type, type strain	ATCC
Δ695		*pg0695*-deletion mutant from ATCC 33277, Cm^r [a]	This study
Δ694		*pg0694*-deletion mutant from ATCC 33277, Cm^r	This study
Δ695-694		*pg0695*- and *pg0694*-deletion mutant from ATCC 33277, Cm^r	This study
abfD mutant		*abfD* mutant of ATCC 33277 with an *ermF-ermAM* insertion in *abfD*, Em^r [a]	This study
W83		Wild type, the genome sequenced	(6)
Escherichia coli			
TOP10		as chemically competent cells, F^- *mcr*A *Δ*(*mrr-hsd*RMS-*mcr*BC) *Φ*80*lac*Z *Δ*M15 *Δlac*X74 *rec*A1 *deo*R *ara*D139 *Δ*(*ara-leu*)7697 *gal*U *gal*K *rps*L (Str^R) *end*A1 *nup*G	Invitrogen Corporation
DH5*α*	PKD260	a derivative of pACYC184 with deletion of a 1.1-kbp *Hinc*II fragment, bearing *cat* gene, Cm^r	a gift from K. Nakayama[b]
—	pCR-Blunt II-TOPO	a cloning vector, linearized with DNA topoisomerase I bound to the 3' end of each DNA strand, Km^r [a]	Invitrogen Corporation

[a] Cm^r, chloramphenicol resistance; Em^r, erythromycin resistance; Km^r, kanamycin resistance.

[b] Division of Microbiology and Oral Infection, Department of Developmental and Reconstructive Medicine, Nagasaki University Graduate School of Biomedical Sciences.

TOPO was grown in Luria-Bertani medium supplemented with 25 μg/ml kanamycin. *E. coli* DH5α carrying pKD260 was grown in Luria-Bertani medium supplemented with 25 μg/ml chloramphenicol (Cm) as described previously (13).

Construction of deletion mutants.

We applied the PCR-based overlap extension method (14) to construct DNA fragments that allowed the replacement of *pg0695*, *pg0694* or both genes with the *cat* gene in the *P. gingivalis* chromosome. The primers and their annealing sites are shown in Table 2 and Fig. 1A, respectively. The *cat* gene was amplified from the ATG start codon to the TAA stop codon with primers AGU-01 and AGU-02 to generate a 660 bp product from pKD260. For construction of the *pg0695*-deletion cassette, the flanking sequence upstream of *pg0695* was amplified with primers AGU-32 and AGU-36, which have homology to the 5' end of the *cat* fragment. The flanking sequence downstream of *pg0695* was amplified with AGU-33 and AGU-37, which have homology to the 3' end of the cat fragment. The *cat*, *pg0695*-upstream and *pg0695*-downsteam fragments were used as templates for overlap extension PCR to generate a deletion cassette in which *pg0695* was replaced by *cat*.

The deletion cassettes of *pg0694* and *pg0695/0694* were generated by similar procedures. Each deletion cassette created was ligated into pCR-Blunt II-TOPO, and the resulting recombinant plasmids were transformed into competent cells of *E. coli* TOP10 according to the manufacturer's directions (Invitrogen Corporation). Constructs to be introduced for making mutants were sequenced before electroporation to rule out unintended base changes. A similar deletion of an adjacent gene downstream from *pg0694* (*abfD*) was also done as described previously (15).

Electroporation of *P. gingivalis* was performed essentially as described by Fletcher et al. (16). The plasmid constructs were linearized by digestion with endonucleases *Kpn*I and *Xba*I, and introduced into electrocompetent cells of *P. gingivalis*. After 6 hours of anaerobic incubation in sTSB, the pulsed cells were plated on BHK agar supplemented with 12 μg/ml Cm, and the plates were incubated anaerobically at 37°C for 7 days. Possible recombinants were verified by PCR and restriction enzyme digestion of their PCR products.

Table 2. Primer list[a]

Name	Sequence (5'- 3')[b]
AGU-01	atggagaaaaaaatcactgga
AGU-02	ttacgccccgccctgccactc
AGU-32	gatgaagtcgccaaaggtgtc
AGU-33	cggaagtaaaccacattgtca
AGU-34	tttaattccatgggtaggtgttg
AGU-35	ctactgaattcattgagggacga
AGU-36	ccagtgatttttttctccatagttttacttttctaagtgtatttta
AGU-37	gcagggcggggcgtaattcatctgagacttttgttggataata
AGU-38	ccagtgatttttttctccataattctgtatgtcattttatattatccaac
AGU-39	gcagggcggggcgtaatctcaaatatccccacaaataaatg
AGU-40	tacgagcctaattctcccatg
AGU-41	cttgtattcgtccatctctgc

[a]Primer binding sites are shown in Fig. 1.
[b]Underlines show overlapping regions of 5' or 3' end of *cat*.

Membrane preparations.

Separation of whole envelopes and the outer membrane from *P. gingivalis* strains was performed essentially as described previously (5). Briefly, bacterial cells were washed with 10 mM HEPES-NaOH (pH 7.4) containing 0.15 M NaCl and then resuspended in 10 mM HEPES-NaOH (pH 7.4) containing 0.1 mM N α-*p*-tosyl-L-lysinechloromethyl ketone, 0.2 mM phenylmethylsulfonyl fluoride, and 0.1 mM leupeptin (HEPES buffer). The cells were disrupted by sonication, and the remaining undisrupted bacterial cells were removed by centrifugation at 1,000 × *g* for 10 min. The envelope was collected as a pellet by centrifugation at 100,000 × *g* for 60 min at 4°C. The pellet was washed once by resuspending in HEPES buffer and recentrifugation. The final pellet was suspended in HEPES buffer, and the outer membrane was obtained from the cell envelopes by the differential detergent extraction method (5). The protein content of the membrane preparation was estimated by the Bradford method (17).

SDS-PAGE and Western blotting.

SDS-PAGE was performed in a 1.0-mm-thick 12% gel as described by Lugtenberg et al. (18). Two-dimensional (2-D), diagonal SDS-PAGE was performed essentially as described previously (19). The samples were usually solubilized in SDS buffer with or without 2-ME at 100°C for 5 min (20). For 2-D, diagonal SDS-PAGE, cell envelopes were applied to the 12% slab gel under nonreducing conditions as the first dimension. After electrophoresis the gel strip was cut out, placed at the top of the second gel, and overlaid with the SDS buffer containing 2-ME to provide reducing conditions. The gels were stained with Coomassie Brilliant Blue R-250 (CBB).

Western blotting was performed as described previously (21). Proteins in SDS-PAGE gel were electrophoretically transferred to a nitrocellulose membrane. The membrane was blocked with 1% BSA (Frac. V) in 20 mM Tris-HCl (pH 7.5) and 0.5 M NaCl. Then the membrane was reacted with the anti-Pgm6/7 serum followed by incubation with peroxidase-conjugated anti-rabbit IgG (MP Biomedicals Inc., Aurora, OH). After the membrane was washed, signals of Pgm6/7 were detected with 0.01% 4-chloro-1-naphthol in 20 mM Tris-HCl (pH 7.5), and 0.5M NaCl supplemented with hydrogen peroxide.

Reduction of the Pgm6/7 protein trimer.

In SDS-PAGE, a solubilization-reduction mixture containing a high concentration of 2-ME was used for reduction of samples. Although the final concentration of 2-ME was about 300 to 700 mM, this could have an unknown solvent effect on proteins (22). Therefore, Pgm6/7 were also tested for dissociation of trimers to monomers by reduction with various concentrations of DTT. The dissociation of Pgm6/7 trimers in low pH was also attempted in the absence of the reducing agent as described by Luckey et al. (23).

Purification of heterotrimer and homotrimer of Pgm6/7.

The heterotrimer of Pgm6/7 and each homotrimer were electrophoretically purified from bacterial envelopes. Briefly, the envelope fraction was subjected to SDS-PAGE under nonreducing conditions. Protein bands (120, 115, and 130 kDa) stained with CBB were cut out from gels with a clean blade. After gel pieces containing the protein were applied again to another SDS-PAGE gel under reducing or nonreducing conditions, bands that migrated either as 120 or 40 kDa protein were excised, and proteins were eluted from gels using an electrophoretic sample concentrator (Isco, Inc., Lincoln, NE).

Chemical cross-linking.

Whole purified Pgm6/7 proteins (120 kDa) were mixed with 500 μl of 0.1 M triethanolamine-HCl buffer (pH 8.5) containing 0.1% SDS. The cross-linker disuccinimidyl suberate (11 Å length, Sigma-Aldrich Co.) dissolved in dimethylsulfoxide was added to it at a final concentration of 50 mM. After incubation at room temperature (20°C) for 1 or 2 h, the cross-linking

reaction was stopped by the addition of 50 μl of 0.1 M Tris-HCl (pH 8.0). Reaction mixtures were analyzed by SDS-PAGE under nonreducing and reducing conditions.

Protein analyses by N-terminal amino acid sequencing and mass spectrometry (MS).

The Pgm6/7 protein heterotrimers were partially digested with *Staphylococcus aureus* V8 protease to analyze the internal sequences as described previously (5). Heterotrimers and homotrimers were also analyzed by matrix-assisted laser-desorption ionization-time-of-flight (MALDI-TOF) MS. After in gel trypsin digestion, resulting peptides were extracted, concentrated, and applied to a Voyage-DE STR BioSpectrometry Workstation (Applied Biosystems, Foster City, CA) in the reflector mode essentially as described by Fountoulakis et al. (24). The identities of the proteins were deduced from MS peaks via MS-Fit peptide mass fingerprinting methods in ProteinProspector (http://prospector.ucsf.edu/).

Permeability of the outer membrane in intact cells.

Permeability of the outer membrane was determined by measuring the rate of hydrolysis of *p*-nitrophenylphosphate by intact cells (25). Alkaline phosphatase is known to be located in the periplasmic space of *P. gingivalis* (25, 26). Bacterial cells were washed and suspended in 10 mM Tris-HCl (pH 7.4) containing 1 mM $MgCl_2$ and 0.15 M NaCl, and cell suspensions were adjusted to an OD_{600} of 1.0. One portion was sonicated to release all alkaline phosphatase activity into the solution, and a part of the other portion was centrifuged to examine the enzyme that leaked out from bacterial cells into the supernatant, and remaining portion was used for determination of the activity of intact cells in the suspension. The hydrolysis of *p*-nitrophenylphosphate was determined in a reaction mixture containing 50 mM Tris-HCl buffer (pH 8.0) and 1 mM *p*-nitrophenylphosphate. After incubation at 37°C for 10 min, the enzymatic reaction was terminated by the addition of NaOH at a final concentration of 0.4 M. The released *p*-nitrophenol was quantified by measuring the OD_{400}. Experiments were carried out in duplicate and repeated separately three times.

Liposome swelling assay.

The assay was performed essentially as described by Nikaido et al. (27). Liposomes were made from 2.6 μmol egg phosphatidylcholine (Avanti Polar Lipids, Alabaster, AL) and 0.2 μmol dicetylphosphate (Sigma-Aldrich Co). Envelope fractions (200 μg protein) from several organisms and strains were used for the reconstitution of proteoliposomes that were suspended in Dextran T-40 (Amersham Biosciences Corp., Piscataway, NJ) solution and diluted into an iso-osmotic solution of arabinose (*Mr*, 150). The permeability was estimated by measuring the initial rates of the OD_{400} of the proteoliposome suspension.

Preparation of anti-Pgm6/7 serum.

A mixture of Pgm6/7 proteins purified as described above was emulsified with complete Freund's adjuvant and injected into rabbits subcutaneously four times at 2-week intervals.

Chloramphenicol acetyltransferase (CAT) assay.

Because there is only one prior report of *cat* as a resistance marker in *P. gingivalis* (28), we examined if *cat* was properly expressed. Even if mutants are successfully selected with Cm, increased resistance might occur due to a decrease in permeability of the outer membrane caused by deficiency in Pgm6/7 proteins. Bacterial lysates for CAT assay were prepared by the method described previously (29). CAT activities in the bacterial lysate were measured using a Chloramphenicol Acetyltransferase Reporter Gene Activity Detection Kit (Sigma-Aldrich Co.).

Antimicrobial susceptibility.

Penicillin G was obtained from Meiji Seika Kaisha, Ltd., Tokyo, Japan. Ampicillin and carbenicillin were obtained from Wako Pure Chemical Industries,

Ltd. Cefotaxime, cefoxitin, ceftriaxone, cefuroxime, cephalexin, erythromycin, Cm, tetracycline, minocycline, gentamicin and norfloxacin were purchased from Sigma-Aldrich Co. MIC was evaluated by agar dilution assay, as recommended by the National Committee for Clinical Laboratory Standards (NCCLS) (30). Briefly, serial dilutions of the corresponding antibiotics were added to BHK agar. After the bacteria were grown to the late logarithmic phase in sTSB, the bacterial culture (2 μl) was spotted on the antibiotic-containing agar. After two days of anaerobic incubation, the susceptibilities breakpoints were determined.

Bioinformatics tools.

Database searches for homologs of OmpA and Pgm6/7 were performed with the BLAST program (31). The program's three-dimensional position-specific scoring matrix (3D-PSSM), which can assign homologous proteins based on a structural prediction (32), and three programs for prediction of transmembrane β-sheets were used in this study (33-35).

Nucleotide sequence accession number.

The nucleotides of *pg0695*, *pg0694*, and their flanking regions of *P. gingivalis* ATCC 33277 were sequenced, and the sequences have been deposited in the GenBank database under accession number AB187516.

Results

Pgm6/7 (Pg0695/0694) homologous to E. coli OmpA.

The *P. gingivalis* genome has six ORFs that share homology with *E. coli* OmpA, but none that are homologous to OmpF and OmpC (20). Among the six ORFs, PgmA (20) and Pgm6/7 (PG33/32) have been identified and inferred to be a protein for fimbriation and candidates for porins, respectively, as OmpA homologs in this organism (5, 36). However, based on BLAST searches, Pgm6/7 have homology to OmpA only in the C-terminal regions that contain a putative peptidoglycan-binding motif (5, 8). Therefore, we performed two analyses to dertermine whether Pgm6/7 are structural homologs of OmpA or other outer membrane proteins such as lipoproteins (37). The program 3D-PSSM (32) predicted that Pgm6/7 were structurally homologous to OmpA with significant confidence e-values of 8.1×10^{-7} and 5.3×10^{-7}, respectively. Both proteins were also predicted to have structural homology to the peptidoglycan-binding lipoproteins as the second highly homologous protein with a less significant e-value of more than 3.0×10^{-2}. Since conventional hydropathy methods for predicting membrane topology are useless for strong hydrophilic membrane proteins like porins and OmpA, the structural prediction was performed by the method of Jeanteur (34) and Wimley (35) with the help of Drs. H. Nikaido (University of California, Berkeley) and W. C. Wimley (Tulane University Health Sciences Center), as well as by the Bigelow method (33). All results convincingly predicted that Pgm6/7 were similar to OmpA and had eight-stranded β-barrels in the N-terminal domain as does OmpA, although the overall β-barrel score of Pgm6 was low by the Wimley method (data not shown).

The Pgm6/7 locus in ATCC 33277 was sequenced and compared with those in W50 (AF175714.1 and AF175715.1) and W83 (6). The DNA sequence in the locus appeared to be the same in W50 and W83, but was slightly different in ATCC 33277. Pgm6 and Pgm7 in ATCC 33277 carried one (Phe to Leu^{199} in the middle; numbering from the N-terminal amino acid of mature protein) and four amino acid substitutions (Gly, Tyr, Met, and Leu to Ser^{55}, Asp^{126}, Ile^{144}, and Met^{154}, respectively) in the N-terminal half, respectively.

Construction of deletion mutants.

We constructed three deletion mutants from *P. gingivalis* wild type strain ATCC 33277 by the PCR-based overlap extension method, in which *orfs pg0695* and/or *pg0694* were deleted and replaced with *cat*, the gene encoding chloramphenicol acetyltransferase. The overall design for construction of the mutants is shown in Fig. 1A. To confirm the replacement of *orfs pg0695* and/or *pg0694* with *cat*, the cloning sites were amplified from flanking regions by PCR using each mutant chromosome as a template with primers of AGU-40

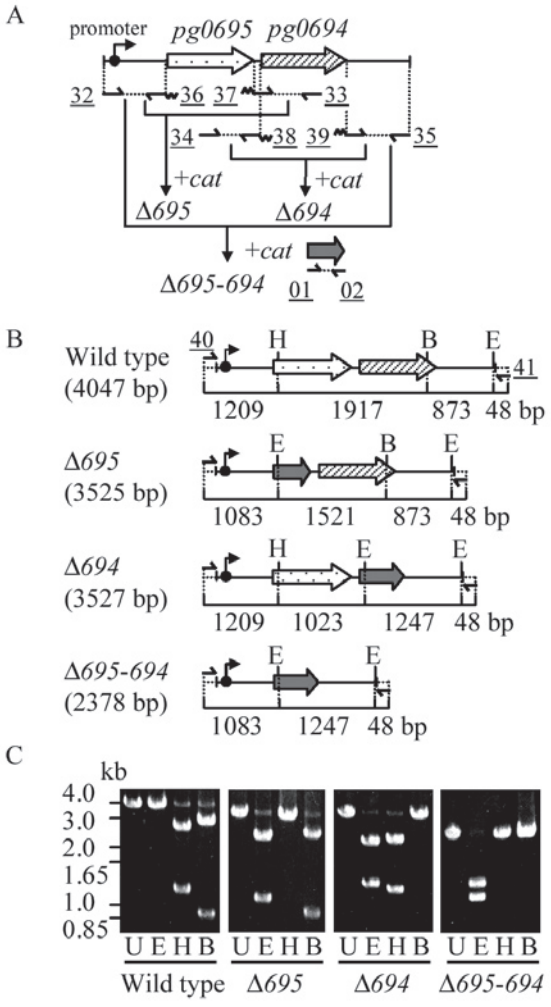

Fig. 1. Construction of *pg0695*- and *pg0694*-deletion mutants from *P. gingivalis* ATCC 33277. (A) The gene arrangement in the chromosome and procedure for construction of allele-exchange gene-deletion and location of primers. (B) Restriction sites and predicted lengths of the DNA regions in each genotype. Sizes of the DNA regions are shown as bp under the names and lines. (C) Verification of the mutants by gel electrophoresis of PCR products. After amplification by PCR with primers of AGU-40 and AGU-41 shown at the top of the panel (B) as 40 and 41, respectively, the PCR products were digested with the restriction enzymes described below and subjected to electrophoresis. Dotted arrows: *pg0695*, Diagonal-line arrows: *pg0694*, Gray arrows: *cat*, Small arrows: primers, Wavy line: overlap regions on *cat*, Underlined numbers: primer designation in a simplified manner (see Table 1 for details), U: undigested, E: digested with *Eco*RI, H: with *Hpa*I, B: with *Ban*II.

and AGU-41 as shown in Fig. 1B. Amplified PCR products were then digested with selected restriction enzymes. Since *Eco*RI cuts within *cat* (as well as 48 bp from the 3' flanking end), *Hpa*I cuts within *pg0695*, and *Ban*II cuts within *pg0694*, these enzymes were used to verify the genotypes of the putative mutants. As shown in Fig. 1C, gel electrophoresis of digested DNA yielded the predicted fragments.

SDS-PAGE, Western blot, and protein analyses.

Bacterial envelopes denatured in SDS were subjected to SDS-PAGE. As shown previously (38), Pgm6/7 formed 40 kDa and 120 kDa bands with and without 2-ME that were interpreted as Pgm6/7 monomers and trimers, respectively (Fig. 2A). No such bands were seen for the mutants.

To verify these assignments, a specific antiserum against Pgm6/7 was used for Western blot analysis (Fig. 2B). No immunoreactive bands appeared in the double mutant, confirming that Pgm6/7 are products of *pg0695/0694*. When reduced with 2-ME, a heavy band at the 40 kDa position was detected in the wild type, and weak bands at the same position appeared in *⊿695* and *⊿694*. No other band was detected. Under nonreducing conditions, a strong band at the 120 kDa position and two minor bands were observed in the wild type. Bands slightly lower (115 kDa) and higher (130 kDa) than the 120 kDa protein band with lower intensities were detected in *⊿695* and *⊿694*, respectively, and several minor bands were detected especially in *⊿694* (the right panel of Fig. 2B). Interestingly, the most slowly migrating bands in *⊿695* and *⊿694* appeared to be homotrimers of Pgm7 and Pgm6, respectively. Different sizes of monomers of Pgm7 (40 kDa) and Pgm6 (41 kDa), based on hypothetical translation of DNA sequences, could explain the differences in trimer mobility. The immunoreactive bands with molecular weights lower than the 120 and 130kDa bands in the wild type and *⊿694* could be partially dissociated (or degradation) products of Pgm6/7 and Pgm6 trimers, respectively.

The 120 kDa band disappeared upon treatment with 1 mM DTT, regardless of whether it was from envelopes or pure protein preparations, and full conver-

sion to monomers occurred in the presence of 5 mM DTT. The dissociated protein (40 kDa) partially returned to the 120 kDa position upon dialysis against distilled water, indicating that the dissociation was due to reduction, not to an unknown solvent effect of 2-ME (22), and the conversion was partially reversible (data not shown). In the absence of the reducing agent, the dissociation did not occur at low pH (data not shown).

To confirm the composition of the proposed Pgm6/7 heterotrimers and of Pgm6 or Pgm7 homotri-

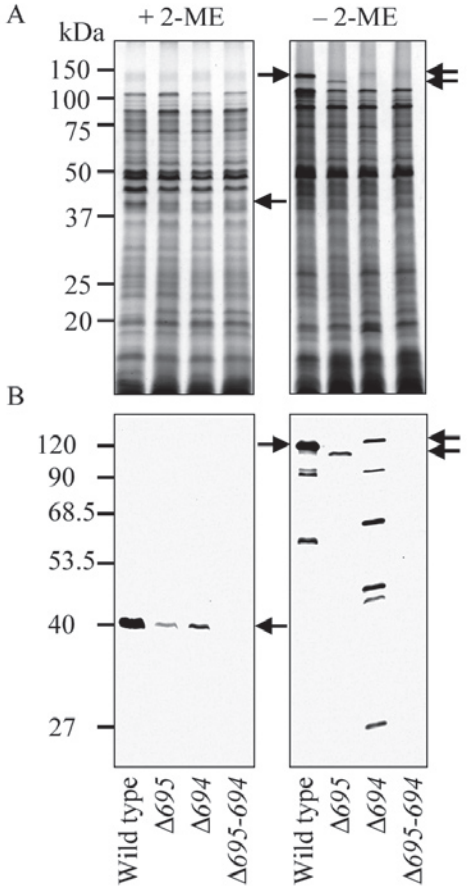

Fig. 2. Typical protein patterns and Western blots of envelope fractions. Bacterial envelopes were denatured in SDS with or without 2-mercaptoethanol (2-ME) at 100°C for 5 min, and then loaded to SDS-PAGE gels. The gels were stained with CBB (A) and subjected to Western blot analysis with anti-Pgm6/7 serum (B). Each 50 μg protein was applied to each lane of gel. Arrows show the predicted monomers and trimers that consisted of Pg0695 (Pgm6 monomer, 41 kDa) and/or Pg0694 (Pgm7 monomer, 40 kDa). Monomers of Pgm6 and Pgm7 were not discriminated from each other in SDS-PAGE.

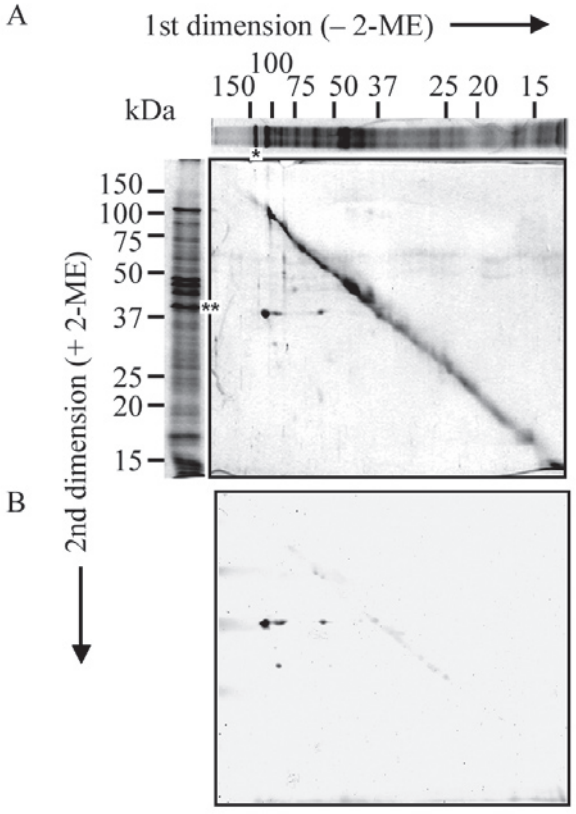

Fig. 3. Two-dimensional, diagonal SDS-PAGE and Western blotting of *P. gingivalis* wild-type envelope fraction. Envelopes (100 μg) were denatured in SDS at 100°C for 5 min under nonreducing conditions before the first-dimension electrophoresis. A gel strip was cut out from the first gel and placed on a well of the second gel. Then the strip in the well was overlaid with a buffer containing 2-ME. After the second electrophoresis, the gel was stained with CBB (A) or subjected to Western blotting with the anti-Pgm6/7 serum (B). The upper and left parts of the figure show protein patterns in one dimension of the sample treated without and with 2-ME, respectively, to more easily understand the result in the central panel. The asterisk and double asterisks show the 120 (predicted trimer) and 40 kDa (monomer) band, respectively.

mers, the envelope fraction of the wild type strain was subjected to 2-D diagonal electrophoresis with the first dimension under nonreducing conditions and the second dimension under reducing conditions. If a protein complex contains disulfide (SS) bonds, its components will appear as spots below the diagonal that reflect their individual molecular weights. Both a CBB-stained gel and a Western blot using the anti-Pgm6/7 serum showed a major 40 kDa spot and several minor spots at the off-diagonal position (Fig. 3). The main 40 kDa spot appeared to come from the major trimer band (120 kDa), and two minor 40 kDa spots were presumably derived from the dimer (90 kDa) and monomer (55 kDa) in the nonreducing dimension. The specific antibody reacted with these three spots and a smaller spot of lower molecular weight, indicating that all spots at the off-diagonal position came from proteins with modified SS-bonds. Next, 120 kDa heterotrimers and 115 and 130 kDa homotrimers were purified from SDS-PAGE gels, and the N-terminal amino acids of partially-digested peptides were sequenced and analyzed by MS. Five major peptides derived from 120 kDa heterotrimers treated with V8 protease were sequenced. The sequences of two peptides were identified as internal peptides of Pg0694 and Pg0695, and three peptides produced no sequence, presumably because they were blocked by an N-terminal pyroglutamyl residue (5, 36). In MS, peptides from heterotrimers were assigned with very high probability to Pgm6 (10 peaks of mass values were matched [matched peaks] and the matched peptides covered 47% of the protein [coverage]) and Pgm7 (42% coverage from 9 matched peaks). Those from 115 and 130 kDa homotrimers derived from the single-deletion mutants were assigned to Pgm7 (42% coverage from 11 matched peaks), and Pgm6 (42% coverage from 9 matched peaks), respectively. No other peptides were assigned to any protein or possible ORF in the *P. gingivalis* genome. This confirmed that Pgm6/7 were mainly present as heterotrimers in the outer membrane of the wild type, and the 115 and 130 kDa proteins from the single mutants were presumably homotrimers, based on their subtle differences in mobility.

Cross-linking experiment.

Purified Pgm6/7 proteins of the wild-type strain were treated with the cross-linker, disuccinimidyl suberate, and electrophoresed under nonreducing conditions (Fig. 4, the left panel). A diffuse band migrated at the position of 120 kDa, suggesting that the cross-linker indeed bound to the 120 kDa protein. When electrophoresed under reducing conditions (Fig. 4, the right panel), most Pgm6/7 migrated at the positions assigned to trimers (120 kDa), dimers (80 kDa) and monomers (40 kDa). In Western blots, the anti-Pgm6/7 serum reacted with all three bands, further supporting the trimeric structure of Pgm6/7 (data not shown).

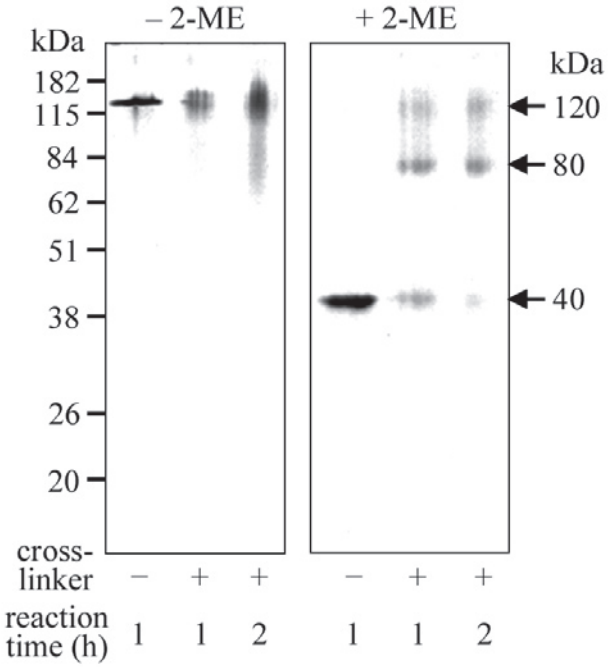

Fig. 4. Cross-linking of *P. gingivalis* wild-type Pgm6/7 proteins. The samples were treated with disuccinimidyl suberate as a cross-linker for 1 or 2 h. The cross-linked samples, denatured in SDS with or without 2-ME, were loaded to SDS-PAGE gels, and gels were stained with CBB.

Growth in rich and synthetic media.

An early-stationary phase culture in sTSB was inoculated into rich and synthetic media at a 1:20 ratio. Growth experiments were repeated at least twice, and typical results are shown in Fig. 5. In sTSB, a rich medium, the three mutants showed growth rates similar to the wild type and reached the stationary phase within 24 h. In a chemically defined medium (CDM), the wild type reached the stationary phase by 36 h, while all mutants grew more slowly and reached the same level as the wild type at about 96 h. In CDM supplemented with NaCl, the growth rate of the wild type did not change dramatically, whereas the three mutants grew more slowly (0.15 M) or did not grow (0.2 M) (Fig. 5). Similar growth inhibition by NaCl (or KCl) was obtained with sTSB (data not shown). We found that *P. gingivalis* could also grow in DMEM, a cell culture medium, as long as 1% BSA, a lower concentration than in CDM, was added. As shown in the bottom of Fig. 5, no significant differences were observed between growth in pure and crude BSA preparations, suggesting that growth of *P. gingivalis* and growth retardation of the mutants were not influenced by contaminants in BSA. The wild type and mutants substantially digested BSA during growth (data not shown).

Outer membrane permeability.

The permeability of the outer membrane in the wild type, as measured by alkaline phosphatase activi-

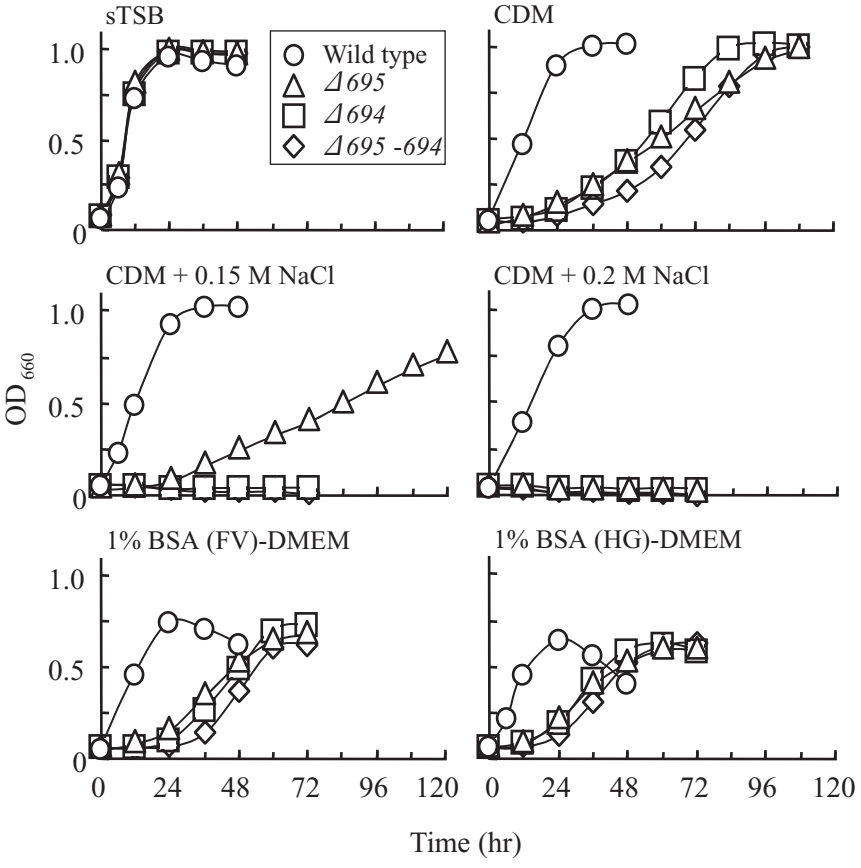

Fig. 5. Growth curves in various media. *P. gingivalis* ATCC 33277 (wild type), *Δ695*, *Δ694*, and *Δ695-694* were cultured in sTSB, CDM (chemically defined medium), CDM supplemented with 0.15 M NaCl or 0.2 M NaCl, and DMEM (Dulbecco's modified Eagle medium) supplemented with 1% BSA (FV, fraction V) or 1% BSA (HG, high grade purified).

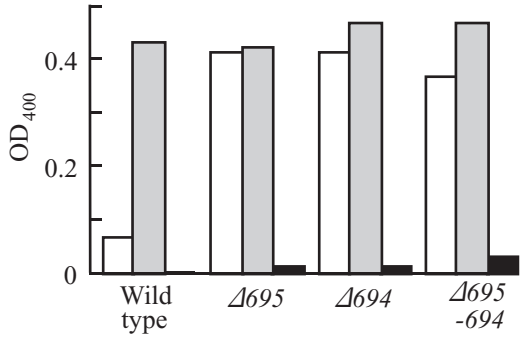

Fig. 6. Permeability of outer membranes in *P. gingivalis* wild type and the mutants. Permeability of the outer membranes was estimated by hydrolysis of *p*-nitrophenylphosphate with alkaline phosphatase. The released *p*-nitrophenol was determined by measuring the OD_{400}. Values are means of duplicate determinations. Similar results were obtained in three independent assays. Open bar, intact cell suspension; dotted bar, sonicated broken cells; closed bar, supernatant obtained from intact cell suspension.

ty with whole intact cells and cell lysates, was much lower than those of the mutants (Fig. 6). Intact cells of the mutants showed high alkaline phosphatase activities almost equal to the total enzyme activities in sonicated cells. Negligible levels of leaked-out enzyme activity were found in both single deletion strains, and a low level of activity was found in the double mutant. A different substrate, thymolphthalein monophosphate (*Mr*, 509) showed similar results (data not shown). Outer membranes lacking either or both Pgm6/7 seemed to be freely permeated by low molecular-weight substances such as *p*-nitrophenylphosphate (*Mr*, 217), but not alkaline phosphatase (a high molecular weight periplasmic enzyme). These experiments were independently done several times, and a typical result is shown in Fig. 6.

Pore-forming activity.

Channel-forming activities of various protein preparations were determined following incorporation of the preparation into liposomes. The liposome swelling rates by incorporation of envelopes from wild type *P. gingivalis* were measurable, but 10- to 100-fold lower than those obtained by incorporation of *E. coli* envelopes and even lower by incorporation of *Pseudomonas aeruginosa* envelopes when the same amount of envelopes was incorporated (data not shown) (39). The swelling rates obtained with envelopes of wild type *P. gingivalis* and those with the envelopes of the three mutants showed no significant differences. In addition, the swelling rate produced by the incorporation of a given amount of purified Pgm6/7 (120 kDa) protein was much lower than what was produced by the incorporation of the envelopes containing an equivalent amount of the protein. Moreover, an interesting finding on a transposon-insertion mutant of *P. gingivalis*, having an unrelated mutation in the *pg0694/0695* locus, was obtained during the liposome experiments. Envelopes from this uncharacterized mutant, containing the same amount of Pgm6/7 as the wild type, incorporated in liposomes resulted in a much lower swelling rate than that obtained by incorporation of envelopes of strains, including the wild type or the single and double mutants, indicating that other protein(s) lost in this mutant may form major channels (data not shown). This is under further investigation.

Antimicrobial susceptibility.

There was no significant difference of MIC values between the wild type and mutants. Strong CAT activities were detected only in the mutants where *cat* had been introduced (data not shown). MICs for Cm to *P. gingivalis* wild type strains ATCC 33277 and W83 were 3 μg/ml, while those to the three mutants ranged from 33 to 39 μg/ml, presumably due to the strong CAT expression. However, MICs for other antibiotics did not differ significantly between the wild type strains and the three mutants (Table 3). Most MIC tests were repeated three times.

Discussion

This study was conducted to further define the structures and functions of Pgm6/7, which are major outer membrane proteins of *P. gingivalis*. Pgm6/7 were predicted to be OmpA homologs. We construct-

Table 3. MICs of various antibiotics to *P. gingivalis* wild type strains and mutants

	MIC (μg/ml)[a]										
	Chloram-phenicol	Penicil-lin G	Ampi-cillin	Carbe-nicillin	Cepha-lexin	Cefo-xitin	Ceftri-axone	Cefota-xime	Tetra-cycline	Mino-cycline	Genta-micin
ATCC 33277	3.0	0.038	0.125	0.50	2.0	1.0	0.250	0.125	0.125	0.031	> 512
W83	3.0	0.038	0.063	0.125	1.0	0.50	0.031	0.031	0.125	0.031	256
*⊿*695	39.0	0.075	0.063	0.250	2.0	0.50	0.125	0.063	0.250	0.031	> 512
*⊿*694	39.0	0.038	0.125	0.125	2.0	0.50	0.125	0.063	0.250	0.063	> 512
⊿695-694	33.0	0.038	0.125	0.250	1.0	0.50	0.125	0.063	0.125	0.063	> 512

[a]The MICs of cefuroxime, erythromycin, and norfloxacin were 0.5, 0.5, and 4 μg/ml, respectively, for all the strains tested.

ed three disruption mutants, *⊿695*, *⊿694*, and *⊿695-694*, in which *orfs* encoding Pgm6, Pgm7, and both, respectively, were deleted and replaced with *cat* (Fig. 1). The amount of Pgm6 protein produced by *⊿694* seemed to be greater than the amount of Pgm7 protein produced by *⊿695*, based on the intensity of the immunoreactive 40 kDa band (Fig. 2B). However, an exact comparison of Pgm6 and Pgm7 production in the single mutants is difficult because the anti-Pgm6/7 antibody may have a different affinity for each protein. It is possible that the insertion of *cat* between the promoter and the *pg0694* in *⊿695* reduced the expression of the downstream *pg0694*. However, the defects seen in the mutants were probably not due to a polar effect on a downstream gene(s) because a mutant having *ermF-ermAM* inserted into a gene downstream of *pg0694* (*abfD*) (40) did not have any apparent effect on the Pgm6/7 production or on growth (data not shown).

The proposed heterotrimers (120 kDa protein) and homotrimers (115 and 130 kDa proteins) were analyzed by MS and N-terminal amino acid sequencing of peptides derived from digested proteins. All results indicated that the 120 kDa protein was composed of Pgm6 (41 kDa) and Pgm7 (40 kDa), and the 115 and 130 kDa proteins were of Pgm7 and Pgm6, respectively. No other protein was detected in these analyses. The heterotrimer band (120 kDa) was estimated to contain equal amounts of Pgm6 and Pgm7, based on detection of amino acid residues at nearly the same concentration from two peptides, during the N-terminal amino acid sequencing in a previous report (5). This result suggested that there was no observable preference for the formation of either 2:1 or 1:2 heterotrimers of Pgm6:Pgm7 since such a preference would skew the relative abundance of the two proteins in the sample. This has to be examined further because a mechanism producing such random assortment of heterotrimers is interesting, as discussed below.

It has been claimed that Omp40/41 in strain W50, which correspond to Pgm6/7, form heterodimers, based on observation of 34 to 35 kDa (monomer) and 70 kDa (dimer) bands (36, 41). Although we detected a minor 90 kDa protein in Western blots of single dimensional (see the right panel in Fig. 2B) and 2-D gels (Fig. 3B), we observed no 35 kDa or 70 kDa bands. However, it may be pertinent to emphasize that we found unusual resistance against dissociation of outer membrane proteins in the sample buffer for SDS-PAGE and encountered difficulties in control of their degradation by an intrinsic strong proteolytic activity in *P. gingivalis* (5). These unique properties intrinsic to this organism may be clues to overcome the differences between the two groups in the future.

In this work, Western blots of an SDS-solubilized and boiled 120 kDa protein complex that dissociated upon treatment with reducing agents revealed that the Pgm6/7 heterotrimer was stabilized by SS-bonds. A prior report also implicated SS-bond formation in the creation of the Omp40/41 (70 kDa) heterodimer (36).

Indeed, Pgm6/7 both have a conserved sequence, RPVSCPECPE, with two closely arranged cysteine residues in the C-terminal region. No other cysteine residue exists in mature Pgm6/7 proteins. However, they could form a stable intramolecular SS-bond as in LamB in *E. coli*, where Cys^{22} and Cys^{38} form an SS-bond that contributes to trimer stability (23). Dissociation of the LamB trimer was shown to be reversible by low pH in the absence of the reducing agent, but we found that Pgm6/7 did not dissociate into dimers or monomers under these conditions. Thus it seems that the Cys residues of Pgm6/7 form two intermolecular SS-bonds that covalently link monomers into heterotrimers, although intermediate heterodimers may partially exist. Given the close proximity of the two Cys residues within each monomer, it was unusual to find that an outer membrane protein formed a covalent trimer via disulfide linkages in the soluble periplasmic domain. Furthermore, due to the addition of DTT to the medium, the periplasm was predicted to have a reducing potential that would disrupt oxidized SS-bonds. Therefore, a mechanism must exist in *P. gingivalis* to facilitate intermolecular SS-bond formation in reducing conditions. Such an oxidation mechanism in the periplasmic space has also been proposed in another anaerobe, *Fibrobacter succinogenes* (42). As described in "Results" and below, because physiological phenotypes of the single mutants losing either protein were almost the same as those of the null mutant, the heterotrimer is likely to be a more stable and functional form than the homotrimer (or homooligomers) in the outer membrane for an unknown reason. We tentatively think that the formation of a heterodimer, an intermediate, would occur via two intermolecular SS-bonds as the first step and then either the subunit of Pgm6 or Pgm7 would associate to the dimer with an equal chance and finally form a heterotrimer by three intermolecular SS-bonds through partial reduction of the SS-bond and reoxidation among three molecules as the second step. If heterodimers formed as intermediates are assumed to be a transiently stable state in the whole heterotrimer population, some heterodimers would be preferentially detected under certain experimental conditions as reported previously (36). More work is needed to explore the possible mechanism of the heterotrimer formation, what components are involved in this mechanism, and where it occurs.

Growth and permeability experiments using intact cells suggested that the three mutants had a somewhat defective, weak, and leaky outer membrane open to limited substances with small molecular weights due to a considerable reduction of or the complete loss of Pgm6/7 as an anchor to the peptidoglycan layer. A rich medium such as sTSB did not affect the growth of the mutants, but the synthetic CDM medium (with 3% BSA), which apparently supports good growth of wild type this organism, dramatically affected growth of the mutants (Fig. 5), suggesting that an intact outer membrane is essential for growth under certain nutritional conditions. BSA is essential for the growth in CDM, and the mutants as well as the wild type appeared to equally digest BSA (data not shown). When NaCl was added to CDM at moderate concentrations (0.15 or 0.2 M), growth of the mutants was severely inhibited. In *P. aeruginosa*, an OmpA homolog, OprF, functions as a major porin (27, 39, 43) and also plays an important role in maintaining the structural integrity of the outer membrane (44-46). Evidence of this structural role is that *P. aeruginosa* OprF-deficient mutants were unable to grow or grew very slowly in low-osmolality media. In contrast, the *P. gingivalis* mutants were unable to grow in the presence of 0.2 M NaCl. These results may indicate that Pgm6/7 play an important role in the ability of *P. gingivalis* to survive in inflamed periodontal pockets, an oral environment with high osmotic pressure (47). Preliminary analysis by 2-D gel electrophoresis showed that more protein spots with strong intensity were observed in the rich medium, sTSB, than in the poor medium, CDM, suggesting that there was a global regulation mechanism depending on a shift from rich to poor nutritional circumstances. In CDM, the loss of Pgm6/7 as anchors between the outer membrane and the peptidogycan layer may be critical in *P. gingivalis*, and they could not produce essential components working together with Pgm6/7 for growth against a highly osmotic condition.

The three Pgm6/7 mutants had a strong tendency to autoagglutinate and to settle to the bottom of culture tubes, suggesting an alteration of their cell surfaces. Permeability of the outer membrane in the mutants

changed, and they became more permeable to *p*-nitrophenylphosphate (M_r, 217) and thymolphthalein monophosphate (M_r, 509), showing loss of crypticity, but did not allow alkaline phosphatase to leak-out, although the double mutant leaked a small amount of enzyme into the supernatant (Fig. 6). However, MICs of various antibiotics that have to pass through the outer membrane did not change even for the double mutant. As an exception, MICs of Cm were 33 to 39 μg/ml for the mutants and 3 μg/ml for the wild type and W83 strains (Table 3). The increases of Cm resistance were probably due to the higher CAT enzyme activity (data not shown), and not to decreases in Cm-penetration through their outer membranes. These observations as to unchanged MICs and loss of crypticity seem paradoxical. However, this is not so unusual because increases or decreases in outer membrane permeability do not necessarily produce large changes in MICs if agents are not efficiently inactivated or pumped out (48). As shown in Table 3, various antibiotics showed very low MICs to *P. gingivalis* wild types that have been considered to be intrinsically susceptible to most antibiotics, including β-lactams, partially due to the absence of β-lactamase (15, 49). The antibiotics tested may pass through the outer membrane efficiently enough to reach targets in this rather slow growing organism, and limited increases in outer membrane permeability seen for alkaline phosphatase activity may not affect MICs, even based on the assumption that no change occurs in the efflux and inactivation systems.

Most of the proteins found in the outer membrane appear to be channel-forming proteins, and they are classified as porins, specific channels, and high affinity receptors (10). *P. gingivalis* major outer membrane proteins have been designated Pgm1 through Pgm7 (5) and, of these, Pgm1 (RagA), Pgm4 (RagB), and Pgm6/7 are inferred to be channel-forming proteins without specific evidence. RagA and RagB appear to be expressed together and have been assumed to function as a specific channel (50) because RagA is a homolog of the TonB-linked receptors. Since this organism does not seem to have "classical porins", OmpF and OmpC homologs in the chromosome (6, 20), Pgm6/7 have been strongly inferred to be candidates for major porin in this organism because of their abundance in the outer membrane and the OmpA homology (5). OmpA type porins are called "monomeric or slow porins" without strong evidence for a stable oligomeric structure like OprF (5, 22). In swelling experiments using proteoliposomes containing bacterial envelopes, no obvious difference of permeability of the liposomes was detected between the wild type and Pgm6/7 mutants. However, preliminary findings that a protein(s) other than Pgm6/7 may play a major role in pore-forming activities were obtained using a transposon-insertion mutant of *P. gingivalis* unrelated to the mutants created here.

In conclusion, Pgm6/7 seem to form heterotrimers as a stable structure to function mainly as stabilizers of the outer membrane, presumably by anchoring to the peptidoglycan layer through the C-terminal domain, and are unlikely to function as a major porin.

Acknowledgments

This has been modified for this report the paper published in Journal of Bacteriology (Vol. 187, No. 4 2005, p. 902-911) with permission of the publisher. I thank Keiji Nagano, Erik K. Read, Yukitaka Murakami, Takashi Masuda, and Toshihide Noguchi for their great contribution. This study was also supported by Grants-in-Aid for Scientific Research (16791149 to K. N., 15591957 to F. Y. and 15591958 to Y. M.) from the Japan Society for the Promotion of Science (JSPS) and the AGU High-Tech Research Center Project from The Ministry of Education, Culture, Sports, Science and Technology, Japan. E. K. R. was supported by a JSPS postdoctoral fellowship for US researchers (short-term, ID No.: PU02209). The author especially thanks Dr. H. Nikaido for valuable suggestions.

References

(1) Lamont, R. J., and H. F. Jenkinson. 1998. Life below the gum line: pathogenic mechanisms of *Porphyromonas gingivalis*. Microbiol. Mol. Biol. Rev. **62**:1244−1263.

(2) Lamont, R. J., and H. F. Jenkinson. 2000. Subgingival colonization by *Porphyromonas gingivalis*. Oral Microbiol. Immunol. **15**:341−349.

(3) Laine, M. L., and A. J. van Winkelhoff. 1998. Virulence of six capsular serotypes of *Porphyromonas gingivalis* in a mouse model. Oral Microbiol. Immunol. **13**:322−325.
(4) van Winkelhoff, A. J., B. J. Appelmelk, N. Kippuw, and J. de Graaff. 1993. K-antigens in *Porphyromonas gingivalis* are associated with virulence. Oral Microbiol. Immunol. **8**:259−265.
(5) Murakami, Y., M. Imai, H. Nakamura, and F. Yoshimura. 2002. Separation of the outer membrane and identification of major outer membrane proteins from *Porphyromonas gingivalis*. Eur. J. Oral Sci. **110**:157−162.
(6) Nelson, K. E., R. D. Fleischmann, R. T. DeBoy, I. T. Paulsen, D. E. Fouts, J. A. Eisen, S. C. Daugherty, R. J. Dodson, A. S. Durkin, M. Gwinn, D. H. Haft, J. F. Kolonay, W. C. Nelson, T. Mason, L. Tallon, J. Gray, D. Granger, H. Tettelin, H. Dong, J. L. Galvin, M. J. Duncan, F. E. Dewhirst, and C. M. Fraser. 2003. Complete genome sequence of the oral pathogenic bacterium *Porphyromonas gingivalis* strain W83. J. Bacteriol. **185**:5591−5601.
(7) Ross, B. C., L. Czajkowski, D. Hocking, M. Margetts, E. Webb, L. Rothel, M. Patterson, C. Agius, S. Camuglia, E. Reynolds, T. Littlejohn, B. Gaeta, A. Ng, E. S. Kuczek, J. S. Mattick, D. Gearing, and I. G. Barr. 2001. Identification of vaccine candidate antigens from a genomic analysis of *Porphyromonas gingivalis*. Vaccine **19**:4135−4142.
(8) De Mot, R., and J. Vanderleyden. 1994. The C-terminal sequence conservation between OmpA-related outer membrane proteins and MotB suggests a common function in both gram-positive and gram-negative bacteria, possibly in the interaction of these domains with peptidoglycan. Mol. Microbiol. **12**:333−334.
(9) Sugawara, E., and H. Nikaido. 1992. Pore-forming activity of OmpA protein of *Escherichia coli*. J. Biol. Chem. **267**:2507−2511.
(10) Nikaido, H. 1994. Porins and specific diffusion channels in bacterial outer membranes. J. Biol. Chem. **269**:3905−3908.
(11) Koebnik, R., K. P. Locher, and P. Van Gelder. 2000. Structure and function of bacterial outer membrane proteins: barrels in a nutshell. Mol. Microbiol. **37**:239−253.
(12) Milner, P., J. E. Batten, and M. A. Curtis. 1996. Development of a simple chemically defined medium for *Porphyromonas gingivalis*: requirement for α-ketoglutarate. FEMS Microbiol. Lett. **140**:125−130.
(13) Ueda, O., and F. Yoshimura. 2003. Transposon-induced norfloxacin-sensitive mutants of *Bacteroides thetaiotaomicron*. Microbiol. Immunol. **47**:17−25.
(14) Horton, R. M., S. N. Ho, J. K. Pullen, H. D. Hunt, Z. Cai, and L. R. Pease. 1993. Gene splicing by overlap extension. Methods Enzymol. **217**:270−279.
(15) Ikeda, T., and F. Yoshimura. 2002. A resistance-nodulation-cell division family xenobiotic efflux pump in an obligate anaerobe, *Porphyromonas gingivalis*. Antimicrob. Agents Chemother. **46**:3257−3260.
(16) Fletcher, H. M., H. A. Schenkein, R. M. Morgan, K. A. Bailey, C. R. Berry, and F. L. Macrina. 1995. Virulence of a *Porphyromonas gingivalis* W83 mutant defective in the *prtH* gene. Infect. Immun. **63**:1521−1528.
(17) Bradford, M. M. 1976. A rapid and sensitive method for the quantitation of microgram quantities of protein utilizing the principle of protein-dye binding. Anal. Biochem. **72**:248−254.
(18) Lugtenberg, B., J. Meijers, R. Peters, P. van der Hoek, and L. van Alphen. 1975. Electrophoretic resolution of the "major outer membrane protein" of *Escherichia coli* K12 into four bands. FEBS Lett. **58**:254−258.
(19) Kennell, W., and S. C. Holt. 1990. Comparative studies of the outer membranes of *Bacteroides gingivalis*, strains ATCC 33277, W50, W83, 381. Oral Microbiol. Immunol. **5**:121−130.
(20) Hongo, H., E. Osano, M. Ozeki, T. Onoe, K. Watanabe, O. Honda, H. Tani, H. Nakamura, and F. Yoshimura. 1999. Characterization of an outer membrane protein gene, *pgmA*, and its gene product from *Porphyromonas gingivalis*. Microbiol. Immunol. **43**:937−946.
(21) Nishikawa, K., and F. Yoshimura. 2001. The re-

sponse regulator FimR is essential for fimbrial production of the oral anaerobe *Porphyromonas gingivalis*. Anaerobe **7**:255−262.
(22) Nikaido, H. 2003. Molecular basis of bacterial outer membrane permeability revisited. Microbiol. Mol. Biol. Rev. **67**:593−656.
(23) Luckey, M., R. Ling, A. Dose, and B. Malloy. 1991. Role of a disulfide bond in the thermal stability of the LamB protein trimer in *Escherichia coli* outer membrane. J. Biol. Chem. **266**:1866−1871.
(24) Fountoulakis, M., and H. Langen. 1997. Identification of proteins by matrix-assisted laser desorption ionization-mass spectrometry following in-gel digestion in low-salt, nonvolatile buffer and simplified peptide recovery. Anal. Biochem. **250**:153−156.
(25) Yoshimura, F., and H. Nikaido. 1982. Permeability of *Pseudomonas aeruginosa* outer membrane to hydrophilic solutes. J. Bacteriol. **152**:636−642.
(26) Yamashita, Y., K. Toyoshima, M. Yamazaki, N. Hanada, and T. Takehara. 1990. Purification and characterization of alkaline phosphatase of *Bacteroides gingivalis* 381. Infect. Immun. **58**:2882−2887.
(27) Nikaido, H., K. Nikaido, and S. Harayama. 1991. Identification and characterization of porins in *Pseudomonas aeruginosa*. J. Biol. Chem. **266**:770−779.
(28) Shi, Y., D. B. Ratnayake, K. Okamoto, N. Abe, K. Yamamoto, and K. Nakayama. 1999. Genetic analyses of proteolysis, hemoglobin binding, and hemagglutination of *Porphyromonas gingivalis*. Construction of mutants with a combination of *rgpA*, *rgpB*, *kgp*, and *hagA*. J. Biol. Chem. **274**:17955−17960.
(29) Hruby, D. E., and E. M. Wilson. 1992. Use of fluorescent chloramphenicol derivative as a substrate for chloramphenicol acetyltransferase assays. Methods Enzymol. **216**:369−376.
(30) National Committee for Clinical Laboratory Standards. 1997. Methods for antimicrobial susceptibility testing of anaerobic bacteria, 5th ed, vol. 21. Approved standard M11-A5. National Committee for Clinical Laboratory Standards, Wayne, PA.
(31) Altschul, S. F., T. L. Madden, A. A. Schaffer, J. Zhang, Z. Zhang, W. Miller, and D. J. Lipman. 1997. Gapped BLAST and PSI-BLAST: a new generation of protein database search programs. Nucleic Acids Res **25**:3389−3402.
(32) Kelley, L. A., R. M. MacCallum, and M. J. Sternberg. 2000. Enhanced genome annotation using structural profiles in the program 3D-PSSM. J. Mol. Biol. **299**:499−520.
(33) Bigelow, H. R., D. S. Petrey, J. Liu, D. Przybylski, and B. Rost. 2004. Predicting transmembrane beta-barrels in proteomes. Nucleic Acids Res. **32**:2566−2577.
(34) Jeanteur, D., J. H. Lakey, and F. Pattus. 1991. The bacterial porin superfamily: sequence alignment and structure prediction. Mol. Microbiol. **5**:2153-2164.
(35) Wimley, W. C. 2002. Toward genomic identification of β-barrel membrane proteins: Composition and architecture of known structures. Protein Sci. **11**:301−312.
(36) Veith, P. D., G. H. Talbo, N. Slakeski, and E. C. Reynolds. 2001. Identification of a novel heterodimeric outer membrane protein of *Porphyromonas gingivalis* by two-dimensional gel electrophoresis and peptide mass fingerprinting. Eur. J. Biochem. **268**:4748−4757.
(37) Cascales, E., A. Bernadac, M. Gavioli, J. C. Lazzaroni, and R. Lloubes. 2002. Pal lipoprotein of *Escherichia coli* plays a major role in outer membrane integrity. J. Bacteriol. **184**:754−759.
(38) Murakami, Y., N. Higuchi, H. Nakamura, F. Yoshimura, and F. G. Oppenheim. 2002. *Bacteroides forsythus* hemagglutinin is inhibited by N-acetylneuraminyllactose. Oral Microbiol. Immunol. **17**:125−128.
(39) Yoshimura, F., L. S. Zalman, and H. Nikaido. 1983. Purification and properties of *Pseudomonas aeruginosa* porin. J. Biol. Chem. **258**:2308−2314.
(40) Diaz, P. I., P. S. Zilm, V. Wasinger, G. L. Corthals, and A. H. Rogers. 2004. Studies on NADH oxidase and alkyl hydroperoxide reductase produced by *Porphyromonas gingivalis*. Oral. Microbiol.

Immunol. **19**:137−143.
(41) Ross, B. C., L. Czajkowski, K. L. Vandenberg, S. Camuglia, J. Woods, C. Agius, R. Paolini, E. Reynolds, and I. G. Barr. 2004. Characterization of two outer membrane protein antigens of *Porphyromonas gingivalis* that are protective in a murine lesion model. Oral Microbiol. Immunol. **19**:6−15.
(42) MacLellan, S. R., and C. W. Forsberg. 2001. Properties of the major non-specific endonuclease from the strict anaerobe *Fibrobacter succinogenes* and evidence for disulfide bond formation *in vivo*. Microbiology **147**:315−323.
(43) Hancock, R. E., and F. S. Brinkman. 2002. Function of *Pseudomonas* porins in uptake and efflux. Annu. Rev. Microbiol. **56**:17−38.
(44) Gotoh, N., H. Wakebe, E. Yoshihara, T. Nakae, and T. Nishino. 1989. Role of protein F in maintaining structural integrity of the *Pseudomonas aeruginosa* outer membrane. J. Bacteriol. **171**:983−990.
(45) Rawling, E. G., F. S. Brinkman, and R. E. Hancock. 1998. Roles of the carboxy-terminal half of *Pseudomonas aeruginosa* major outer membrane protein OprF in cell shape, growth in low-osmolarity medium, and peptidoglycan association. J. Bacteriol. **180**:3556−3562.
(46) Woodruff, W. A., and R. E. Hancock. 1989. *Pseudomonas aeruginosa* outer membrane protein F: structural role and relationship to the *Escherichia coli* OmpA protein. J. Bacteriol. **171**:3304−3309.
(47) Griffiths, G. S. 2003. Formation, collection and significance of gingival crevice fluid. Periodontol. 2000 **31**:32−42.
(48) Nikaido, H. 1989. Outer membrane barrier as a mechanism of antimicrobial resistance. Antimicrob. Agents Chemother. **33**:1831−1836.
(49) Pajukanta, R., S. Asikainen, B. Forsblom, M. Saarela, and H. Jousimies-Somer. 1993. beta-Lactamase production and in vitro antimicrobial susceptibility of *Porphyromonas gingivalis*. FEMS Immunol. Med. Microbiol. **6**:241−244.
(50) Bonass, W. A., P. D. Marsh, R. S. Percival, J. Aduse-Opoku, S. A. Hanley, D. A. Devine, and M. A. Curtis. 2000. Identification of *ragAB* as a temperature-regulated operon of *Porphyromonas gingivalis* W50 using differential display of randomly primed RNA. Infect. Immun. **68**:4012−4017.

Mechanism of Generation of NK1.1$^-$ Vα14$^+$ NKT Cells in the Liver of *Listeria monocytogenes* Infected Mice and Possible Role of These Cells in Protection from the Infection

Masashi Emoto

Laboratory of Immunology, Department of Laboratory Sciences, Gunma University School of Health Sciences, Maebashi, Gunma 371-8511, Japan

Introduction

Natural killer (NK)T cells represent a unique T cell population which shares characteristic features with NK cells. Notably, both cell types surface-express the type II C-type lectin, NKR-P1B and C (NK1.1) (1). In the mouse, the majority of NKT cells express an invariant T cell receptor (TCR)α chain encoded by Vα14 gene segments paired with Jα281 and a TCRVβ highly skewed towards Vβ8.2, 7 and 2 (1). The development of Vα14$^+$ NKT cells depends on CD1d, which is surface expressed together with β2-microglobulin (β2m) (1-4). Although the natural ligand for this T cell population remains enigmatic, α-galactosylceramide (α-GalCer) derived from a marine sponge is recognized by these Vα14$^+$ NKT cells in the context of CD1d (5). The Vα14$^+$ NKT cells are abundant in the liver, and the majority express CD4 and the minority express neither CD4 nor CD8 (6). Liver Vα14$^+$ NKT cells rapidly secrete large amounts of both interferon (IFN)-γ and interleukin (IL)-4 upon activation through their TCR (6-9).

Listeria monocytogenes is a facultative intracellular bacterium, which preferentially replicates in macrophages and liver parenchymal cells (10). Type 1 cytokines, notably IL-12 and IFN-γ, play a pivotal role in protection against *L. monocytogenes* infection (10), whereas type 2 cytokines such as IL-4 exacerbate listeriosis (11-14). After systemic infection, the vast majority of *L. monocytogenes* organisms are rapidly trapped in the liver (15). Hence, immunocompetent cells which reside in the liver are critical for control of infection (10,16). Although sterile eradication of this pathogen is ultimately achieved by conventional T cells (10), innate immunity performed by granulocytes in concert with monocytes and macrophages controls replication of this bacterium before conventional T cells enter this stage (10-16). In addition, IFN-γ-secreting NK1$^+$ cells seem to participate in protection against *L. monocytogenes* infection (10,17-20).

We have previously shown that cells stained with mAbs against CD4 and NK1 (CD4$^+$ NKT cells) disappear in the liver of mice following *L. monocytogenes* infection (8, 21). Disappearance of NKT cells soon after infection could be taken as an argument against contribution of this population to antibacterial defense. Since down-modulation of the NK1 marker on NKT cells upon activation has been suggested (22, 23), NKT cells could outwardly become undetectable due to down-modulation of NK1.

In the present study, we analyzed NK1 expression on Vα14$^+$ NKT cells in the liver of mice following *L. monocytogenes* infection using α-GalCer/CD1d tetramers. We found that during listeriosis, the α-GalCer/CD1d tetramer-reactive T cells lacking NK1 derived from an NK1$^+$ subpopulation and increased independently of the presence of a thymus and that they could secrete IFN-γ, but not IL-4. Since listeriosis in mice deficient in Vα14$^+$ NKT cells was ameliorated, our

findings suggest that the $NK1^+$ subsets which produce IL-4 in addition to IFN-γ are of detriment to the host, whereas the $NK1^-$ subsets which exclusively produce IFN-γ may contribute to antibacterial protection.

Materials and Methods

Mice.

Female adult thymectomized (ATX) (8 wks after birth) C57BL/6 mice were purchased from the Jackson Laboratory. Breeding pairs of $J\alpha281^{-/-}$ (5) and C57BL/6 $V\beta^a$ ($V\beta^a$) mice were kindly provided by Drs. M. Taniguchi and A. M. Livingstone, respectively. These mutants backcrossed onto C57BL/6 ($J\alpha281^{-/-}$ and $J\alpha281^{+/-}$, 8th generation; $V\beta^a$, 18th generation), and C57BL/6 mice were maintained under specific pathogen-free conditions, and weight-matched female mice were used at 8 to 12 weeks of age.

Antibodies.

Monoclonal antibodies (mAbs) against TCRα/β (H57-597), CD3ε (145-2C11), NK1.1 (PK136), CD4 (YTS.191.1), Fcγreceptor (R) (2.4G2), IL-12 (p40/p70) (C17.8), IL-4 (11B11, BVD6-24G2), and IFN-γ (R4-6A2, XMG1.2) were purified from hybridoma culture supernatants. MAbs against IFN-γ (XMG1.2) and IL-4 (BVD6-24G2) were biotinylated, and mAbs against TCRα/β and CD3 were conjugated with fluorescein isothiocyanate (FITC) by conventional methods. FITC-conjugated mAbs against CD11a (M17/4), CD54 (H9.2B8), CD25 (7D4), CD122 (TM-β1), CD49d (R1-2), CD69 (H1.2F3), CD4 (H129.19), NK1.1 (PK136) and mouse IgG2a (R19-15), and biotinylated mAbs against NK1.1 (PK136) and mouse IgG2a (R19-15) were purchased from BD PharMingen. Rabbit anti-asialo GM1 (ASGM1) Ab and rabbit IgG were obtained from Wako Chemicals and Sigma-Aldrich, respectively.

Bacteria and infection.

L. monocytogenes (strain EGD) recovered from infected liver were grown in tryptic soy broth (Difco Laboratories) at 37 °C for 18 h and aliquots were frozen at −80 °C until used. The final concentration of viable bacteria was enumerated by plate counts on tryptic soy agar (Difco). Mice were infected i.v. with 2×10^3 *L. monocytogenes*.

In vivo treatment.

Mice were treated i.p. with recombinant (r)IL-12 (1 μg) (Genzyme). To deplete $NK1^+$ cells, mice were treated i.p. with anti-NK1.1 mAb (300 μg) 4 and 2 days before infection. For depletion of NK cells, mice were treated i.p. with anti-ASGM1 Ab (5 mg) 3 days before infection. To deplete $CD4^+$ cells, mice were treated i.p. with anti-CD4 mAb (300 μg) 4 and 2 days before infection. Depletion of $NK1^+$ cells (> 95 %), NK cells (> 95 %) and $CD4^+$ cells (> 98 %) was verified by immunohistochemistry and/or flow cytometry. For endogenous IL-12 neutralization, mice were treated i.p. with anti-IL-12 mAb (500 μg) 2 h before infection. Isotype-matched mAbs with other specificity but purified by the same procedure as for specific mAbs or PBS used for mAb purification were used as control. Rabbit IgG was used as control for anti-ASGM1 Ab.

Mouse CD1d/β2m tetramer.

Mouse CD1d/β2m tetramers were prepared by baculovirus expression system using a CD1d-construct with a BirA biotinylation site followed by a His-6 tag as described previously (24). In brief, Sf9 insect cell line (BD Biosciences) was infected with mouse CD1d/β2m-expressing virus stock kindly provided by Dr. M. Kronenberg (24) at a multiplicity of infection of 0.1 for expanding the viral stock. Culture supernatants were harvested on day 4 post infection (pi) and used for infection at high multiplicity of infection of 1 to 5. These large-scale cultures were performed in Sf-900 II serum-free medium (Gibco Invitrogen Corp.) and harvested on day 3 or 4 by centrifugation. Supernatants were concentrated by passing through a hollow fiber tangential flow module (MiniKros 1100 cm^2, Spectrum, MembraPure). The CD1d molecules were purified by metal chelating chromatography (Chelating

sepharose Fast flow, Amersham Pharmacia Biotech) on an NTA-sepharose column (Amersham Pharmacia Biotech) charged with cobalt chloride (Roth). Protein was eluted with 200 mM imidazol (Merck) and pooled fractions were concentrated to 0.5 ml by ultrafiltration (Ultrafree Units, Millipore). Purity and protein amount were assessed by SDS-PAGE and Bradford reagent (BioRad), respectively. Purified CD1d protein was subsequently biotinylated with BirA enzyme (Avidity) according to the manufacturer's instructions. Biotinylated CD1d proteins were purified by gel-filtration (Superdex 200 HR10/30, Amersham Pharmacia Biotek). Soluble biotinylated CD1d/β2m protein was loaded with or without α-GalCer (kindly provided by KIRIN BREWERY Co. Ltd.) which was dissolved in PBS containing 0.5 % Tween 20 at 220 μg/ml, at a molar ratio of 1:3 (protein:lipid) overnight at room temperature. For tetramerization, streptavidin (SA)-conjugated PE (MobiTec) was added to α-GalCer/CD1d/β2m monomers at a 1:4 (monomer : SA-conjugated PE) molar ratio. The purification of phycoerythrine (PE)-labeled CD1d/β2m tetramers loaded with or without α-GalCer was performed by gel-filtration (Superdex 200 HR10/30, Amersham Pharmacia Biotek).

Cell preparation and flow cytometry.

Mice were killed by cervical dislocation and organs were collected. Hepatic leukocytes (HL) were prepared as described previously (7). Bone marrow (BM) plugs in the femura were collected by flushing with RPMI 1640 containing 10 % fetal calf serum (FCS) and T cells were enriched by passing through a nylon wool column. Splenocytes were prepared by conventional methods. For staining with mAbs, cells were incubated with anti-FcγR mAb and then stained with conjugated mAbs at 4 °C for 15 min. Biotinylated mAbs were visualized by SA-conjugated CyChrome (BD PharMingen). Stained cells were washed with PBS containing 0.1 % bovine serum albumin (BSA) (Serva) and 0.1 % sodium azide (Merck), fixed with 1 % paraformaldehyde (Merck), applied on FACScan® (BD Biosciences), and the lymphoid cells were analyzed with CellQuest software. For staining with α-GalCer/CD1d tetramer, cells were stained with PE-labeled α-GalCer/CD1d tetramer for 15 min at room temperature after blocking.

Cell sorting.

α-GalCer/CD1d tetramer-reactive cells were positively sorted by MACS (Miltenyi Biotec) following the manufacturer's instruction. In brief, HL were stained with PE-labeled α-GalCer/CD1d tetramer for 15 min at room temperature after blocking and subsequently incubated with anti-PE microbeads (Miltenyi Biotec) for 15 min at 6 °C. Cell suspensions were applied to a MS+/RS+ column (Miltenyi Biotec) and then α-GalCer/CD1d tetramer-reactive cells were enriched by flushing out. Purity of α-GalCer/CD1d tetramer-reactive cells was always > 95 %.

Enzyme-linked immunospot assay.

IFN-γ and IL-4 production was measured by the Enzyme-linked immunospot (ELISPOT) method as described previously (7,8) with a slight modification. Briefly, cells were cultured for 18 h in the presence or absence of phorbol myristate acetate (PMA) (10 ng/ml) and ionomycine (1 μg/ml) in ELISPOT plates (Millipore) precoated with anti-IFN-γ mAb (R4-6A2) or anti-IL-4 mAb (11B11). After washing, plates were incubated with biotinylated anti-IFN-γ mAb (XMG1.2) or biotinylated anti-IL-4 mAb (BVD6-24G2), respectively. For developing spots, SA-conjugated alkaline phosphatase (Dianova) and 5-bromo-4-chloro-3-indolyl phosphate/nitro blue tetrazolium tablets (Sigma-Aldrich) were used. Numbers of cytokine-secreting cells were estimated by counting spots using a dissecting microscope.

Statistical analysis.

The statistical significance was determined by Student's *t*-test. A p value < 0.05 was regarded as significant.

Results

Differential kinetics of NK1$^+$ and NK1$^-$ α-GalCer/CD1d tetramer-reactive T cells in the liver following L. monocytogenes infection.

C57BL/6 mice were infected with *L. monocytogenes* and the kinetics of the fate of liver Vα14$^+$ T cells was followed using α-GalCer/CD1d tetramers. High proportions of α-GalCer/CD1d tetramer-reactive T cells as well as NK1$^+$ TCRα/β cells were detected in the liver before infection (Fig. 1A). Consistent with recent findings (25), the majority of α-GalCer/CD1d tetramer-reactive T cells coexpressed NK1, and a small population lacked this marker. α-GalCer/CD1d tetramer-reactive T cells were undetectable in Jα281$^{-/-}$ mice, verifying that Vα14$^+$ T cells are specifically detected by α-GalCer/CD1d tetramers (data not shown). The proportions of α-GalCer/CD1d tetramer-reactive T cells as well as NK1$^+$ TCRα/β cells were markedly reduced by day 2 pi and were still low on day 4 pi. At these days, only a minority of α-GalCer/CD1d tetramer-reactive T cells coexpressed the NK1 marker and the majority lacked it (Fig.1A).

Numbers of recovered HL gradually increased following infection (Fig. 1B). Absolute numbers of α-GalCer/CD1d tetramer-reactive NK1$^+$ T cells were

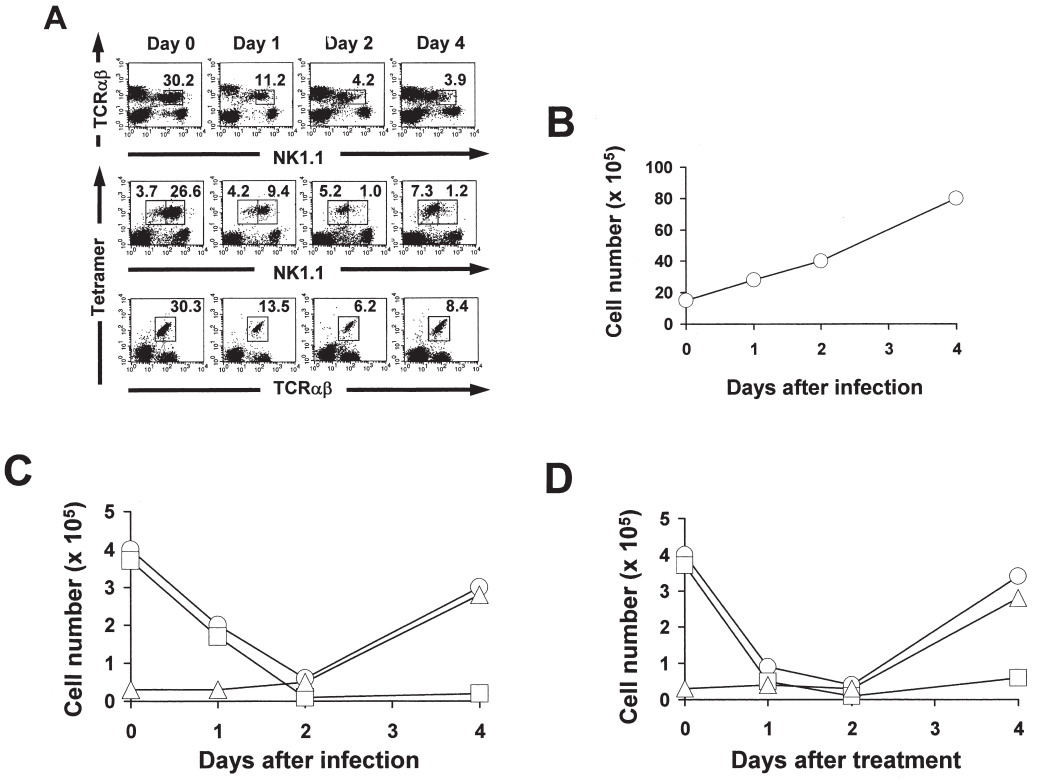

Fig. 1. Appearance of α-GalCer/CD1d tetramer-reactive T cells in the liver of C57BL/6 mice following *L. monocytogenes* infection or rIL-12 treatment. Mice were infected with *L. monocytogenes* (A, B, C) or treated with rIL-12 (D) on day 0, and HL were collected on the days indicated in the Figure. Cells were stained with FITC-conjugated anti-TCRα/β mAb, biotinylated anti-NK1.1 mAb and PE-labeled α-GalCer/CD1d tetramers, followed by SA-conjugated CyChrome. (A) Data are expressed as dot plots after gating on lymphoid cells. Numbers in the dot plots represent percentages of each cell population within the square. Representative staining patterns from 3 to 6 mice at each time point are shown. (B) Data represent numbers of recovered HL and are expressed as means of 3 to 6 mice at each time point. (C,D) Data represent absolute numbers of α-GalCer/CD1d tetramer-reactive NK1$^+$ T cells (□), α-GalCer/CD1d tetramer-reactive NK1$^-$ T cells (△) and total α-GalCer/CD1d tetramer-reactive T cells (○), and are expressed as means of 3 to 6 mice at each time point.

markedly diminished by day 2 pi, whereas those of α-GalCer/CD1d tetramer-reactive NK1$^-$ T cells increased subsequently and were dominant among α-GalCer/CD1d tetramer-reactive T cells on days 2 and 4 pi (Fig. 1C). Similar results were obtained in the mice treated with rIL-12 (Fig.1D). Note that no inverse relationship was found in kinetics of NK1$^+$ and NK1$^-$ α-GalCer/CD1d tetramer-reactive T cells following *L. monocytogenes* infection. Similar results were obtained in Vβ^a mice (data not shown). Thus, NK1$^+$ and NK1$^-$ α-GalCer/CD1d tetramer-reactive T cells showed different kinetics in response to *L. monocytogenes* infection.

Selective expansion of the α-GalCer/CD1d tetramer-reactive NK1$^-$ T cell population following L. monocytogenes infection is mediated by IL-12.

We have previously shown that IL-12 contributes to the reduction of the liver NKT cell population coexpressing CD4 following *L. monocytogenes* infection (21). To determine whether IL-12 is involved in the expansion of the α-GalCer/CD1d tetramer-reactive NK1$^-$ T cell population, the influence of rIL-12 on liver α-GalCer/CD1d tetramer-reactive T cells was examined. Consistent with recent findings (23), absolute numbers of α-GalCer/CD1d tetramer-reactive NK1$^+$ T cells were markedly diminished by day 2 after rIL-12 treatment, whereas those of α-GalCer/CD1d tetramer-reactive NK1$^-$ T cells were virtually unaffected at this time point and increased thereafter (Fig. 1D). Supporting this finding, reduction of the α-GalCer/CD1d tetramer-reactive NK1$^+$ T cell population and subsequent increase of the α-GalCer/CD1d tetramer-reactive NK1$^-$ T cell population following *L. monocytogenes* infection were completely abrogated by anti-IL-12 mAb treatment (data not shown). Similar results were obtained in Vβ^a mice (data not shown). Hence, IL-12 plays a critical role both in the reduction of the α-GalCer/CD1d tetramer-reactive NK1$^+$ T cell population and in the subsequent increase of the α-GalCer/CD1d tetramer-reactive NK1$^-$ T cell population.

α-GalCer/CD1d tetramer-reactive NK1$^-$ T cells are derived from NK1$^+$ subpopulation.

We raised the question whether the appearance of α-GalCer/CD1d tetramer-reactive NK1$^-$ T cells in the liver of *L. monocytogenes*-infected mice was due to down-modulation of the NK1 marker. We determined effect of NK1$^+$ cell-depletion on the fate of α-GalCer/CD1d tetramer-reactive NK1$^-$ T cells during *L. monocytogenes* infection. In addition to NK (CD3$^-$NK1$^+$) cells, total NKT (CD3$^+$NK1$^+$) cells as well as α-GalCer/CD1d tetramer-reactive NK1$^+$ T cells became virtually undetectable in the liver after anti-NK1.1 mAb treatment, whereas the proportion of α-GalCer/CD1d tetramer-reactive NK1$^-$ T cells increased (Fig. 2A). In accordance with the NK1$^+$ cell depletion, numbers of recovered HL were reduced (data not shown). Some cells which were slightly stained with anti-NK1.1 mAb still remained in the liver even after anti-NK1.1 mAb treatment. We consider it likely that this was caused by biotin-mediated nonspecific reaction, because (i) similar staining patterns were obtained when cells were stained with biotinylated anti-mouse IgG2a (secondary mAb for detection of anti-NK1.1 mAb) and (ii) NK1 staining was completely negative when FITC-conjugated mAbs against NK1.1 or mouse IgG2a were used (data not shown). Importantly, the increase of both, proportion and absolute number, of α-GalCer/CD1d tetramer-reactive NK1$^-$ T cells after *L. monocytogenes* infection was prevented by NK1$^+$ cell depletion (Figs. 2A and 2B). These results suggest that NK1$^+$ cells are essential for the emergence of α-GalCer/CD1d tetramer-reactive NK1$^-$ T cells in the liver following *L. monocytogenes* infection.

Because some T cells bearing CD8α and/or TCRγ/δ also express NK1 (26, 27), we examined whether these cells are involved in increase of α-GalCer/CD1d tetramer-reactive NK1$^-$ T cells. No measurable alterations were found in the numbers of α-GalCer/CD1d tetramer-reactive NK1$^-$ T cells in the liver of *L. monocytogenes*-infected mice by CD8α$^+$ or TCRγ/δ$^+$ cell depletion (data not shown). These results exclude that NK1$^+$ cells expressing CD8α and/or TCRγ/δ are involved in the increase of the α-GalCer/

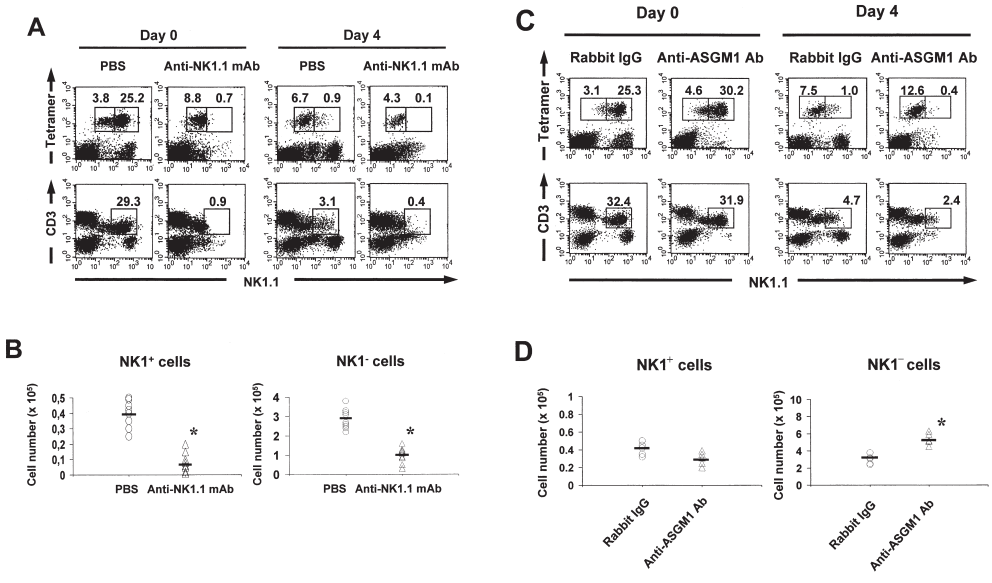

Fig. 2. Influence of anti-NK1.1 mAb or anti-ASGM1 Ab treatment on α-GalCer/CD1d tetramer-reactive T cells in the liver of C57BL/6 mice before and after *L. monocytogenes* infection. Mice were treated with anti-NK1.1 mAb or PBS on days −4 and −2 (A,B), or with anti-ASGM1 Ab or rabbit IgG on day −3 (C,D), infected with *L. monocytogenes* on day 0, and HL were prepared on days 0 (A,C) and/or 4 (A,B,C,D). Cells were stained with FITC-conjugated anti-CD3ε mAb, biotinylated anti-NK1.1 mAb and PE-labeled α-GalCer/CD1d tetramer, followed by SA-conjugated CyChrome. (A) Data are expressed as dot plots after gating on lymphoid cells. Numbers in dot plots represent percentages of each cell population within the square. Representative staining patterns from 8 mice in each group are shown. Because no significant difference was found between anti-human transferrin R mAb (isotype-matched mAb for anti-NK1.1 mAb)-treated and PBS-treated group in another experiment, PBS was used as a control. (B) Data represent absolute numbers of α-GalCer/CD1d tetramer-reactive NK1$^+$ and NK1$^-$ T cells. Each symbol represents an individual animal and bars represent means of 8 mice. *, $p < 0.01$, anti-NK1.1 mAb-treated group vs. PBS-treated group. (C) Data are expressed as dot plots after gating on lymphoid cells. Numbers in dot plots represent percentages of each cell population within the square. Representative staining patterns from 5 mice per group are shown. (D) Data represent absolute numbers of α-GalCer/CD1d tetramer-reactive NK1$^+$ and NK1$^-$ T cells. Each symbol represents an individual animal and bars represent means of 5 mice. *, $p < 0.01$, anti-ASGM1 Ab-treated group vs. rabbit IgG-treated group.

CD1d tetramer-reactive NK1$^-$ T cell population.

Because not only NKT cells, but also NK cells express NK1, we examined whether NK cells participate in the increase of α-GalCer/CD1d tetramer-reactive NK1$^-$ T cells. C57BL/6 mice were treated with anti-ASGM1 Ab, infected with *L. monocytogenes* and the appearance of α-GalCer/CD1d tetramer-reactive NK1$^-$ T cells was determined. Consistent with our previous findings (28, 29), NK cells became virtually undetectable in the liver after anti-ASGM1 Ab treatment, whereas α-GalCer/CD1d tetramer-reactive T cells were virtually unaffected (Fig. 2C). In accordance with the NK cell depletion, numbers of recovered HL were reduced (data not shown). In contrast to anti-NK1.1 mAb treatment, both proportion and absolute numbers of α-GalCer/CD1d tetramer-reactive NK1$^-$ T cells following *L. monocytogenes* infection were increased by anti-ASGM1 Ab treatment (Figs. 2C and 2D). These results indicate that NK cells prevent the emergence of α-GalCer/CD1d tetramer-reactive NK1$^-$ T cells in the

liver following *L. monocytogenes* infection. We conclude that the majority of α-GalCer/CD1d tetramer-reactive NK1$^-$ T cells which emerged in the liver following *L. monocytogenes* infection were derived from NK1$^+$ subpopulation.

α-GalCer/CD1d tetramer-reactive NK1$^+$ T cells in the thymus are unaffected by L. monocytogenes infection.

Mice were treated with PBS(control) or anti-NK1.1 mAb and numbers of α-GalCer/CD1d tetra-

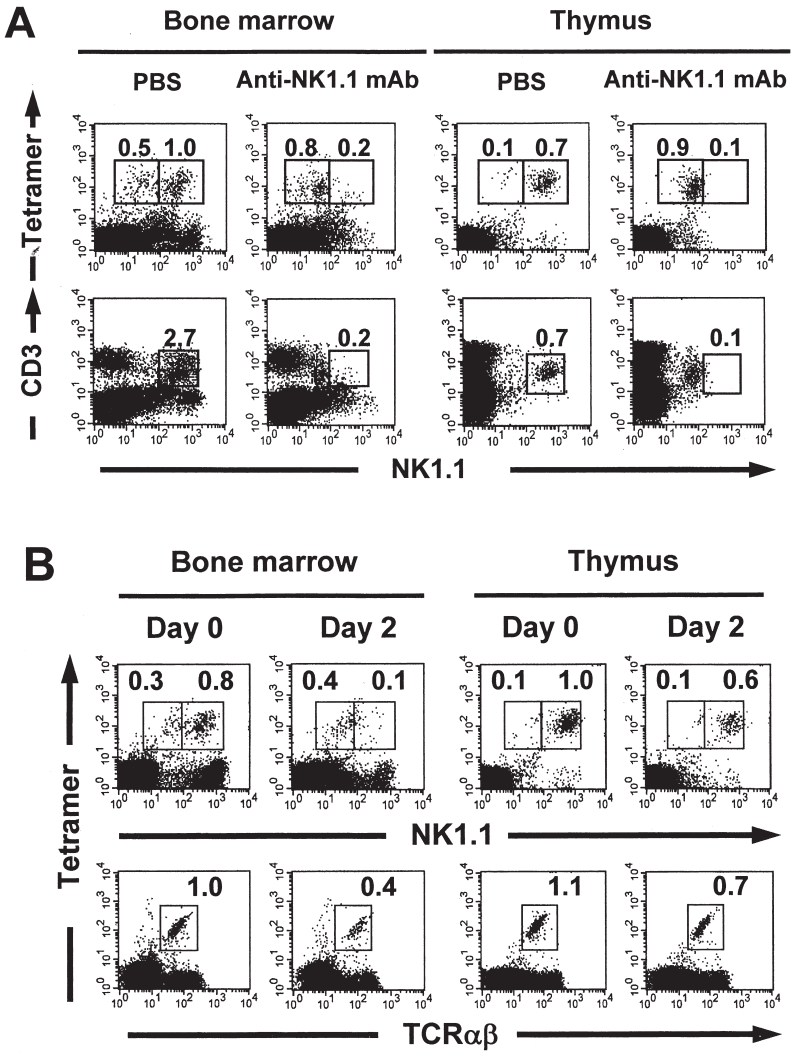

Fig. 3. Influence of NK1$^+$ cell depletion or *L. monocytogenes* infection on α-GalCer/CD1d tetramer-reactive T cells in the BM and thymus of C57BL/6 mice. (A) Mice were treated with anti-NK1.1 mAb or PBS on days 0 and 2, and BM cells and thymocytes were collected on day 4. Cells were stained and analyzed as in Fig. 2 A. Representative staining patterns from 8 mice in each group are shown. Because no significant difference was found between anti-human transferrin R mAb (isotype-matched mAb for anti-NK1.1 mAb)-treated and PBS-treated groups in another experiment, PBS was used as control. (B) Mice were infected with *L. monocytogenes*, and BM cells and thymocytes were collected on days 0 and 2 pi. Cells were stained and analyzed as in Fig. 1 A. Representative staining patterns from 3 to 6 mice in each group are shown.

mer-reactive NK1$^+$ T cells in the BM and thymus were determined. A small, but distinct population of α-GalCer/CD1d tetramer-reactive T cells was detected in the BM and the majority coexpressed NK1, whereas a minor subpopulation lacked this marker. In contrast, virtually all α-GalCer/CD1d tetramer-reactive T cells in the thymus coexpressed NK1 on their cell surface (Fig.3A). Like in the liver, α-GalCer/CD1d tetramer-reactive NK1$^+$ T cells in the BM and thymus became virtually undetectable after anti-NK1.1 mAb treatment. This was also true in other organs including spleen (data not shown). In parallel to the reduction of the α-GalCer/CD1d tetramer-reactive NK1$^+$ T cell population, proportion of α-GalCer/CD1d tetramer-reactive NK1$^-$ T cells increased in both organs after anti-NK1.1 mAb treatment (Fig. 3A), although absolute number of this cell population remained unchanged (data not shown). Although after anti-NK1.1 mAb treatment some cells were slightly stained with anti-NK1.1 mAb, this was caused by biotin-mediated nonspecific reaction (data not shown). Thus, α-GalCer/CD1d tetramer-reactive NK1$^+$ T cells were depleted from lymphoid organs by anti-NK1.1 mAb treatment.

Like in the liver, α-GalCer/CD1d tetramer-reactive NK1$^+$ T cells became virtually undetectable in the BM following *L. monocytogenes* infection (Fig. 3B). In contrast, in the thymus of *L. monocytogenes*-infected mice considerable numbers of α-GalCer/CD1d tetramer-reactive NK1$^+$ T cells persisted and the α-GalCer/CD1d tetramer-reactive NK1$^-$ T cell population did not expand. This discrepancy is probably due to difference in the levels of IL-12 in the two organs. IL-12-producing cells were detected in the BM with high frequencies during *L. monocytogenes* infection as in the liver, whereas virtually no IL-12 producing cells were detected in the thymus (data not shown). Thus, α-GalCer/CD1d tetramer-reactive NK1$^+$ T cells in the thymus should not be affected by *L. monocytogenes* infection.

Thymus-independent emergence of α-GalCer/CD1d tetramer-reactive NK1$^-$ T cells.

ATX mice were infected with *L. monocytogenes* and numbers of liver Vα14$^+$ T cells were determined by α-GalCer/CD1d tetramers. Similar to euthymic mice, high numbers of α-GalCer/CD1d tetramer-reactive T cells were detected in the liver before infection, and the majority of the α-GalCer/CD1d tetramer-reactive T cells coexpressed NK1 (Fig. 4). Absolute numbers of α-GalCer/CD1d tetramer-reactive NK1$^+$ T cells were markedly diminished by day 4 pi, whereas abso lute numbers of α-GalCer/CD1d tetramer-reactive NK1$^-$ T cells were increased (Fig. 4). Thus, NK1$^+$ and NK1$^-$ α-GalCer/CD1d tetramer-reactive T cells were numerically reduced and increased, respectively in response to *L. monocytogenes* infection regardless of the presence of thymus.

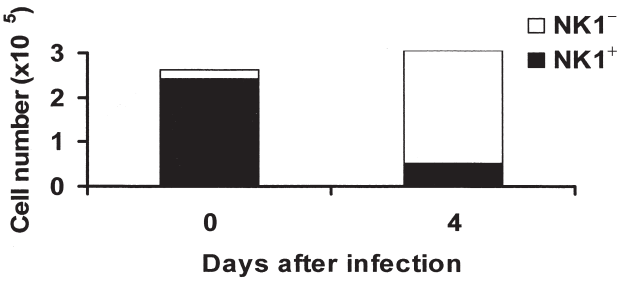

Fig. 4. Appearance of α-GalCer/CD1d tetramer-reactive T cells in the liver of ATX mice following *L. monocytogenes* infection. Mice were infected with *L. monocytogenes* on day 0, and HL were collected on days 0 and 4 pi. Cells were stained as described in Fig. 1 legend. Data represent absolute numbers of α-GalCer/CD1d tetramer-reactive NK1$^+$ T cells (closed bar) and α-GalCer/CD1d tetramer-reactive NK1$^-$ T cells (open bar) and are expressed as mean of three mice at each time point.

Up-regulation of activation markers on α-GalCer/CD1d tetramer-reactive NK1$^-$ T cells during L. monocytogenes infection.

We compared surface expression of various markers on α-GalCer/CD1d tetramer-reactive T cells before and after *L. monocytogenes* infection. In uninfected mice, the vast majority of α-GalCer/CD1d tetramer-reactive T cells expressed CD122 and high levels of CD11a, and this expression pattern remained unchanged during infection (data not shown). In contrast, expression of the CD69, CD54, CD25, and CD49d

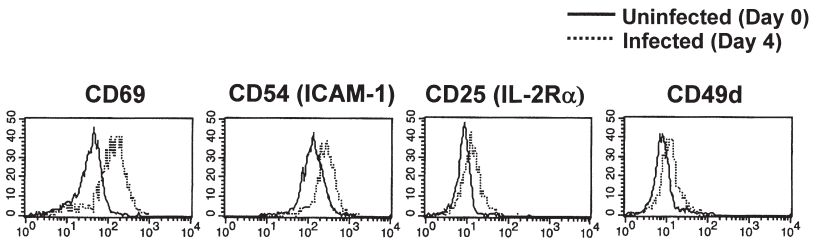

Fig. 5. Cell surface phenotype of α-GalCer/CD1d tetramer-reactive T cells in the liver of C57BL/6 mice before and after *L. monocytogenes* infection. Mice were infected with *L. monocytogenes*, and HL were collected on days 0 and 4 pi. Cells were stained with PE-labeled α-GalCer/CD1d tetramer and FITC-conjugated or biotinylated mAbs indicated in the Figure, followed by SA-conjugated CyChrome. Data are expressed as histograms after gating on α-GalCer/CD1d tetramer-reactive T cells. Representative staining patterns from 3 to 6 mice are shown.

was up-regulated after infection (Fig. 5). Since the majority of α-GalCer/CD1d tetramer-reactive T cells lacked NK1 during *L. monocytogenes* infection, these results suggest that α-GalCer/CD1d tetramer-reactive $NK1^-$ T cells are highly activated.

IFN-γ, but not IL-4, production by α-GalCer/CD1d tetramer-reactive $NK1^-$ T cells following L. monocytogenes infection.

We raised the question whether α-GalCer/CD1d tetramer-reactive $NK1^-$ T cells which emerge in the liver following *L. monocytogenes* infection are functionally active. α-GalCer/CD1d tetramer-reactive T cells were purified from the liver before and after infection, and IFN-γ- and IL-4-producing activities were analyzed by ELISPOT assay. Substantial numbers of IFN-γ and IL-4 producers were detected among α-GalCer/CD1d tetramer-reactive T cells from uninfected animals after in vitro stimulation with PMA and ionomycine (Fig. 6A). Considerable numbers of IFN-γ producers were detected among α-GalCer/CD1d tetramer-reactive T cells from *L. monocytogenes*-infected mice, whereas IL-4-producing cells became virtually undetectable. These results suggest that α-GalCer/CD1d tetramer-reactive $NK1^-$ T cells which emerged in the liver following *L. monocytogenes* infection lack IL-4-producing activities and hence express a Th1-like phenotype.

Selective reduction of CD4-coexpressing $V\alpha14^+$ T cell numbers following L. monocytogenes infection.

We compared CD4 expression on α-GalCer/CD1d tetramer-reactive T cells in the liver before and after *L. monocytogenes* infection. Before infection, the majority (≈ 80 %) of α-GalCer/CD1d tetramer-reactive T cells coexpressed CD4 and a minority (≈ 20 %) lacked this marker (Fig. 6B). In contrast, percentages of $CD4^+$ and $CD4^-$ cells among α-GalCer/CD1d tetramer-reactive T cells shifted to 65 % and 35 %, respectively on day 4 pi. Hence, the $CD4^+$ rather than $CD4^-8^-$ α-GalCer/CD1d tetramer-reactive T cell population was primarily reduced following *L. monocytogenes* infection.

IFN-γ production by $CD4^-8^-$, but not $CD4^+$ α-GalCer/CD1d tetramer-reactive $NK1^-$ T cells following L. monocytogenes infection.

We examined whether among α-GalCer/CD1d tetramer-reactive T cells, $CD4^+$ T cells, $CD4^-8^-$ T cells, or both are responsible for IL-4 and IFN-γ production. Mice were treated with either anti-CD4 mAb or anti-NK1.1 mAb, infected with *L. monocytogenes*, and frequencies of IL-4 and IFN-γ producers among α-GalCer/CD1d tetramer-reactive T cells in the liver were determined by ELISPOT assay. $CD4^+$ and $NK1^+$ cells became undetectable after anti-CD4 mAb (data not

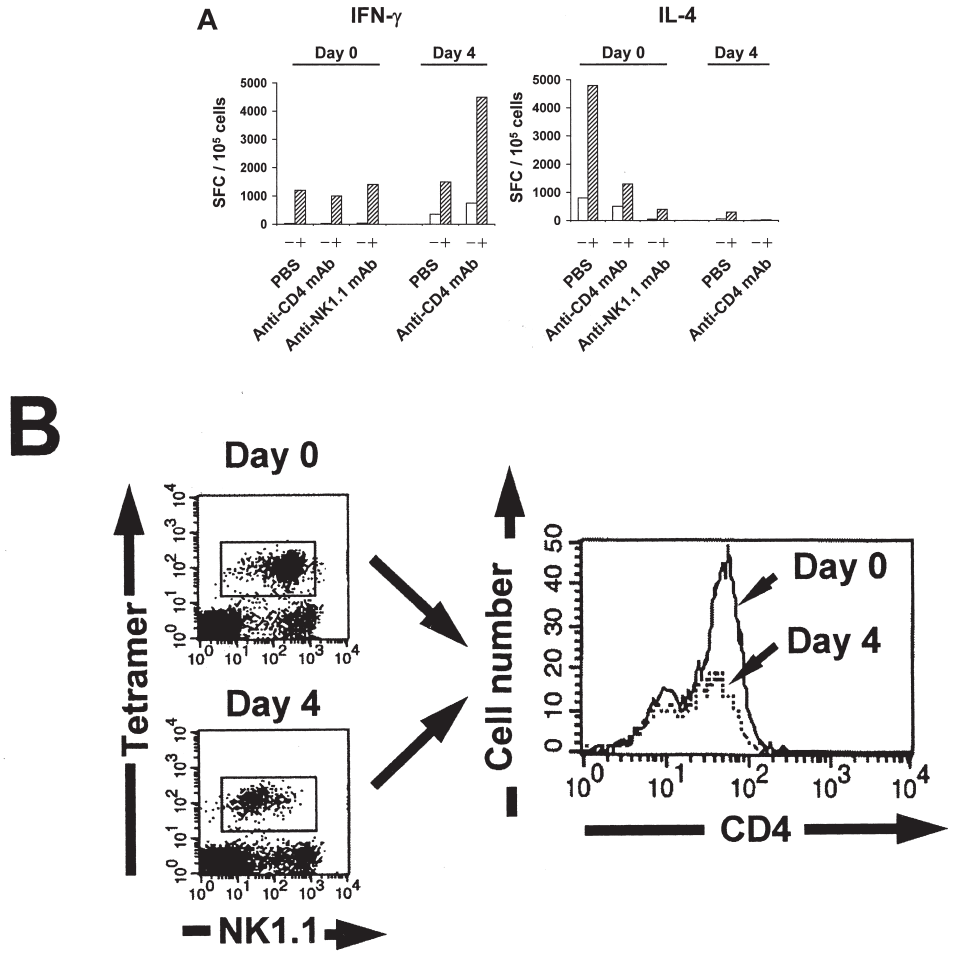

Fig. 6. Influence of $CD4^+$ or $NK1^+$ cell depletion on frequencies of IFN-γ and IL-4 producers among α-GalCer/CD1d tetramer-reactive T cells, and surface expression of CD4 on α-GalCer/CD1d tetramer-reactive T cells in the liver of C57BL/6 mice before and after *L. monocytogenes* infection. (A) Mice were treated with anti-CD4 mAb, anti-NK1.1 mAb or PBS on days −4 and −2, infected with *L. monocytogenes* on day 0, and HL were collected on days 0 and/or 4. Cells were stained with PE-labeled α-GalCer/CD1d tetramer followed by anti-PE microbeads. α-GalCer/CD1d tetramer-reactive cells were positively sorted by MACS, and cultured in the presence or absence of PMA and ionomycin on ELISPOT plates coated with either anti-IFN-γ mAb or anti-IL-4 mAb. Data are expressed as means of duplicate cultures (SD <10 %). Experiments were performed three times with comparable results. +, in the presence of PMA and ionomycin; −, in the absence of PMA and ionomycin. Because virtually all α-GalCer/CD1d tetramer-reactive T cells in the liver on day 4 pi lacked NK1, anti-NK1.1 mAb treatment was not performed in infected mice. (B) Mice were infected with *L. monocytogenes* and HL were collected on days 0 and 4 pi. Cells were stained with FITC-conjugated anti-CD4 mAb, biotinylated anti-NK1.1 mAb and PE-labeled α-GalCer/CD1d tetramer, followed by SA-conjugated CyChrome. Data of NK1.1 vs. α-GalCer/CD1d tetramer are expressed as dot plots after gating on lymphoid cells. Profiles of CD4 are expressed as histograms after gating on α-GalCer/CD1d tetramer-reactive T cells. Representative staining patterns from 5 mice per group are shown.

shown) or anti-NK1.1 mAb (see Fig. 2A and 2B) treatment, respectively: virtually all α-GalCer/CD1d tetramer-reactive T cells from anti-CD4 mAb- or anti-NK1.1 mAb-treated mice lacked CD4 or NK1, respectively. Before infection, numbers of IL-4-producing cells among α-GalCer/CD1d tetramer-reactive T cells from $CD4^+$ or $NK1^+$ cell-depleted mice were markedly lower as compared to cells from non-depleted mice, whereas numbers of IFN-γ producers were comparable among these groups (Fig. 6A). In contrast, after infection frequencies of IFN-γ producers among α-GalCer/CD1d tetramer-reactive T cells were 3.5-fold higher in $CD4^+$ cell-depleted mice than in non-depleted mice. These results suggest that $CD4^-8^-$, but not $CD4^+$ α-GalCer/CD1d tetramer-reactive $NK1^-$ T cells which emerged in the liver following *L. monocytogenes* infection are responsible for IFN-γ production.

Jα28$^{-/-}$ mice are more resistant to L. monocytogenes infection than heterozygous littermates.

We compared Jα281$^{-/-}$and heterozygous littermates for susceptibility to *L. monocytogenes* infection. Jα281$^{-/-}$ and Jα281$^{+/-}$ mice were infected with *L. monocytogenes* and CFUs in livers and spleens were determined on day 4 pi. The CFUs in both livers and spleens were significantly lower in Jα281$^{-/-}$ mice than in Jα281$^{+/-}$ mice (Fig. 7). Thus, Jα281$^{-/-}$ mice were more resistant to *L. monocytogenes* infection than

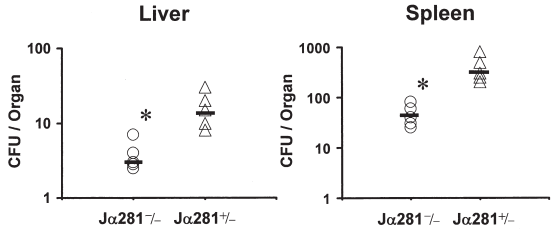

Fig. 7. CFU in livers and spleens of Jα281$^{-/-}$ and Jα281$^{+/-}$ mice following *L. monocytogenes* infection. Mice were infected with *L. monocytogenes* and CFUs in livers and spleens were determined on day 4 pi. Data are from 5 mice and each symbol represents CFU in an individual animal. Horizontal bars represent mean CFU. *, $p < 0.02$, Jα281$^{-/-}$ vs. Jα281$^{+/-}$. Experiments were performed twice with comparable results.

Jα281$^{+/-}$ mice. These findings suggest that the α-GalCer/CD1d tetramer-reactive T cells comprise a heterogeneous population which in its entirety does not contribute to antibacterial protection and may even exacerbate disease.

Discussion

Our findings reveal that IL-4-producing glycolipid/CD1d-specific Vα14$^+$NK1$^+$ T cells vanish in the liver following *L. monocytogenes* infection, whereas IFN-γ-producing glycolipid/CD1d-specific Vα14$^+$NK1$^-$ T cells emerge, and that IL-12 is involved in this mechanism. Thus, the NK1 surface expression on glycolipid/CD1d-specific Vα14$^+$ T cells and their functional activities are markedly influenced by microbial infection.

Similar kinetics of α-GalCer/CD1d tetramer-reactive T cells were seen in Vβ^a mice, in which Vα14$^+$ T cells express TCRVβ7 or 2, but not Vβ8 (30), as in C57BL/6 mice. Moreover, the majority of α-GalCer/CD1d tetramer-reactive $NK1^-$ T cells in the *L. monocytogenes*-infected liver expressed TCRVβ8 and a minority expressed TCRVβ7 and Vβ2 (our unpublished observation). We conclude that the reduction of the α-GalCer/CD1d tetramer-reactive $NK1^+$ T cell population and subsequent expansion of $NK1^-$ subpopulation occurs independently of TCRVβ usage.

IL-15 plays a central role in the proliferation of both NK cells and NKT cells (31-33). Recent study has shown that depletion of NK cells by anti-ASGM1 Ab treatment enhances expansion of thymus-derived Vα14$^+$ NKT cells in the liver due to increased level of IL-15 in the liver microenvironment (34). We consider it likely that similar mechanisms were responsible for the numerical increase of α-GalCer/CD1d tetramer-reactive $NK1^-$ T cells after NK cell depletion. We have previously reported that NK cells play a central role in accumulation of thymic Vα14$^+$ T cells in the liver (28). Because different mechanisms have been suggested for accumulation of Vα14$^+$T calls in the liver under normal condition and under inflammatory condition (35), Vα14$^+$ T cells could accumulate in the liver during infection even in the absence of NK cells.

The Vα14$^+$NK1$^+$ T cells in the periphery were re-

cently found to be derived from thymic NK1$^-$ subpopulation (36). In this study, NK1 surface expression on Vα14$^+$ T cells was acquired in the periphery after the cells had left the thymus during ontogeny. In our study, however, Vα14$^+$NK1$^-$ T cells which emerged in the liver following *L. monocytogenes* infection were derived from NK1$^+$ subpopulation. Hence, we consider it likely that accumulation of Vα14$^+$ NKT cells in the liver is regulated differently under normal condition and inflammatory condition (35).

It has been reported that Vα14$^+$ T cells expand in vivo in response to α-GalCer (37, 38). Because (i) NK cells increased numerically after *L. monocytogenes* infection as well and (ii) expansion of Vα14$^+$ T cells was severely impaired in the presence of NK cells (34, 39), we consider it unlikely that α-GalCer/CD1d tetramer-reactive NK1$^-$ T cells in the liver expanded in situ. Since during listeriosis the increase of the α-GalCer/CD1d tetramer-reactive NK1$^-$ T cell population depends on IL-12, we consider it likely that the fate of Vα14$^+$ T cells is regulated differently by specific antigen, (α-GalCer), and by IL-12. Because BM has been reported to be a source of peripheral Vα14$^+$ T cells during inflammation (35), we consider that α-GalCer/CD1d-specific NK1$^-$ T cells which emerged in the liver are derived from BM and that after leaving the BM, α-GalCer/CD1d tetramer-reactive NK1$^+$ T cells encounter endogenous IL-12 in the peripheral organs including liver, which causes the loss of NK1 marker on the surface.

Although we postulated that curtailment of IL-4-producing Vα14$^+$ T cells favors protection from infection and avoids default leading towards disease exacerbation (8, 21), studies using Vα14$^+$ T cell-deficient β2m$^{-/-}$ and CD1d$^{-/-}$ mice revealed virtually unimpaired Th2 cell responses (2-4). This finding argues against a mandatory role of Vα14$^+$ T cells in polarization towards type 2-immune responses. Because α-GalCer/CD1d tetramer-reactive NK1$^-$ T cells, which increased in the liver following *L. monocytogenes* infection, secreted IFN-γ, but not IL-4, we consider it likely that these cells promote type 1-immune responses.

CD4$^+$ NKT cells differ from CD4$^-$8$^-$NKT cells with regard to cytokine production (40-45). In these studies, CD4$^+$ rather than CD4$^-$8$^-$ NKT cells are responsible for IL-4 production albeit at varying levels in different organs. (i) In the liver CD4$^+$ cells dominate over CD4$^-$8$^-$ cells among Vα14$^+$ T cells (6,7). (ii) IL-4-producing cells among HL are markedly reduced by NK1$^+$ cell depletion (7). (iii) Large numbers of IL-4 producers are detected among purified liver CD4$^+$NK1$^+$ cells after TCR ligation (8). (iv) Numbers of IL-4 producers were low among α-GalCer/CD1d tetramer-reactive T cells from CD4$^+$ or NK1$^+$ cell-depleted mice (this study). Thus, it appears that under normal conditions Vα14$^+$ CD4$^+$NK1$^+$ T cells are mainly responsible for IL-4 production at least in the liver. The α-GalCer/CD1d tetramer-reactive T cell population has been shown to express both IL-4 and IFN-γ mRNA upon stimulation (46, 47). The discrepancy is probably due to difference in stimulant: i.e. specific antigen vs. IL-12.

Since listeriosis preferentially affected CD4$^+$ cells among α-GalCer/CD1d tetramer-reactive T cells (this study, 8, 21), CD4$^+$ and CD4$^-$8$^-$ cells must be differently regulated by endogenous IL-12. Although we did not address the question why the two populations show different kinetics in response to IL-12, we consider it likely that these differences are caused by difference in the intracellular signal transduction pathways after signaling through IL-12R, because IL-12R expression was comparable in the CD4$^+$ and CD4$^-$ α-GalCer/CD1d tetramer-reactive T cell populations (our unpublished observation).

Although Vα14$^+$NKT cells have been considered to undergo apoptosis easily after activation (35), recent studies demonstrate that Vα14$^+$NKT cells are resistant to activation-induced cell death (37, 38). Consistent with these findings (37, 38), we were unable to detect apoptotic cells among Vα14$^+$NKT cells from infected animals (our unpublished observation). We therefore assume that Vα14$^+$NKT cells become undetectable because of NK1 marker down-modulation. In addition to NK1 surface expression, TCR expression on Vα14$^+$NKT cells has recently been suggested to be down-modulated upon activation (37, 38, 48, 49). At present, we cannot formally exclude the possibility that TCR expression on Vα14$^+$NKT cells is down-modulated following *L. monocytogenes* infection. Yet, it is possible that the TCR expression is differently in-

fluenced by specific antigen and IL-12.

At first sight, the finding that listeriosis in Vα14$^+$ T cell-deficient mice was ameliorated argues against a protective role of the Vα14$^+$ T cells in listeriosis. However, as shown here two populations of Vα14$^+$ T cells exist: First, the CD4$^+$NK1$^+$ cells which produce IL-4 and hence should be of no benefit for combat against listeriosis. At early stages of listeriosis, the exacerbating effect of this T cell population seems to dominate and hence depletion of the total Vα14$^+$ T cell population results in amelioration. This notion is consistent with previous findings that anti-CD1 mAb treatment ameriolates listeriosis (50). Second, the CD4$^-$NK1$^-$ cells which produce IFN-γ could be beneficial for control of listeriosis. Contribution of α-GalCer/CD1d tetramer-reactive NK1$^-$ T cells to protection against listeriosis at later stage was observed but not essential, because conventional T cells have already assumed the task of protection. These very subtle effects of Vα14$^+$ NK1$^-$ T cells cannot be visualized in mouse mutants devoid of the entire Vα14$^+$ T cell population because gene knockout mutants only allow identification of essential phenotypic corollary of gene deletion.

Conclusion

We show that the NK1 surface expression on α-GalCer/CD1d-reactive T cell population is influenced by microbial infection. Although Vα14$^+$ NKT cells produce both IFN-γ and IL-4 in naive mice, upon *L. monocytogenes* infection the majority of this cell population produces IFN-γ, but not IL-4. The majority of IFN-γ-producing Vα14$^+$ T cells lacking NK1 are probably derived from thymic NK1$^+$ subset in the BM. Therefore, it is tempting us to assume that distinct Vα14$^+$ NKT cell populations play different roles in infection. Of these, Vα14$^+$ NKT cells expressing NK1 are ineffectual, whereas Vα14$^+$ NKT cells devoid of NK1 seem to participate in protection from bacterial infection by means of IFN-γ.

References

(1) Bendelac, A., M. N. Rivera, S. Park, and J. H. Roark. 1997. Mouse CD1-specific NK1 T cells: development, specificity, and function. *Annu. Rev. Immunol*. **15**: 535.

(2) Chen, Y., N. M. Chiu, M. Mandal, N. Wang, and C. Wang. 1997. Impaired NK1$^+$ T cell development and early IL-4 production in CD1-deficient mice. *Immunity* **6**: 459.

(3) Mendiratta, S. K., W. D. Martin, S. Hong, A. Boesteanu, S. Joyce, and L. van Kaer. 1997. CD1d1 mutant mice are deficient in natural T cells that promptly produce IL-4. *Immunity* **6**: 469.

(4) Smiley, S. T., M. H. Kaplan, and M. J. Grusby. 1997. Immunoglobulin E production in the absence of interleukin-4-secreting CD1-dependent cells. *Science* **275**: 977.

(5) Kawano, T., J. Cui, Y. Koezuka, I. Toura, Y. Kaneko, K. Motoki, H. Ueno, R. Nakagawa, H. Sato, E. Kondo, H. Koseki, and M. Taniguchi. 1997. CD1d-restricted and TCR-mediated activation of Vα14NKT cells by glycosylceramides. *Science* **278**: 1626.

(6) Emoto, M., and S. H. E. Kaufmann. 2003. Liver NKT cells: an account of heterogeneity. *Trends Immunol*. **24**: 364.

(7) Emoto, M., Y. Emoto, and S. H. E. Kaufmann 1995. IL-4 producing CD4$^+$ TCR$\alpha\beta^{int}$ liver lymphocytes: influence of thymus, β_2-microglobulin and NK1.1 expression. *Int. Immunol*. **7**: 1729.

(8) Emoto, M., Y. Emoto, and S. H. E. Kaufmann. 1995. Interleukin-4-producing CD4$^+$ NK1.1$^+$ TCR$\alpha/\beta^{intermediate}$ liver lymphocytes are down-regulated by *Listeria monocytogenes*. *Eur. J. Immunol*. **25**: 3321.

(9) Emoto, M., Y. Emoto, I. B. Buchwalow, and S. H. E. Kaufmann. 1999. Induction of IFN-γ-producing CD4$^+$ natural killer T cells by *Mycobacterium bovis* bacillus Calmette Guérin. *Eur. J. Immunol*. **29**: 650.

(10) Kaufmann, S. H. E. Immunity to intracellular bacteria. In *Fundamental Immunology* 5th. Ed. W. E. Paul, ed. Lippincott-Raven Pubishers, Philadelphia, PA. in press.

(11) Haak-Frendscho M, J. F. Brown, Y. Iizawa, R. D. Wagner, and C. J. Czuprynski. 1992. Administration of anti-IL-4 monoclonal antibody 11B11 in-

creases the resistance of mice to *Listeria monocytogenes* infection. *J. Immunol*. **148**: 3978.
(12) Wagner, R. D., and C. J. Czuprynski. 1993. Cytokine mRNA expression in livers of mice infected with *Listeria monocytogenes. J. Leukoc. Biol*. **53**: 525.
(13) Teixeira, H. C., and S. H. E. Kaufmann. 1994. Role of NK1.1$^+$ cells in experimental listeriosis. NK1$^+$ cells are early IFN-γ producers but impair resistance to *Listeria monocytogenes* infection. *J. Immunol*. **152**: 1873.
(14) Szalay, G., C. H. Ladel, C. Blum, and S. H. E. Kaufmann. 1996. IL-4 neutralization or TNF-α treatment ameliorate disease by an intracellular pathogen in IFN-γ receptor-deficient mice. *J. Immunol.* **157**: 4746.
(15) Mackaness, G. P. 1962. Cellular resistance to infection. *J. Exp. Med*. **116**: 381.
(16) Gregory, S. H., and E. J. Wing. 1998. Neutrophil-Kupffer cell interaction in host defenses to systemic infections. *Immunol. Today* **19**: 507.
(17) Holmberg, L. A., and K. A. Ault. 1986. Characterization of *Listeria monocytogenes*-induced murine natural killer cells. *Immunol. Res.* **5**: 50.
(18) Bancroft, G. J., R. D. Schreiber, G. C. Bosma, M. J. Bosma, and E. R. Unanue. 1987. A T cell-independent mechanism of macrophage activation by interferon-γ. *J. Immunol*. **139**: 1104.
(19) Poston, R. M., and R. J. Kurlander. 1991. Analysis of the time course of IFN-γ mRNA and protein production during primary murine listeriosis. The immune phase of bacterial elimination is not temporally linked to IFN production in vivo. *J. Immunol*. **146**: 4333.
(20) Bancroft, G. J., R. D. Schreiber, and E. R. Unanue. 1991. Natural immunity: a T-cell-independent pathway of macrophage activation, defined in the *scid* mouse. *Immunol. Rev.* **124**: 5.
(21) Emoto, Y., M. Emoto, and S. H. E. Kaufmann 1997. Transient control of interleukin-4-producing natural killer T cells in the livers of *Listeria monocytogenes*-infected mice by interleukin-12. *Infect. Immun.* **65**: 5003.
(22) Chen, H., H. Huang, and W. E. Paul. 1997. NK1.1$^+$CD4$^+$ T cells lose NK1.1 expression upon in vitro activation. *J. Immunol.* **158**: 5112.
(23) Park, S., T. Kyin, A. Bendelac, and C. Carnaud. 2003. The contribution of NKT cells, NK cells, and other γ-chain-dependent non-T non-B cells to IL-12-mediated rejection of tumors. *J. Immunol.* **170**: 1197.
(24) Matsuda, J. L., O. V. Naidenko, L. Gapin, T. Nakayama, M. Taniguchi, C. R. Wang, Y. Koezuka, and M. Kronenberg. 2000. Tracking the response of natural killer T cells to glycolipid antigens using CD1d tetramer. *J. Exp. Med.* **192**: 741.
(25) Benlagha K., A. Weiss, A. Beavis, L. Teyton, and A. Bendelac. 2000. In vivo identification of glycolipid antigen-specific T cells using fluorescent CD1d tetramer. *J. Exp. Med.* **191**: 1895.
(26) Emoto, M., J. Zerrahn, M. Miyamoto, B. Perarnau, and S. H. E. Kaufmann. 2000. Phenotypic characterization of CD8$^+$NKT cells. *Eur. J. Immunol.* **30**: 2300.
(27) Emoto, M., M. Miyamoto, Y. Emoto, J. Zerrahn, and S. H. E. Kaufmann. 2001. A critical role of T-cell receptor γ/δ cells in antibacterial protection in mice early in life. *Hepatology* **33**: 887.
(28) Miyamoto, M., M. Emoto, V. Brinkmann, N. van Rooijen, R. Schmits, E. Kita, and S. H. E. Kaufmann. 2000. Contribution of NK cells to the homing of thymic CD4$^+$NKT cells to the liver. *J. Immunol.* **165**: 1729.
(29) Emoto, M., M. Miyamoto, K. Namba, R. Schmits, N. van Rooijen, E. Kita, and S. H. E. Kaufmann. 2000. Participation of leukocyte function-associated antigen-1 and NK cells in the homing of thymic CD8$^+$NKT cells to the liver. *Eur. J. Immunol.* **30**: 3049.
(30) Ohteki, T., and H. R. MacDonald. 1996. Stringent Vβ requirement for the development of NK1.1$^+$ T cell receptor-α/β^+ cells in mouse liver. *J. Exp. Med.* **183**: 1277.
(31) Ohteki, T., H. Shirley, H. Suzuki, T. W. Mak, and P. S. Ohashi. 1997. Role for IL-15/IL-15Rβ chain in NK1.1$^+$ T cell receptor-$\alpha\beta^+$ cell development. *J. Immunol.* **159**: 5931.
(32) Kennedy, M. K., M. Glaccum, S. N. Brown, E. A. Butz, J. L. Viney, M. Embers, N. Matsuki, K. Charrier, L. Sedger, C. R. Willis, K. Brasel, P. J.

Morrissey, K. Stocking, J. C. Schuh, S. Joyce, and J. J. Peschon. 2000. Reversible defects in natural killer and memory CD8 T cell lineages in interleukin 15-deficient mice. *J. Exp. Med.* **191**: 771.

(33) Lodolce, J. P., D. L. Boone, S. Chai, R. E. Swain, T. Dassopoulos, S. Trettin, and A. Ma. 1998. IL-15 receptor maintains lymphoid homeostasis by supporting lymphocyte homing and proliferation. *Immunity* **9**: 669.

(34) Matsuda, J. L., L. Gapin, S. Sidobre, W. C. Kieper, J. T. Tan, R. Ceredig, C. D. Surh, and M. Kronenberg. 2002. Homeostasis of Vα14i NKT cells. *Nat. Immunol*. **3**: 966.

(35) Eberl, G, and H. R. MacDonald. 1998. Rapid death and regeneration of NKT cells in anti-CD3-ε- or IL-12-treated mice—a major role for bone marrow in NKT cell homeostasis. *Immunity* **9**: 345.

(36) Benlagha, K., T. Kyin, A. Beavis, L. Teyton, and A. Bendelac. 2002. A thymic precursor to the NK T cell lineage. *Science* **296**: 553.

(37) Wilson, M.T., C. Johansson, D. Olivares-Villagomez, A.K. Singh, A.K. Stanic, C. Wang, S. Joyce, M.J. Wick, and L. van Kaer. 2003. The response of natural killer T cells to glycolipid antigens is characterized by surface receptor down-modulation and expansion. *Proc. Natl. Acad. Sci. U S A.* **100**: 10913.

(38) Crowe, N.Y., A.P. Uldrich, K. Kyparissoudis, K.J.L. Hammond, Y. Hayakawa, S. Sidobre, R. Keating, M. Kronenberg, M.J. Smyth, and D.I. Godfrey. 2003. Glycolipid antigen drives rapid expansion and sustained cytokine production by NK T cells. *J. Immunol*. **171**: 4020.

(39) Ranson, T., C. A. Vosshenrich, E. Corcuff, O. Richard, V. Laloux, A. Lehuen, and J. P. Di Santo. 2003. IL-15 availability conditions homeostasis of peripheral natural killer T cells. *Proc. Natl. Acad. Sci. U S A.* **100**: 2663

(40) Davodeau, F., M. A. Peyrat, A. M.A., Necker, R. A., Dominici, F. R., Blanchard, C. F., Leget, J. C., Gaschet, P. J., Costa, Y. P., Jacques, A. Y., Godard, H. A., Vie, A. H., Poggi, F. A., Romagne, F., and M. Bonneville, M. 1997. Close phenotypic and functional similarities between human and murine $\alpha\beta$ T cells expressing invariant TCR α-chains. *J. Immunol.* **158**: 5603.

(41) Hammond, K. J., S. B. Pelikan, N. Y. Crowe, E. Randle-Barrett, T. Nakayama, M. Taniguchi, M. J. Smyth, I. R. van Driel, R. Scollay, A. G. Baxter, and D. I. Godfrey. 1999. NKT cells are phenotypically and functionally diverse. *Eur. J. Immunol.* **11**: 3768.

(42) Hameg, A., I. Apostolou, M. Leite-De-Moraes, J. M. Gombert, C. Garcia, Y. Koezuka, J. F. Bach, and A. Herbelin. 2000. A subset of NKT cells that lacks the NK1.1 marker, expresses CD1d molecules, and autopresents the α-galactosylceramide antigen. *J. Immunol.* **165**: 4917.

(43) Takahashi, T., M. Nieda, Y. Koezuka, A. Nicol, S. A. Porcelli, Y. Ishikawa, K. Tadokoro, H. Hirai, and T. Juji. 2000. Analysis of human Vα24$^+$CD4$^+$NKT cells activated by α-glycosylceramide-pulsed monocyte-derived dendritic cells. *J. Immunol.* **164**: 4458.

(44) Gumperz, J. E., S. Miyake, T. Yamamura, and M. B. Brenner. 2002. Functionally distinct subsets of CD1d-restricted natural killer T cells revealed by CD1d tetramer staining. *J. Exp. Med.* **195**: 625.

(45) Lee, P. T., K. Benlagha, L. Teyton, and A. Bendelac. 2002. Distinct functional lineages of human Vα24 natural killer T cells. *J. Exp. Med.* **195**: 637.

(46) Matsuda JL., L. Gapin, JL. Baron, S. Sidobre, DB. Stetson, M. Mohrs, RM. Locksley, and M. Kronenberg. 2003. Mouse Vα14i natural killer T cells are resistant to cytokine polarization *in vivo. Proc. Natl. Acad. Sci. U S A* **100**: 8395.

(47) Stetson DB. M. Mohrs, RL Reinhardt, JL. Baron, ZE. Wang, L. Gapin, M. Kronenberg, and RM. Locksley. 2003. Constitutive cytokine mRNAs mark natural killer (NK) and NKT cells poised for rapid effector function. *J. Exp. Med.* **198**: 1069.

(48) Dieli, F., M. Taniguchi, M. Kronenberg, S. Sidobre, J. Ivanyi, L. Fattorini, E. Iona, G. Orefici, G. de Leo, D. Russo, N. Caccamo, G. Sireci, C. di Sano, A. Salerno. 2003. An anti-inflammatory role for Vα14 NK T cells in *Mycobacterium bovis* bacillus Calmette-Guerin-infected mice. *J. Im-*

munol. **171**: 1961.
(49) Harada, M., K. Seino, H. Wakao, S. Sakata, Y. Ishizuka, T. Ito, S. Kojo, T. Nakayama, M. Taniguchi. 2004. Down-regulation of the invariant Vα14 antigen receptor in NKT cells upon activation. *Int. Immunol.* **16**: 241.
(50) Szalay, G., C. H. Ladel, C. Blum, L. Brossay, M. Kronenberg, and S. H. E. Kaufmann. 1999. Anti-CD1 monoclonal antibody treatment reverses the production patterns of TGF-β2 and Th1 cytokines and ameliorates listeriosis in mice. *J. Immunol.* **162**: 6955.

Immune Response of Lymphocytes Infected with *Chlamydia pneumoniae*

Yoshimasa Yamamoto

Laboratory of Molecular Microbiology, Department of Basic Laboratory Sciences, Graduate School of Medicine, Osaka University, Osaka 565-0871, Japan

Introduction

Chlamydia (Chlamydophila) pneumoniae, an obligate intracellular bacterium, causes a wide spectrum of respiratory tract infections (1-3). Current studies indicate that this pathogen is associated with not only respiratory diseases but also chronic inflammatory diseases, such as atherosclerosis, endocarditis, asthma, and arthritis (4-7). However, even though there are a large number of reports relating *C. pneumoniae* infection and certain chronic inflammatory diseases, the mechanisms of development of such diseases by this pathogen are not clear. Lymphocytes are known to play a central role in the development of such chronic inflammatory diseases by their diverse functions. In this regard, a study by Kaul et al. (8) showed that *C. pneumoniae* DNA could be recovered from $CD3^+$ peripheral blood leukocytes obtained from the patients attending a cardiology clinic. In addition, our current study demonstrates that this pathogen can infect and multiply in lymphocytes *in vitro* (9). These findings suggest new potential target cells in *C. pneumoniae* infection. Since lymphocytes are another major immune cell type besides macrophages in the development of chronic inflammatory diseases, particularly atherosclerosis (10), interaction between lymphocytes and this pathogen may contribute to the pathogenesis of atherosclerosis as well as other chronic inflammatory diseases associated with *C. pneumoniae*. For instance, it can be conjectured that modulation of lymphocyte functions by infection with *C. pneumoniae* may lead to inappropriate response and/or over stimulation of the immune system. In order to analyze details of the lymphocyte-*C. pneumoniae* interaction, we determined cytokine responses as well as expression of activation markers in defined human T lymphocyte and B lymphocyte cell line cells after infection with *C. pneumoniae*.

Materials and Methods

Cells.

The human monocyte cell line THP-1 and human lymphocyte cell lines Molt-4 (mature T-cell) and P3HR1 (mature B-cell) were utilized in this study. The cells were cultured in RPMI 1640 medium containing 10% heat-inactivated fetal calf serum (FCS) and antibiotics (gentamycin sulfate, 10 μg/ml; vancomycin, 10 μg/ml; amphotericin B, 1 μg/ml) (Sigma Chemical, St. Louis, MO, USA) at 37°C in 5% CO_2.

Bacteria.

C. pneumoniae TW183 strain was kindly provided by G. Byrne, University of Wisconsin, Madison, WI, USA. Mycoplasma-free of the bacteria culture was confirmed by PCR, as described previously (11). The bacteria were propagated in the HEp-2 cell culture system according to the methods described previously (12). *C. pneumoniae* elementary bodies (EBs) were purified by density gradient centrifugation with Percoll (Sigma) (13). Purified EBs were suspended in sucrose-phosphate-gultamic acid buffer (0.2 M sucrose, 3.8 mM KH_2PO_4, 6.7 mM Na_2HPO_4, 5 mM L-gultamic

acid, pH 7.4) and then stored at −70°C until used. Inclusion forming units (IFU) of prepared EBs were determined by counting *Chlamydia* inclusions in HEp-2 cell monolayers, as described previously (12,14).

C. pneumoniae infection.

Cultures of each cell line (1×10^6 cells/well, 24-well plates) were infected with bacteria (1×10^7 bacteria) by centrifugation at $700 \times g$ for 1 h. The cells were then washed to remove non-infected bacteria with Hanks' balanced salt solution (HBSS) by centrifugation, resuspended in the medium and incubated for 72 h at 37°C in 5% CO_2. In some experiments, Molt-4 and P3HR1 cells were stimulated with 250 ng phorbol myristate acetate (PMA; Sigma) per ml and 50 ng ionomycin (Sigma) per ml, nonspecific stimulators, as a cell activation control. In the case of THP-1 cells, 1 μg bacterial lipopolysaccharide (LPS; Sigma) per ml was also used as a nonspecific stimulator for a cell activation control.

Determination of chlamydial inclusions.

The infected cells on a microscopic slide were centrifuged by a Cytospin (Shandon, Sewickley, PA, USA). After fixing with ethanol, the cells were then stained with *Chlamydia*-specific fluorescein isothiocyanate (FITC)-conjugated monoclonal antibody (Research Diagnostics, Flanders, NJ, USA), as described previously (15). The presence of chlamydial inclusions in the sample was then determined by fluorescence microscopy.

RNA extraction and RT-PCR.

The total RNA was extracted from infected cells using an RNeasy Mini Kit (Qiagen, Valencia, CA, USA) according to the manufacturer's instructions. In some expereiments, RNA was extracted by a single step method using guanidine thiocyanate reagent (TRI Reagent; Sigma), as described previously (16). The concentration of RNA was quantified by spectrophotometry, and RNA was stored at −70°C until used. The extracted RNAs were treated with DNase (DNA-free; Ambion, Austin, TX, USA) to eliminate the contaminating DNA. DNA-free of the treated RNAs was confirmed by PCR without reverse transcription (RT). The RT of 2 μg of RNA was performed using avian myeloblastosis virus transcriptase (Promega, Madison, WI, USA) with random primers in a commercial reaction mixture (20 μl; Reverse Transcription System; Promega). The resulting cDNAs (2 μl) were then subjected to real-time PCR.

The real-time PCR with primers specific for *C. pneumoniae* 16S rRNA was performed in the master mixture (SYBR Green PCR Master Mix; Applied Biosystems, Foster City, CA, USA) with primers and cDNAs in an iCycler thermal cycler (Bio-Rad, Hercules, CA, USA), as described previously (15). The primer sequences for *C. pneumoniae* 16S rRNA were described previously (17).

The real-time PCR specific for tumor necrosis factor (TNF)-α, interferon (IFN)-γ, *BIC* (a lymphocyte activation marker gene), and β-actin was also performed. The primer sequences for β-actin were described previously (18). The sequences of primer for TNF-α were 5'-TCT CGA ACC CCG AGT GAC A-3' (sense) and 5'-GGC CCG GCG GTT CA-3' (antisense). The primer sequences for *BIC* were 5'-TGG AGG AAG AAA CAG GCT TAG AA-3' (sense) and 5' -TTC AAG TTC AAT AGC TTA GCC ACA TAA-3' (antisense) (19). The primer sequences for IFN-γ were 5'-AGC GGA TAA TGG AAC TCT TTT CTT AG-3' (sense) and 5'-AAG TTT GAA GTA AAA GGA GAC AAT TTG G-3' (antisense). The thermal cycling conditions were 95°C for 10 min, and 50 cycles of 95°C for 40 s, 60°C (58°C for IFN-γ, β-actin) for 40 s and 72°C for 30 s.

As a standard for *C. pneumoniae* 16S rRNA, a series of diluted *C. pneumoniae* DNA extracted from purified EBs was used. In the case of an activating marker gene (*BIC*), TNF-α, IFN-γ as well as β-actin genes, cDNAs of these messages generated by PCR were purified from gels by QiAquick Gel Extraction Kit (Qiagen) and were utilized for standard curves of real-time PCR. The levels of mRNAs as well as *C. pneumoniae* transcripts are represented as an x-fold increase in the expression.

Statistical analysis.

All experiments were repeated at least three times and the statistical significance of difference was assessed by Student's *t*-test.

Results

Chlamydia infection of lymphocytes.

The previous study by us demonstrated that *C. pneumoniae* infects and replicates vigorously in established lymphoid cell line cells in the presence of cycloheximide (20), which is an enhancer of *Chlamydia* growth in cells (21). However, cycloheximide may modulate the response of lymphocytes to *Chlamydia* infection due to the inhibitory activity of this compound on the protein synthesis of the host cells. Therefore, we attempted to establish *Chlamydia* infection model in lymphoid cells not treated with cycloheximide in this study. The cells of both T-lymphocyte Molt-4 and B-lymphocyte P3HR1 established cell line cells were infected with *C. pneumoniae* by centrifugation and then cultured for up to 3 days without cycloheximide. Bacterial growth in the cells was assessed by determination of chlamydial inclusions as well as bacterial transcripts. The cells of both lymphoid cell-lines showed the presence of obvious chlamydial inclusion bodies stained with FITC-labeled anti-*Chlamydia* antibody at 72 hr after infection, but not at time zero (immediately after infection) (data not shown). However, the size and number of inclusion bodies were small and limited in comparison with those in the cells cultured in the presence of cycloheximide (20).

The detection of bacterial transcripts as a marker of viable and metabolically active bacteria has been utilized for a wide variety of bacteria, including *C. pneumoniae* (17, 22, 23). Because mRNA is turned over rapidly in living bacterial cells, i. e., most mRNA species having a half-life of only a few minutes (24), the presence of certain bacterial mRNAs can be regarded as a valid and convincing criterion for assessing the levels of the viable bacteria. In this regard, the levels of *C. pneumoniae* 16S rRNA transcripts in lymphocytes infected with *C. pneumoniae* were measured during the infection by quantitative RT-PCR. As shown in Fig. 1, 16S rRNA transcripts were detected at certain levels which were maintained through the infection for up to 72 hrs tested. No difference in the susceptibility to *C.pneumoniae* infection was found between T cell line Molt-4 cells and B cell line P3HR1 cells by determination of intracellular chlamidia inclusions and chlamidia 16S rRNA transcripts during the course of infection. These results indicate that *C. pneumoniae* may infect persistently both T and B lymphocytes in human.

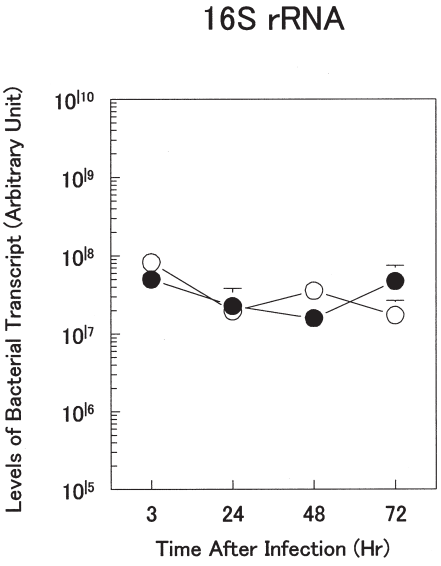

Fig. 1. *C. pneumoniae* transcript levels in infected cells. Cells were infected with *C. pneumoniae*, washed to remove non-ingested bacteria and then total RNA was extracted from the cells at the indicated time point. Bacterial transcript levels were determined by real-time RT-PCR. Data are mean + standard deviation (SD) for 3 experiments. ●, Molt-4; ○, P3HR1.

TNF-α response of C. pneumoniae infected lymphocytes.

To determine which kind of lymphoid cells could respond to *Chlamydia* infection, lymphoid cells of T cell line Molt -4 or B cell line P3HR1 were infected with *C. pneumoniae* and expression levels of cytokine

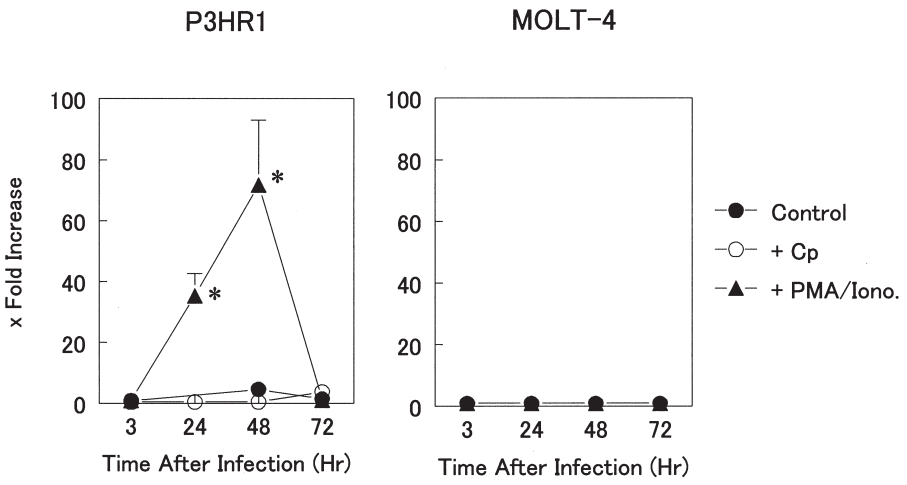

Fig. 2. TNF-α mRNA expression levels in cells without any treatment (control), cells infected with *C. pneumoniae* (Cp), or cells treated with non-specific stimulator PMA/ionomycin (Iono.). The expression levels of TNF-α mRNA in the cells at indicated time point were determined by real-time RT-PCR. The levels of TNF-α mRNA expression were normalized to β-actin mRNA expression. The data are the x-fold increase (mean + SD) vs. time zero (immediately after infection) of TNF-α mRNA levels of 3 experiments. *P<0.05, vs. control culture group at the same time point.

gene in the cells were assessed by quantification of the gene transcripts. TNF-α is known to play a major role in inflammatory response and to regulate the *C. pneumoniae* infection (14), and *C. pneumoniae* infection of cells, including macrophages and epithelial cells, induces this cytokine (15, 25, 26). However, whether lymphocytes infected with *C. pneumoniae* produce TNF-α, particularly by persistent infection, is not known. Therefore, in this study levels of TNF-α gene expression in *C. pneumoniae* infected lymphocytes were assessed by quantitative RT-PCR following the course of the infection. As shown in Fig. 2, lymphoid cells of both T cell line and B cell line did not show any increase in TNF-α messages during the infection with *C. pneumoniae*. Nonspecific activation of P3HR1 (B cell line) cells with PMA/ionomycin resulted in a marked induction of this cytokine messages at 24 and 48 hr after stimulation, indicating that TNF-α messages can be induced in P3HR1 cells. In contrast, Molt-4 cells (T cell line) did not show any increase in TNF-α messages by the stimulation with the same nonspecific stimulators tested under the same experimental conditions. Infection of THP-1 (monocyte cell line) cells with *C. pneumoniae* resulted in a marked induction of TNF-α messages (Fig. 3). These results indicate that TNF-α message expression in P3HRI lymophoid cells can be enhanced with PMA/ionomycin but may not be enhanced by *C. pneumoniae* infection, even though *Chlamydia* infection can enhance this cy-

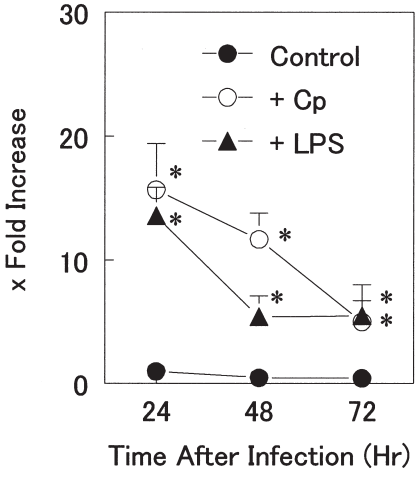

Fig. 3. TNF-α mRNA expression levels in monocytic THP-1 cells without any treatment (control), cells infected with *C. pneumoniae* (Cp), or cells treated with bacterial LPS. See the Figure 2 legend.

tokine message levels in monocytic THP-1 cells.

IFN-γ response of C. pneumoniae infected lymphocytes.

It is widely accepted that immune responses that favor the development of Th1 responses as assessed by measuring cytokines, including IFN-γ, tend to be more protective against intracellular pathogens than immune responses favoring the development of Th2 cytokines (27). In fact, it is demonstrated that IFN-γ activates cells to inhibit intracellular *C. pneumoniae* growth (14, 28-30). Furthermore, this cytokine is mainly produced by activated T-lymphocytes. Therefore, in order to determine the IFN-γ response of *C. pneumoniae* infected lymphocytes, Molt-4 T-lymphocytes were infected with *C. pneumoniae* and levels of the IFN-γ message of the infected cells were assessed by quantitative real-time RT-PCR. As shown in Fig. 4, the levels of IFN-γ messages of Molt-4 cells stimulated with nonspecific stimulators, PMA/ionomycin, were obviously enhanced. However, *Chlamydia* infection of lymphocytes induced only a minimum enhancement, which was not statistically significant, of IFN-γ messages at 48 hrs after infection.

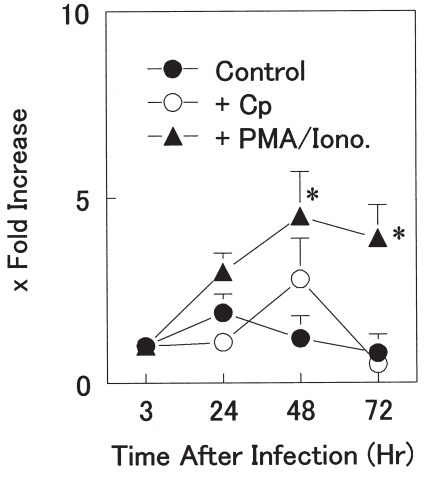

Fig. 4. IFN-γ mRNA expression levels in Molt-4 cells without any treatment (control), cells infected with *C. pneumoniae* (Cp), or cells treated with non-specific stimulator PMA/ionomycin (Iono.). The expression levels of IFN-γ mRNA in cells at indicated time point were determined by real-time RT-PCR. The levels of IFN-γ mRNA expression were normalized to β-actin mRNA expression. The data are the x-fold increase (mean + SD) vs. time zero (immediately after infection) of IFN-γ mRNA levels of 3 experiments. **P*<0.05, vs. control culture group at the same time point.

Lymphocyte activation marker in C. pneumoniae infected cells.

BIC is a proto-oncogene (31) and a marker for an early and sustained lymphocyte activated events (19). Therefore, we determined whether increase in *BIC* messages in lymphocytes occurs by *C. pneumoniae* infection (Fig.5). P3R1 (B cell line) cells and Molt-4 (T cell line) cells which were cultured without any stimulation, or under infection with *C. peumoniae* showed a certain level of *BIC* messages during the culture. Both P3HR1 cells and Molt-4 cells stimulated with nonspecific stimulants, PMA/ionomycin, showed marked increase in message of this activation maker gene, whereas infection with *C. pneumoniae* induced only a limited increase of this gene messages in P3R1 cells and Molt-4 cells during the infection.

Discussion

The importance of lymphocytes in the development of chronic inflammatory diseases, including atherosclerosis, is obvious. For example, it is well documented that the lesions of atherosclerosis contain a focal accumulation of macrophages and T lymphocytes with the capacity to secret a variety of cytokines (32-34). This inflammatory response may result in plaque rupture and thrombosis, eventually causing stroke or myocardial infarction (35). Therefore, an immune response, including regulation of inflammation by immune cells, to *C. pneumoniae* may be critical for the development of not only atherosclerosis but also other chronic inflammatory diseases associated with *C. pneumoniae*. In this regard, we attemted to infect lymphocytes with *C. pneumoniae in vitro* and have demonstrated growth of the bacteria within the lymphocytes (9). In addition, the recovery of *Chlamydia*

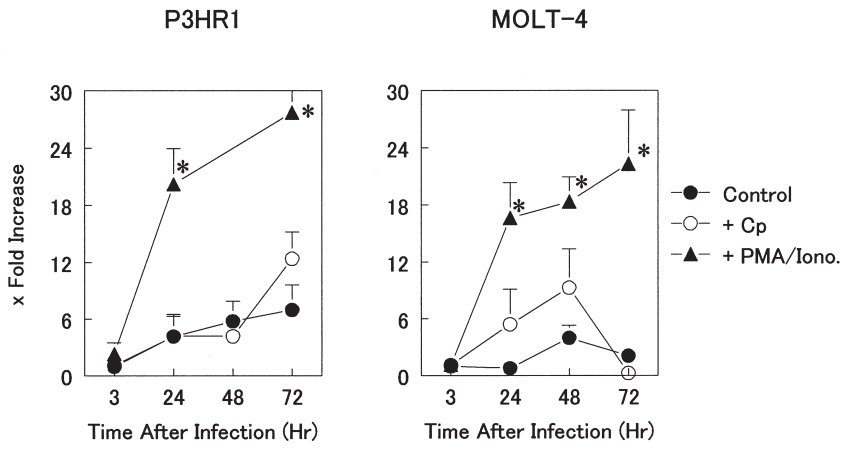

Fig. 5. *BIC* mRNA expression levels in cells without any treatment (control), cells infected with *C. pneumoniae* (Cp), or cells treated with PMA/ionomycin (Iono.). The expression levels of *BIC* mRNA in cells at indicated time point were determined by real-time RT-PCR. The levels of *BIC* mRNA expression were normalized to β-actin mRNA expression. The data are the x-fold increase (mean + SD) vs. time zero (immediately after infection) of *BIC* mRNA levels of 3 experiments. **P*<0.05, vs. control culture group at the same time point.

DNA from lymphocytes of peripheral blood of the patients with cardiovascular disease was also reported (8). Thus, the infection of lymphocytes with *C. pneumoniae* is highly likely in actual diseases associated with this pathogen. From these findings, it can be conjectured that a possible alteration of lymphocyte immune function by the infection may play an important role in the development of atherosclerosis as well as other diseases associated with *C. pneumoniae*.

Effect of *Chlamydia* infection on the cytokine production as well as cell function of the infected lymphocytes is not known, while *C. preumoniae* infection of various kinds of cells, including macrophages and epithelial cells, is known to induce a variety of cytokines from the infected cells (15, 25, 26, 36). In order to find out a possible alteration of such lymphocyte function by *Chlamydia* infection, an *in vitro Chlamydia* infection model of lymphoid cells was examined. Our previous study has demonstrated that both Molt-4 lymphoid cells and P3HR1 lymphoid cells are susceptible to *C. pneumoniae* infection and support a vigorous growth of this pathogen in the presence of cycloheximide (20). However, cycloheximide, which is widely used as an enhancer for *Chlamydia* growth, is an inhibitor for host cell protein synthesis and may affect the response of lymphocytes to *Chlamydia* infection. In the present study, therefore, we did not use cycloheximide in the *in vitro* study of *Chlamydia* infection of lymphocytes. The results obtained in this study indicated that lymphoid cells of both cell lines, Molt-4 T-lymphocytes and P3HR1 B-lymphocytes, supported only a minimum growth of *C. pneumoniae* in the cells as shown by determination of *Chlamydia* inclusion bodies, and that a certain level of viable bacteria was maintained as shown by determination of levels of bacterial transcript. *C. pneumoniae* 16S rRNA transcripts are expressed in all metabolically active stages of *C. pneumoniae* growth, including the stage of noninfectious reticulate bodies in the infected cells (17). In the present study, the expression levels of 16S rRNA transcripts were well maintained during the infection indicating the presence of viable bacteria in cells. Immunohistochemical determination of chlamydial inclusions with FITC-labeled anti-*Chlamydia* antibody showed obvious but small and limited number of inclusions at 72 hrs after infection, but not immediately after infection. Even though in this study only qualitative analysis of *Chlamydia* inclusion body formation was performed, the results indicated clearly that both Molt-4 and P3HR1 lymphocytes permit a

persistent infection of *C. pneumoniae* even without addition of inhibitor for host cell metabolism, such as cycloheximide. No significant difference in the ability to support the intracellular growth of *C. pneumoniae* was observed between T- and B-lymphocytes.

Persistent infection of lymphocytes with *C. pneumoniae* permits only a limited growth of the pathogen in the cells and may not cause serious damage to the host cells. In fact, the level of house-keeping β-actin gene messages of the infected cells was maintained at a constant level without any remarkable loss during the infection (data not shown). The cytokine messages (TNF-α and IFN-γ) of the infected lymphocytes were also maintained at a constant level with only a minimal alteration during the infection. In the case of TNF-α, P3HR1 B-lymphocytes and Molt-4 T-lymphocytes showed a minimal constitutive expression of this cytokine messages. *C. pneumoniae* infection did not induce any enhancement of expression of messages of this cytokine in the lymphocytes, whereas this pathogen induced a marked induction of TNF-α in the infected THP-1 monocytes. The findings that enhancement of TNF-α message in P3HR1 B-lymphocytes was induced by nonspecific stimulators, PMA/ionomycin, indicate that the experimental conditions used were appropriate for enhancement of expression of this cytokine message. However, in the case of Molt-4 T cells TNF-α message was not induced by the nonspecific stimulators tested. Nevertheless, it is obvious from these results that *C. pneumoniae* persistent infection of lymphoid cells may not induce an enhancement of TNF-α in the infected lymphocytes. Similar results were also observed in the case of IFN-γ. That is, Molt-4 T lymphocytes showed a certain level of constitutive expression of IFN-γ messages. Stimulation of the Molt-4 cells with nonspecific stimulators induced a marked enhancement of expression of this message. However, infection of the cells with *C. pneumoniae* induced only a minimal enhancement, which was not statistically significant.

Activation of lymphocytes causes the expression of a number of early response genes (31). In this regard, it has been demonstrated that *BIC* expression is markedly upregulated by the stimulation that leads to activation of lymphocyte (31). Therefore, as an approach to examine whether *C. pneumoniae* infection of lymphocytes affects the activation status of the cells, *BIC* expression levels of the infected lymphocytes were determined. Both P3HR1 B lymphocytes and Molt-4 T lymphocytes used in this study constitutively expressed a certain level of this gene message and showed a marked elevation of expression levels after stimulation with nonspecific stimulators. In contrast, *C. pneumoniae* infection of P3HR1 or Molt-4 lymphocytes induced only a statistically non-significant minimal enhancement of *BIC* message in the cells during the infection.

Thus, the results obtained in this study revealed that the expression levels of genes of cytokines as well as an activation marker gene, *BIC*, were minimally altered by *C. pneumoniae* infection in lymphocytes. Even though only genes for two cytokines and one activation marker were examined in this study, it seems likely that *C. pneumoniae* infection of lymphocytes may tend to be silent regarding cytokine response of the infected cells possibiy because the infection is persistent. Further study regarding the response of *C. pneumoniae* infected lymphocytes to physiological stimulations, such as engagement of T cell receptor to its ligand, is necessary to clarify the details of relation between *C. pneumoniae* infection in lymphocytes and modulation of immune responses.

References

(1) Grayston, J.T. (1989) *Chlamydia pneumoniae*, strain TWAR. Chest **95**: 664−669.

(2) Grayston, J.T., Wang, S.P., Kuo, C.C. and Campbell, L.A. (1989) Current knowledge on *Chlamydia pneumoniae*, strain TWAR, an important cause of pneumonia and other acute respiratory diseases. Eur J Clin Microbiol Infect Dis **8**:191−202.

(3) Kauppinen, M. and Saikku, P. (1995) Pneumonia due to *Chlamydia pneumoniae*: prevalence:clinical features, diagnosis, and treatment. Clin Infect Dis **21**: Suppl 3, S244−252.

(4) Grayston, J.T. (1996) *Chlamydia pneumoniae* and atherosclerosis. Rev Med Interne **17**: Suppl 1, 45S−47S.

(5) Hahn, D.L., Dodge, R.W. and Golubjatnikov, R. (1991) Association of *Chlamydia pneumoniae* (strain TWAR) infection with wheezing, asthmatic bronchitis, and adult-onset asthma. JAMA **266**: 225−230.
(6) Norton, R., Schepetiuk, S. and Kok, T.W. (1995) *Chlamydia pneumoniae* pneumonia with endocarditis. Lancet **345**:1376−1377.
(7) Saario, R. and Toivanen, A. (1993) *Chlamydia pneumoniae* as a cause of reactive arthritis. Br J Rheumatol **32**:1112.
(8) Kaul, R., Uphoff, J., Wiedeman, J., Yadlapalli, S. and Wenman, W.M. (2000) Detection of *Chlamydia pneumoniae* DNA in $CD3^+$ lymphocytes from healthy blood donors and patients with coronary artery disease. Circulation **102**: 2341−2346.
(9) Haranaga, S., Yamaguchi, H., Friedman, H., Izumi, S. and Yamamoto, Y. (2001) *Chlamydia pneumoniae* infects and multiplies in lymphocytes in vitro. Infect Immun **69**: 7753−7759.
(10) Ross, R. (1999) Atherosclerosis—an inflammatory disease. N Engl J Med **340**: 115−126.
(11) Ossewaarde, J.M., de Vries, A., Bestebroer, T. and Angulo, A.F. (1996) Application of a Mycoplasma group-specific PCR for monitoring decontamination of Mycoplasma-infected *Chlamydia* sp. strains. Appl Environ Microbiol **62**: 328−331.
(12) Roblin, P.M., Dumornay, W. and Hammerschlag, M.R. (1992) Use of HEp-2 cells for improved isolation and passage of *Chlamydia pneumoniae*. J Clin Microbiol **30**:1968−1971.
(13) Gaydos, C.A., Summersgill, J.T., Sahney, N.N., Ramirez, J.A. and Quinn, T.C. (1996) Replication of *Chlamydia pneumoniae* in vitro in human macrophages, endothelial cells, and aortic artery smooth muscle cells. Infect Immun **64**: 1614−1620.
(14) Summersgill, J.T., Sahney, N.N., Gaydos, C.A., Quinn, T.C. and Ramirez, J.A. (1995) Inhibition of *Chlamydia pneumoniae* growth in HEp-2 cells pretreated with gamma interferon and tumor necrosis factor alpha. Infect Immun **63**: 2801−2803.
(15) Haranaga, S., Yamaguchi, H., Ikejima, H., Friedman, H. and Yamamoto, Y. (2003) *Chlamydia pneumoniae* infection of alveolar macrophages: a model. J Infect Dis **187**: 1107−1115.
(16) Yamamoto, Y., Retzlaff, C., He, P., Klein, T.W. and Friedman, H. (1995) Quantitative reverse transcription-PCR analysis of *Legionella pneumophila*-induced cytokine mRNA in different macrophage populations by high-performance liquid chromatography. Clin Diagn Lab Immunol **2**:18−24.
(17) Haranaga, S., Ikejima, H., Yamaguchi, H., Friedman, H. and Yamamoto, Y. (2002) Analysis of *Chlamydia pneumoniae* growth in cells by reverse transcription-PCR targeted to bacterial gene transcripts. Clin Diagn Lab Immunol **9**:313−319.
(18) Zhou, L.J. and Tedder, T.F. (1995) A distinct pattern of cytokine gene expression by human CD83+ blood dendritic cells. Blood **86**: 3295−3301.
(19) Haasch, D., Chen, Y.W., Reilly, R.M., Chiou, X.G., Koterski, S., Smith, M.L., Kroeger, P., McWeeny, K., Halbert, D.N., Mollison, K.W., Djuric, S.W. and Trevillyan, J.M. (2002) T cell activation induces a noncoding RNA transcript sensitive to inhibition by immunosuppressant drugs and encoded by the proto-oncogene, BIC. Cell Immunol **217**:78−86.
(20) Yamaguchi, H., Haranaga, S., Friedman, H., Moor, J.A., Muffly, K.E. and Yamamoto, Y. (2002) A *Chlamydia pneumoniae* infection model using established human lymphocyte cell lines. FEMS Microbiol Lett **216**:229−234.
(21) Harper, A., Pogson, C.I., Jones, M.L. and Pearce, J.H. (2000) Chlamydial development is adversely affected by minor changes in amino acid supply, blood plasma amino acid levels, and glucose deprivation. Infect Immun **68**: 1457−1464.
(22) Esposito, G., Blasi, F., Allegra, L., Chiesa, R., Melissano, G., Cosentini, R., Tarsia, P., Dordoni, L., Cantoni, C., Arosio, C. and Fagetti, L. (1999) Demonstration of viable *Chlamydia pneumoniae* in atherosclerotic plaques of carotid arteries by reverse transcriptase polymerase chain reaction. Ann Vasc Surg **13**: 421−425.
(23) Gerard, H.C., Schumacher, H.R., El-Gabalawy, H., Goldbach-Mansky, R. and Hudson, A.P. (2000) *Chlamydia pneumoniae* present in the human

synovium are viable and metabolically active. Microb Pathog **29**:17−24.
(24) Alifano, P., Bruni, C.B. and Carlomagno, M.S. (1994) Control of mRNA processing and decay in prokaryotes. Genetica **94**: 157−172.
(25) Yang, J., Hooper, W.C., Phillips, D.J., Tondella, M.L. and Talkington, D.F. (2003) Induction of proinflammatory cytokines in human lung epithelial cells during *Chlamydia pneumoniae* infection. Infect Immun **71**: 614−620.
(26) Redecke, V., Dalhoff, K., Bohnet, S., Braun, J. and Maass, M. (1998) Interaction of *Chlamydia pneumoniae* and human alveolar macrophages:infection and inflammatory response. Am J Respir Cell Mol Biol **19**: 721−727.
(27) Lucey, D.R., Clerici, M. and Shearer, G.M. (1996) Type 1 and type 2 cytokine dysregulation in human infectious, neoplastic, and inflammatory diseases. Clin Microbiol Rev **9**: 532−562.
(28) Airenne, S., Surcel, H.M., Bloigu, A., Laitinen, K., Saikku, P. and Laurila, A. (2000) The resistance of human monocyte-derived macrophages to *Chlamydia pneumoniae* infection is enhanced by interferon-gamma. Apmis **108**:139−144.
(29) Matsushima, H., Shirai, M., Ouchi, K., Yamashita, K., Kakutani, T., Furukawa, S. and Nakazawa, T. (1999) Lymphotoxin inhibits *Chlamydia pneumoniae* growth in HEp-2 cells. Infect Immun **67**:3175−3179.
(30) Rottenberg, M.E., Gigliotti Rothfuchs, A., Gigliotti, D., Ceausu, M., Une, C., Levitsky, V. and Wigzell, H. (2000) Regulation and role of IFN-gamma in the innate resistance to infection with *Chlamydia pneumoniae*. J Immunol **164**: 4812−4818.
(31) Clurman, B.E. and Hayward, W.S. (1989) Multiple proto-oncogene activations in avian leukosis virus-induced lymphomas: evidence for stage-specific events. Mol Cell Biol **9**: 2657−2664.
(32) Emeson, E.E. and Robertson, A.L., Jr. (1988) T lymphocytes in aortic and coronary intimas. Their potential role in atherogenesis. Am J Pathol **130**: 369−376.
(33) Hansson, G.K., Holm, J. and Jonasson, L. (1989) Detection of activated T lymphocytes in the human atherosclerotic plaque. Am J Pathol **135**: 169 −175.
(34) Munro, J.M., van der Walt, J.D., Munro, C.S., Chalmers, J.A. and Cox, E.L. (1987) An immunohistochemical analysis of human aortic fatty streaks. Hum Pathol **18**: 375−380.
(35) Uyemura, K., Demer, L.L., Castle, S.C., Jullien, D., Berliner, J.A., Gately, M.K., Warrier, R.R., Pham, N., Fogelman, A.M. and Modlin, R.L. (1996) Cross-regulatory roles of interleukin (IL)-12 and IL-10 in atherosclerosis. J Clin Invest **97**: 2130−2138.
(36) Heinemann, M., Susa, M., Simnacher, U., Marre, R. and Essig, A. (1996) Growth of *Chlamydia pneumoniae* induces cytokine production and expression of CD14 in a human monocytic cell line. Infect Immun **64**: 4872−4875.

Aberrant Signal Transduction through T Cell Antigen Receptor and Its Correction in Patients with Systemic Lupus erythematosus

Tsutomu Takeuchi

Division of Rheumatology, Clinical Immunology, Saitama Medical Center, Saitama Medical School, 1981 Kamoda, Tsujido-machi, Kawagoe, Saitama 350-8550, Japan

Systemic lupus erytematosus (SLE) is a prototype autoimmune disease and is characterized by a wide spectrum of clinical manifestations and abundant production of autoantibodies to nuclear antigens, cell surface and serum proteins (1, 2). It is well recognized that the B cells are hyperactive and produce excessive amounts of immunoglobulins and a variety of autoantibodies, resulting in formation of immune complexes, which are central to the effector phase of the disease. On the other hand, it has become evident that SLE T cells participate in the attack on target cells or tissues through overproduction of pro-inflammatory cytokines or an increase in cell-to-cell adhesion, ultimately leading to the apoptosis of the target cells (3). Accumulating evidence suggests that the regulatory function of the T cells in controlling immunoglobulin production by B cells is defective and results in the amplification and perpetuation of the immune response exclusively targeting the autoantigens (4, 5). Thus, it is widely accepted that the SLE T cells play an indispensable role in the pathogenesis of the disease (4). Detailed studies of the molecular mechanism underlying the aberrant function of SLE T cells is now beginning to identify the molecules responsible for that (5).

T-cell Antigen Receptor and Associated Signaling Molecules

In contrast to the up-regulated adhesion molecules and their down-stream signaling molecules in SLE T cells, the antigen receptor and associated molecules are hypo-responsive (5-7). The altered response of SLE T cells reverts to normal, or even much higher than normal, when the cells are stimulated with phorbol ester and ionomycin, which directly activate a protein kinase C located downstream of the TCR-CD3 complex, co-receptors, and membrane-associated tyrosine kinases, as shown in Figure 1. These findings raise the possibility that defects may reside in the proximal signal transduction molecules through T cell antigen receptor (Figure 2). A comprehensive survey of the tyrosine-phosphorylated proteins by stimulation through the TCR-CD3 complex could clearly show the defective tyrosine-phosphorylation and protein expression of the TCR zeta chain (TCR ζ) (8, 9), and defective protein expression of the TCR ζ chain was observed in more than half of SLE patients. It should be noted that most patients exhibit attenuated expression of the TCR ζ chain over several months to years, although the disease activity fluctuates in some patients. The sustained reduction of the TCR ζ chain in SLE is markedly contrasted to the transient reduction observed in cancers, infectious diseases, and other autoimmune diseases (10). The TCR ζ chain possesses three ITAM domains which can transmit signals downstream, while interaction between the TCR ζ chain and ZAP-70 tyrosine kinase is required for subsequent transduction of the signals. It has been demonstrated that the transcriptional regulation is attenuated, when protein expression of the TCR ζ chain is down-regulated (9). At least three transcriptional regulation re-

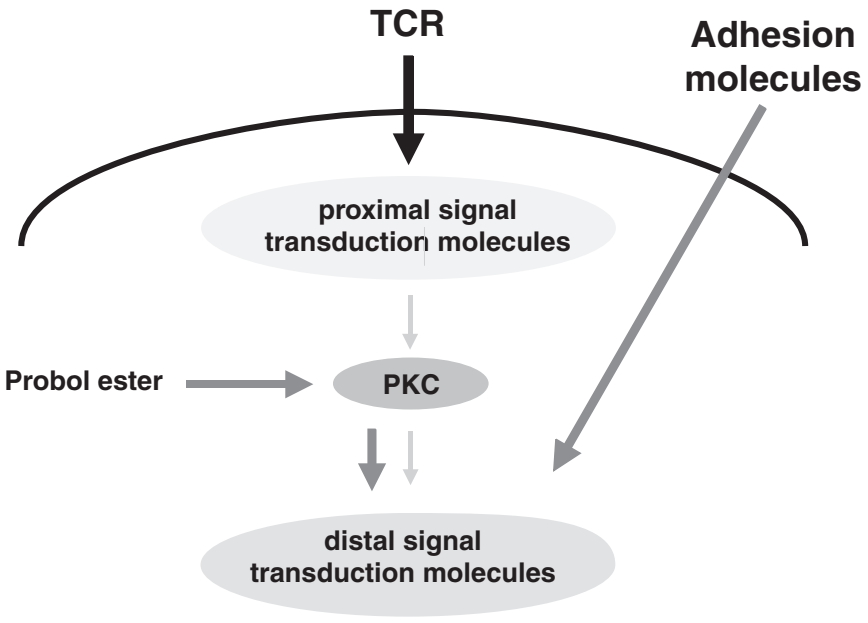

Fig. 1. Functional defects of SLE T cells. The signals delivered via TCR are impaired in SLE T cells, whereas phorbor ester can restore the defects, indicating that the proximal signal transduction molecules may be responsible for the defects. In contrast, the adhesion molecules are upregulated in the function and expression, raising a possibility that the signals via adhesion molecules can bypass the proximal transduction molecules.

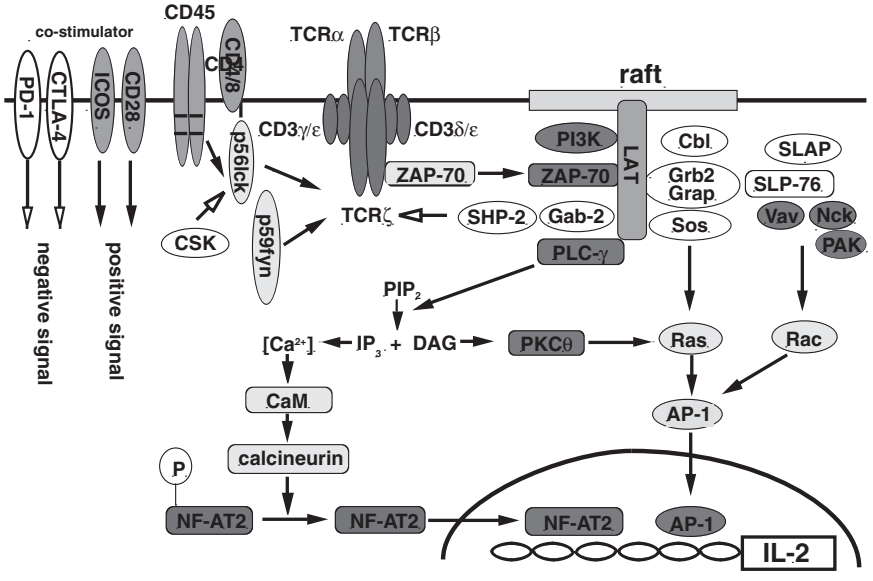

Fig. 2. Signal transduction molecules in T cells leading to transcriptional activation of IL-2.

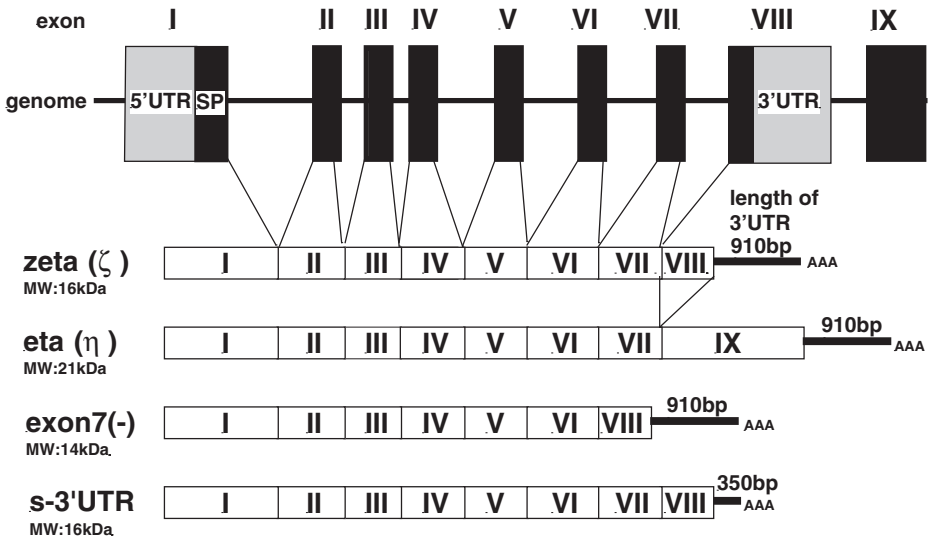

Fig. 3. Structure of spliced variants of TCR ζ chain. Exon-intron organization of TCR ζ chain gene and the transcripts of the wild type and spliced variants found in SLE are shown.

gions have been identified within the 5'-flanking region of the TCR ζ gene in T cells: 1) region −216 to +121 contains the basal promoter; 2) region −561 to −216 confers strong transcriptional activity; and 3) region −784 to −561 contains negative elements (11). Wang et al. have identified no mutations or deletions in the 5'-flanking region of the TCR ζ gene in SLE T cells (11), while other researchers have identified those in 5'-flanking region (12). We and others have detected abnormal transcripts of the TCR ζ chain, such as the splice variants unique to SLE (12, 13). They include a splice variant lacking exon 7, a variant with a short 3' -UTR, and several other variants with base substitutions in the coding regions (8, 13, 14). The eta (ex1-7+ex9) and iota (ex1-7+ex10) variants have been shown to be generated by alternative splicing of the TCR ζ gene on human and mouse chromosome 1q22-23 (15-19); however, the functions of these splice variants are not fully understood. The TCR ζ chain lacking exon 7 and the short 3'- UTR splice variants, which are exclusively detected in SLE T cells, are new-class spliced variants (Figure 3).

Spliced Variants of TCR ζ Chain in SLE

In the splice variant with the short 3'-UTR, a 562bp region containing the consensus sequence for mRNA stabilization is missing (20). In addition, a conserved sequence consisting of 31 nucleotides is also missing; this conserved sequence has been observed in humans, mice, rats and bovines, indicating an essential function. If this conserved region is involved in stabilization, transportation, or localization, the short 3'UTR splice variant may account for the downregulation in protein expression. Clearly, the dominant regulation controls of a variety of critical genes occur during the post-transcriptional stage (21). Since the initiation of transcription requires several hours, post-transcriptional regulation enables a faster response to stimuli. For example, the early lymphocyte-activation antigen CD69 is rapidly induced by stimulation; thereafter, CD69 mRNA levels rapidly decline, with a half-life of less than 60 minutes. The 3' UTR of this mRNA contains AU-rich motifs that, when fused to a previously stable globin transcript, confer instability (22). Since the metabolism of the TCR ζ chain is faster than the metabolism of other components in the TCR-CD3 complex (23), post-transcriptional regulation may be involved in TCR ζ expression. To test the hypothesis that the splice variant of TCR ζ mRNA with the short 3'UTR leads to a downregulation in protein expression, an mRNA stability assay as well as the transfection of cells with the splice variant would be helpful in verification of the role of this region in the regulation

of protein expression.

Transfection of the messages from the two spliced variants into mouse T-cell hybridomas lacking TCR ζ has recently demonstrated that the variants confer instability on TCR ζ mRNA, leading to reduced protein expression (24, 25). Although the exact mechanism responsible for the generation of the spliced variants remains to be clarified, the defective expression of TCR ζ has a considerable effect on the downstream signaling pathway. In this regard, it should be noted that some molecules are upregulated, presumably by compensating for the defective proximal signaling. One example is the FcεRγ1 chain, which has been demonstrated to induce and substitute for the defective TCR ζ chain in SLE T cells (26). A number of signaling molecules in SLE T cells, including transcription factor elf-1, inflammation signal trnasducer NF-kB, and PKC theta, have been reported to malfunction (27, 28). Other signal transduction molecules with aberrant function include protein kinase A (7) and CD45 PTPase (29). We therefore need to know which molecules are induced or reduced secondary to the aberrant TCR ζ in SLE.

TCR ζ Chain Defects as the Target of Therapeutic Intervention in SLE

The biological agents currently used for therapy of SLE are directed at the effector phase of the disease, and targeted therapy to correct the molecular defects in SLE T cells is awaited. However, more information is needed about the molecular targets in SLE T cells, since we still do not know which molecular defects are located upstream in the signaling cascade. Nevertheless, the TCR ζ chain is one of the candidate molecules, because 70% of SLE patients exhibit a decrease in tyrosine-phosphorylation, 55% have decreased protein expression, and 30 % carry some mRNA aberrations, such as exon 7 lacking variant and short 3' UTR variant (8, 13, 30, 31).

Several mechanisms are responsible for the downregulated expression of the TCR ζ chain, including low transcription activity, generation of spliced variants, redox status (32), oxidative stress (33), heat stress (34), chronic exposure to pro-inflammatory cytokines (35), and direct contact with activated macrophages (36). Because of the recent progress in the treatment of inflammatory diseases with biological agents that neutralize TNF (37-39), the expression patterns of the TCR ζ chain after successful treatment with these anti-TNF biologics should be examined. In addition, L-arginine-deficient status, which is induced by arginase-1 from activated macrophages, decreases expression of the TCR ζ chain, giving rise to the intriguing hypothesis that L-arginine supplementation will reverse the defective expression of TCR ζ in SLE (40). In contrast to the extrinsic factors that influence the level of expression of the TCR ζ chain, the intrinsic factors should be considered in SLE, because the defects are stable over a long period of time, regardless of the degree of disease activity or treatment with prednisolone (10, 30, 31, 41) .

Is it possible that in vitro correction of the TCR ζ chain will restore SLE T cells to normal function? Freshly isolated SLE T cells were transfected with TCR ζ chain construct by an efficient nucleoporation technique (42), and the results showed normalization of not only TCR ζ, but calcium influx through TCR-CD3, tyrosine-phosphorylation of the cellular substrates and IL-2 production, suggesting that reconstitution of a deficient TCR ζ chain can restore most of the SLE phenotype to normal. However, it is interesting that forced expression of the TCR ζ chain by retroviral vector in TNF-treated T cell hybridomas with reduced expression of the zeta chain resulted in overexpression of TCR ζ, but failed to rescue receptor proximal signaling, suggesting that this strategy can not be used in this particular situation (43).

Future Perspective

It is understood that no single molecular defect can be responsible for development of SLE, except for complement deficiency. However, it is extremely interesting to know the recent fingings demonstrating that loss of function mutation of ZAP-70 is a cause of autoimmune arthritis mice called SKG, which are characterized by destructive arthritis and autoantibody to type II collagen and rheumatoid factor, resembling human rheumatoid arthritis (44). These findings support

the notion that defects in the proximal signaling molecules can cause autoimmune diseases by altering thymic selection. Although we need to define the detailed cause of TCR ζ defect in SLE, these studies provide new directions of the reserach for autoimmune diseases, such as SLE.

References

(1) Cohen, P.L. 1993. T- and B-cell abnormalities in systemic lupus. *J Invest Dermatol* **100**: 69s−72s.

(2) Mills, J.A. 1994. Systemic lupus erythematosus. *N Engl J Med* **330**: 1871−1879.

(3) Kevil, C.G., and Bullard, D.C. 1999. Roles of leukocyte/endothelial cell adhesion molecules in the pathognenesis of vasculitis. *Am J Med* **106**: 677−687.

(4) Kotzin, B.L. 1996. Systemic lupus erythematosus. *Cell* **85**: 303−306.

(5) Dayal, A.K., and Kammer, G.M. 1996. The T cell enigma in lupus. *Arthritis Rheum* **39**: 23−33.

(6) Sierakowski, S., Kucharz, E.J., Lightfoot, R.W., and Goodwin, J.S. 1989. Impaired T-cell activation in patients with systemic lupus erythematosus. *J Clin Immunol* **9**: 469−476.

(7) Kammer, G.M., Perl, A., Richardson, B.C., and Tsokos, G.C. 2002. Abnormal T cell signal transduction in systemic lupus erythematosus. *Arthritis Rheum* **46**: 1139−1154.

(8) Takeuchi, T., Tsuzaka, K., Pang, M., Amano, K., Koide, J., and Abe, T. 1998. TCR zeta chain lacking exon 7 in two patients with systemic lupus erythematosus. *Int Immunol* **10**: 911−921.

(9) Liossis, S.N., Ding, X.Z., Dennis, G.J., and Tsokos, G.C. 1998. Altered pattern of TCR/CD3-mediated protein-tyrosyl phosphorylation in T cells from patients with systemic lupus erythematosus. Deficient expression of the T cell receptor zeta chain. *J Clin Invest* **101**: 1448−1457.

(10) Takeuchi, T., Tsuzaka, K., and Abe, T. 2004. Altered expression of the T cell receptor-CD3 complex in systemic lupus erythematosus. *Int Rev Immunol* **23**: 273−291.

(11) Wang, L., Bronstein, N., Hsu, V., and Baniyash, M. 1995. Transcriptional regulation of the murine TCR zeta gene. *Int Immunol* **7**: 1627−1635 Issn: 0953−8178.

(12) Nambiar, M.P., Enyedy, E.J., Warke, V.G., Krishnan, S., Dennis, G., and Wong, H.K. 2001. T cell signaling abnormalities in systemic lupus erythematosus are associated with increased mutations/polymorphisms and splice variants of T cell receptor zeta chain messenger RNA. *Arthritis Rheum* **44**: 1336−1350.

(13) Tsuzaka, K., Takeuchi, T., Onoda, N., Pang, M., and Abe, T. 1998. Mutations in T cell receptor zeta chain mRNA of peripheral T cells from systemic lupus erythematosus patients. *J Autoimmun* **11**: 381−385.

(14) Nambiar, M.P., Enyedy, E.J., Warke, V.G., Krishnan, S., Dennis, G., Kammer, G.M., and Tsokos, G.C. 2001. Polymorphisms/mutations of TCR-zeta-chain promoter and 3' untranslated region and selective expression of TCR zeta-chain with an alternatively spliced 3' untranslated region in patients with systemic lupus erythematosus. *J Autoimmun*. **16**: 133−142.

(15) Baniyash, M., Hsu, V.W., Seldin, M.F., and Klausner, R.D. 1989. The isolation and characterization of the murine T cell antigen receptor zeta chain gene. *J Biol Chem* **264**: 13252−13257.

(16) Jin, Y.J., Clayton, L.K., Howard, F.D., Koyasu, S., Sieh, M., Steinbrich, R., Tarr, G.E., and Reinherz, E.L. 1990. Molecular cloning of the CD3 eta subunit identifies a CD3 zeta-related product in thymus-derived cells. *Proc Natl Acad Sci USA* **87**: 3319−3323.

(17) Clayton, L.K., D'Adamio, L., Howard, F.D., Sieh, M., Hussey, R.E., Koyasu, S., and Reinherz, E.L. 1991. CD3 eta and CD3 zeta are alternatively spliced products of a common genetic locus and are transcriptionally and/or post-transcriptionally regulated during T-cell development. *Proc Natl Acad Sci USA* **88**: 5202−5206.

(18) Jensen, J.P., Hou, D., Ramsburg, M., Taylor, A., Dean, M., and Weissman, A.M. 1992. Organization of the human T cell receptor zeta/eta gene and its genetic linkage to the Fc gamma RII-Fc gamma RIII gene cluster. *J Immunol* **148**: 2563−2571.

(19) Nocentini, G., Ronchetti, S., Bartoli, A., Testa, G., D'Adamio, F., Riccardi, C., and Migliorati, G. 1995. T cell receptor iota an alternatively spliced product of the T cell receptor zeta gene. *Eur J Immunol* **25**: 1405−1409.

(20) Tsuzaka, K., Onoda, N., Yoshimoto, K., Setoyama, Y., Suzuki, K., Pang, M., Abe, T., and Takeuchi, T. 2002. T-cell receptor ζ mRNA with an alternatively spliced 3' untranslated region is generated predominantly in the peripheral blood T cells of systemic lupus erythematosus patients. *Mod Rheumatol* **12**: 167−173.

(21) Malter, J.S. 1998. Posttranscriptional regulation of mRNAs important in T cell function. *Adv Immunol* **68**: 1−49.

(22) Santis, A., Lopez-Cabrera, M., Sanchez-Madrid, F., and Proudfoot, N. 1995. Expression of the early lymphocyte activation antigen CD69, a C-type lectin, is regulated by mRNA degradation associated with AU-rich motifs. *Eur J Immunol* **25**: 2142−2146.

(23) Ono, S., Ohno, H., and Saito, T. 1995. Rapid turnover of the CD3 zeta chain independent of the TCR-CD3 complex in normal T cells. *Immunity* **2**: 639−644.

(24) Tsuzaka, K., Fukuhara, I., Setoyama, Y., Yoshimoto, K., Suzuki, K., Abe, T., and Takeuchi, T. 2003. TCR zeta mRNA with an alternatively spliced 3'-untranslated region detected in systemic lupus erythematosus patients leads to the down-regulation of TCR zeta and TCR/CD3 complex. *J Immunol* **171**: 2496−2503.

(25) Tsuzaka, K., Setoyama, Y., Yoshimoto, K., Shiraishi, K., Suzuki, K., Abe, T., and Takeuchi, T. 2005. A splice variant of the TCR zeta mRNA lacking exon 7 leads to the down-regulation of TCR zeta, the TCR/CD3 complex, and IL-2 production in systemic lupus erythematosus T cells. *J Immunol* **174**: 3518−3525.

(26) Enyedy, E.J., Nambiar, M.P., Liossis, S.N., Dennis, G., Kammer, G.M., and Tsokos, G.C. 2001. Fc epsilon receptor type I gamma chain replaces the deficient T cell receptor zeta chain in T cells of patients with systemic lupus erythematosus. *Arthritis Rheum* **44**: 1114−1121.

(27) Tsokos, G.C. 2001. Systemic lupus erythematosus. A disease with a complex pathogenesis. *Lancet* **358**: S65.

(28) Tsokos, G.C., Mitchell, J.P., and Juang, Y.T. 2003. T cell abnormalities in human and mouse lupus: intrinsic and extrinsic. *Curr Opin Rheumatol* **15**: 542−547.

(29) Takeuchi, T., Pang, M., Amano, K., Koide, J., and Abe, T. 1997. Reduced protein tyrosine phosphatase (PTPase) activity of CD45 on peripheral blood lymphocytes in patients with systemic lupus erythematosus. *Clin Exp Immunol* **109**: 20−26.

(30) Pang, M., Setoyama, Y., Tsuzaka, K., Yoshimoto, K., Amano, K., Abe, T., and Takeuchi, T. 2002. Defective expression and tyrosine phosphorylation of T cell receptor zeta chain in peripheral blood T cells from systemic lupus erythematosus patients. *Clin Exp Immunol* **129**: 160−168.

(31) Nambiar, M.P., Mitchell, J.P., Ceruti, R.P., Malloy, M.A., and Tsokos, G.C. 2003. Prevalence of T cell receptor zeta chain deficiency in systemic lupus erythematosus. *Lupus* **12**: 46−51.

(32) Maurice, M.M., Nakamura, H., van der Voort, E.A., van Vliet, A.I., Staal, F.J., Tak, P.P., Breedveld, F.C., and Verweij, C.L. 1997. Evidence for the role of an altered redox state in hyporesponsiveness of synovial T cells in rheumatoid arthritis. *J Immunol* **158**: 1458−1465.

(33) Gringhuis, S.I., Papendrecht-van der Voort, E.A., Leow, A., Nivine Levarht, E.W., Breedveld, F.C., and Verweij, C.L. 2002. Effect of redox balance alterations on cellular localization of LAT and downstream T-cell receptor signaling pathways. *Mol Cell Biol* **22**: 400−411.

(34) Nambiar, M.P., Fisher, C.U., Enyedy, E.J., Warke, V.G., Krishnan, S., and Tsokos, G.C. 2000. Heat stress downregulates TCR zeta chain expression in human T lymphocytes. *J Cell Biochem* **79**: 416−426.

(35) Isomaki, P., Panesar, M., Annenkov, A., Clark, J.M., Foxwell, B.M., Chernajovsky, Y., and Cope, A.P. 2001. Prolonged exposure of T cells to TNF down-regulates TCR zeta and expression of the TCR/CD3 complex at the cell surface. *J Immunol*

166: 5495−5507.
(36) Aoe, T., Okamoto, Y., and Saito, T. 1995. Activated macrophages induce structural abnormalities of the T cell receptor-CD3 complex. *J Exp Med* **181**: 1881−1886.
(37) Abe, T., and Takeuchi, T. 2001. Rheumatoid arthritis and tumor necrosis factor α. *Autoimmunity* **34**: 291−303.
(38) Feldmann, M., Elliott, M.J., Woody, J.N., and Maini, R.N. 1997. Anti-tumor necrosis factor-alpha therapy of rheumatoid arthritis. *Adv Immunol* **64**: 283−350.
(39) Takeuchi, T., Amano, K., and Kameda, H. 2004. Anti-TNF biological agents in rheumatoid arthritis and other inflammatory diseases. *Int Allergol* in press.
(40) Rodriguez, P.C., Zea, A.H., Culotta, K.S., Zabaleta, J., Ochoa, J.B., and Ochoa, A.C. 2002. Regulation of T cell receptor CD3z chain expression by L-arginine. *J Biol Chem* **277**: 21123−21129.
(41) Brundula, V., Rivas, L.J., Blasini, A.M., Paris, M., Salazar, S., and Stekman, I.L. 1999. Diminished levels of T cell receptor zeta chains in peripheral blood T lymphocytes from patients with systemic lupus erythematosus. *Arthritis Rheum* **42**: 1908−1916.
(42) Nambiar, M.P., Fisher, C.U., Warke, V.G., Krishnan, S., Mitchell, J.P., Delaney, N., and Tsokos, G.C. 2003. Reconstitution of deficient T cell receptor zeta chain restores T cell signaling and augments T cell receptor/CD3-induced interleukin-2 production in patients with systemic lupus erythematosus. *Arthritis Rheum* **48**: 1948−1955.
(43) Clark, J.M., Annenkov, A.E., Panesar, M., Isomaki, P., Chernajovsky, Y., and Cope, A.P. 2004. T cell receptor ζ reconstitution fails to restore response of T cells rendered hyporesposive by tumor necrosis factor α. *Proc Natl Acad Sci USA* **101**: 1696−1701.
(44) Sakaguchi, N., Takahashi, T., Hata, H., Nomura, T., Tagami, T., Yamazaki, S., Sakihama, T., Matsutani, T., Negishi, I., Nakatsuru, S., et al. 2003. Altered thymic T-cell selection due to a mutation of the ZAP-70 gene causes autoimmune arthritis in mice. *Nature* **426**: 454−460.

Study on the Prediction and Prevention of Cholera Epidemic among the Children in Bangladesh

Mitsuaki Nishibuchi

Division of Humans and the Environment, Center for Southeast Asian Studies, Kyoto University, 46 Shimoadachi-cho, Yoshida, Sakyo-ku, Kyoto 606-8501, Japan

Introduction

Cholera is considered to be "a disease of poverty" and is still a major health hazard for the people in developing countries. The results of recent researches suggest the involvement of climate factors in diarrhoeal diseases epidemics (1-9). Implication of the optimal climatic conditions for bacterial proliferation in their natural reservoir (10-15) and the ecology of *Vibrio cholerae* have been discussed, and one hypothesis has proposed that *V. cholerae* proliferates in the seawater through a complicated ecological pathway and invades human community just before the epidemic season (16,17).

Two peaks are usually observed for epidemic cholera every year in Dhaka, Bangladesh. This phenomenon suggests that some seasonal factors, which change regularly, are associated with the emergence of the epidemic cholera. As the hypothesis rose above, climate factors such as temperature and rainfall are considered to be the important factors. The considerable proportion of the patients is under 10-year-old children whose condition easily gets worse once *V. cholerae* infects them. Meteorological analysis to forecast "the timing and location of public health intervention (18)" against epidemic cholera is essential to decrease their physical burden. Preventative measures including vaccination would be very effective if applied at a proper timing.

In this study, attempts were made to establish a formula for prediction of the future number of cholera patients from temperature and rainfall data in Dhaka.

Materials and Methods

Patient data.

Daily infection data for the patients under 10-year-old that were diagnosed as the infection by *V. cholerae* O1 (hereinafter abbreviated as O1 cholera) from 1983 to 2002 were obtained from the International Centre for Diarroeal Diseases Research, Bangladesh (ICDDR, B). ICDDR, B is located in Dhaka City, and provides free medical services for the low-income people. According to the data of surveillance between 1996 and 2001, 12.7% of the diarrhoeal diseases were attributable to *V. cholerae* infection (19). At Dhaka Hospital belonging to ICDDR, B, stool cultures were examined for every 25th diarrhoeal patient until 1995 and for every 50th patient after 1995, so that the definite diagnosis of O1 cholera could be confirmed by stool culture. We calculated the number of the monthly O1 cholera patients under 10-year-old from the above data. In Bangladesh, most of the children experience the primary cholera infection before 10-year-old so

that we expect the patients of this age group might more precisely reflect the exposure of bacterial pathogen in an epidemic rather than those of all age groups.

Climate data.

The meteorological data, daily maximum and minimum temperatures and rainfall, which were recorded by the Bangladesh Meteorological Department (BMD) from 1983 to 2001 in Dhaka City, were obtained through the Disaster Prevention Research Institute of Kyoto University. Missing data were interpolated by using the data just before and after the missing data. The daily climate data were used to calculate monthly data; rainfall was added up and average maximum and minimum temperatures were calculated.

Statistical analysis.

Spectral analysis was performed to detect periodicity in the number of patients. A time series analysis was performed to construct an autoregression model for prediction of the number of O1 cholera patients using the monthly data of the mean maximum and minimum temperatures, total rainfall and the total number of O1 cholera patients under 10. The prediction errors of the regression model to be correlated were then examined. In the first step, time lag (lag1 = one month) was set from 0 to 6 for each climate factor against original data, and totally 343 combinations ($=7^3$) were set among the 3 factors. This procedure is considered necessary because there may be some time lag before the changes in the temperature and rainfall influence bacterial proliferation. Then each combination was matched with the patient number in the original data (patient; lead=0). In this step, we tried to estimate the patient number on time n by using the data of maximum and minimum temperatures on a preceding month x and y ($0 \leqq x \leqq 6$, $0 \leqq y \leqq 6$), respectively, and rainfall on a preceding month z ($0 \leqq z \leqq 6$). The "n" means present time. In the second step, we set one lead (=one month ahead) in patient number in trying to estimate the patient number on time (n+1). We calculated the Pearson's coefficient of correlation, and error variance was examined to measure the utility of this regression model. In the above examinations, P values less than 0.05 and 0.01 were considered to be significant for the coefficient of equation and for the Pearson' s coefficient of correlation, respectively. These analyses were conducted using the computer program contained in the SPSS trends 11.5J software (SPSS INC., Chicago, IL, USA).

Results and Discussion

Climate in Dhaka.

The mean maximum and minimum temperatures for the 19-year period was 30.8°C and 21.7°C, respectively. Figure 1 shows mean monthly maximum and minimum temperatures and mean monthly rainfall in Dhaka City from 1983 to 2001. The monthly mean minimum temperature was under 18°C only between December and February with the lowest temperature being 12.9°C in January. The monthly mean maximum temperature ranged from 25°C to 34°C. *V. cholerae* can grow at temperatures between 18°C and 42°C and grows optimally at about 37°C. Therefore, this temperature condition in Dhaka City appears to be suitable for the survival and proliferation of *V. cholerae*. The monthly mean rainfall was above 300 mm between May and September whereas not much rainfall was recorded in the winter season.

Number of O1 cholera patients under 10 year old.

Monthly number of O1 cholera patients under 10 year old during the 19 years is summarized in Fig.2. The two large peaks observed for years 1997 and 1998 are considered to be associated with floods. The spectral analysis was then performed to examine periodicity of the number of O1 cholera patients under 10 years old (Fig.3). The result revealed that the largest spectral density peak appeared between 6 and 7 months. This means that the patient number of under 10-year-old in Dhaka City fluctuates with the periodicity of 6 to 7 months.

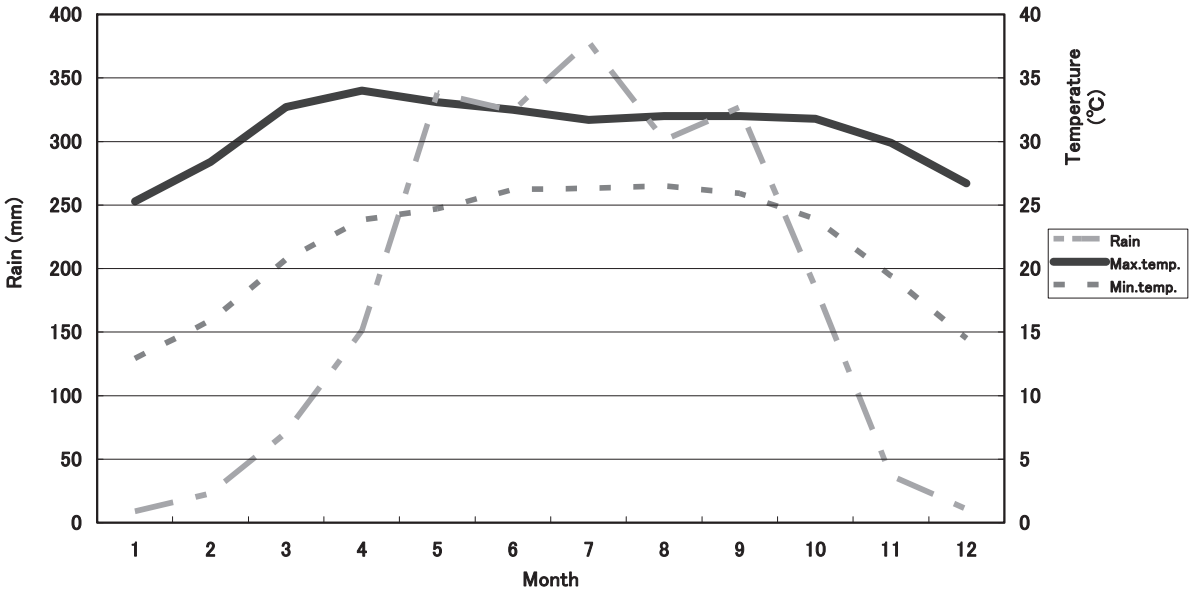

Fig. 1. Mean monthly maximum and minimum temperatures and monthly total rainfall in Dhaka between 1983 and 2001.

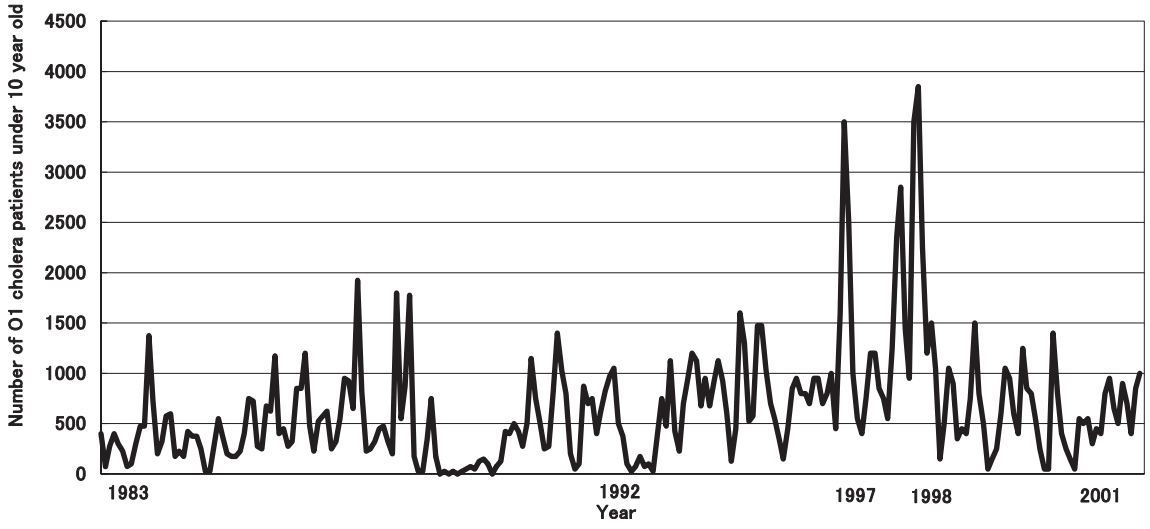

Fig. 2. Monthly O1 cholera patients under 10 years old in Dhaka between 1983 and 2001.

Prediction of the epidemic cholera from climate data.

To evaluate predictability of the patient number from the monthly mean maximum and minimum temperatures and rainfall, regression models were constructed in the time series analysis, and aptness of the models was evaluated as described above. When the patient number was set at lead 0 (= 0 month ahead), Pearson's coefficients of correlation were low (0.63 ～ 0.68) for all 343 combinations of maximum and minimum temperature and rainfall with lag 0 to 6 (= preceding 0 to 6 months), indicating insignificant correlation. The reason for the poor estimation was considered due to the shift of the number of the patients by about one month. Pearson's coefficients of correlation became between 0.9 and 1.0 when the patient number was set at lead 1 (=one month ahead).

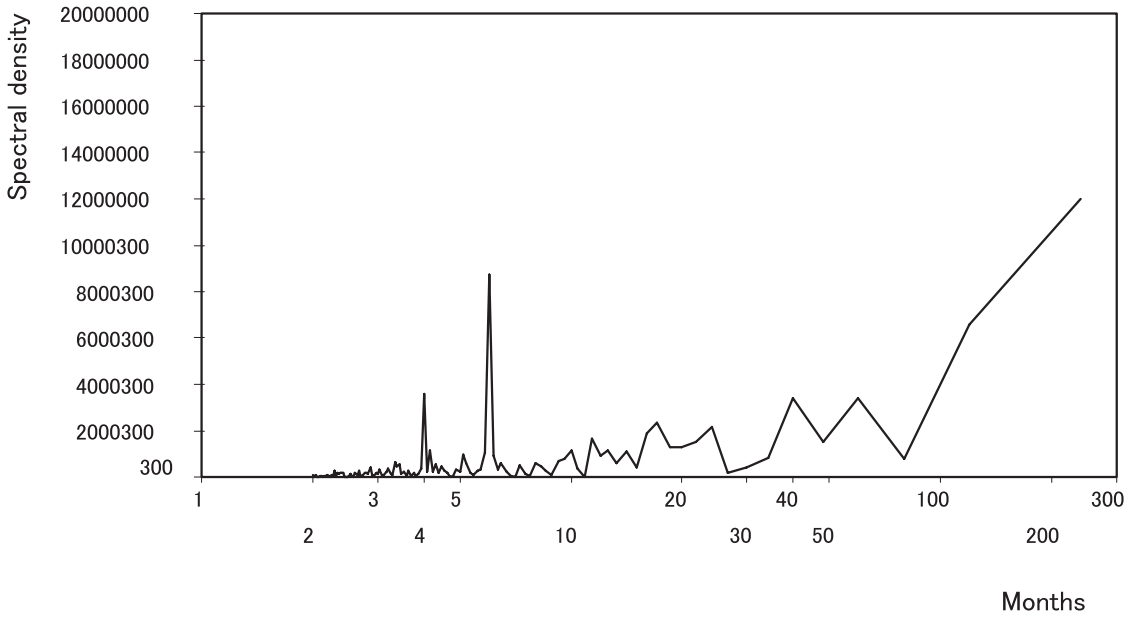

Fig. 3. The result of the spectral analysis for monthly O1 cholera patients under 10 years old in Dhaka between 1983 and 2001.

Among the 343 combinations with patient lead 1, there were 10 combinations for which the p-values were <0.05 in the evaluation of the prediction error of the autoregression. However, the combinations of the temperature and rainfall data with lag 0 or 1 (0 or 1 preceding month) were considered hardly useful for prediction and they were excluded. One remaining combination of maximum temperature with lag 2, minimum temperature with lag 4, and rainfall with lag 3 was chosen from the 10 combinations. Equation for this combination is given below.

$Y = -57.2 \times$ maximum temperature (lag 2) $-23.6 \times$ minimum temperature (lag 4) $+0.53 \times$ rainfall with lag(3)+2829.2+r(t)

$r(t)=0.66 \times r(t-1)+u(t)$

where Y is estimated patient number, r(t) is residue, u(t) is white noise, and The Pearson's coefficient of correlation is 0.95.

We checked the residue and confirmed its white noise for this equation (data not shown).

Fig.4 compares the actual (dotted line) and the estimated (continuous line) number of the patients. The patient numbers were compared at various time points. When the ratio of the estimated and the actual patient number was between 0.8 and 1.2, we arbitrarily interpreted it as "good estimation". When the ratio of the estimated and the actual patient number was outside of this range, it was considered as "poor estimation". The actual patient numbers were plotted for at 226 time points (Fig. 5). The estimations at 89 points (39.4%) are classified as good estimations. Poor estimations tended to be observed where the actual patient number was around or less than 500, indicating good estimation is possible when the size of the epidemic is large.

The result of our study indicates that we can satisfactory estimate the number of O1 cholera patients under 10 year old for any month (n+1) using the data of the preceding two month's maximum temperature, preceding four month's minimum temperature, and the preceding three month's rainfall in Dhaka City. The numerical equation we obtained can be interpreted to mean that the lower the maximum temperature of the preceding two months and the minimum temperature of the preceding four months and the more the rainfall of the preceding 3 months were, the more the patient number of one month following time point n will increase.

As shown in Fig.3, there is a clear seasonal periodicity in the patient number in Dhaka, and thus our result strongly suggests that at least temperature and rain fall are important factors controlling the seasonal epidemic cholera and that there is a time lag between

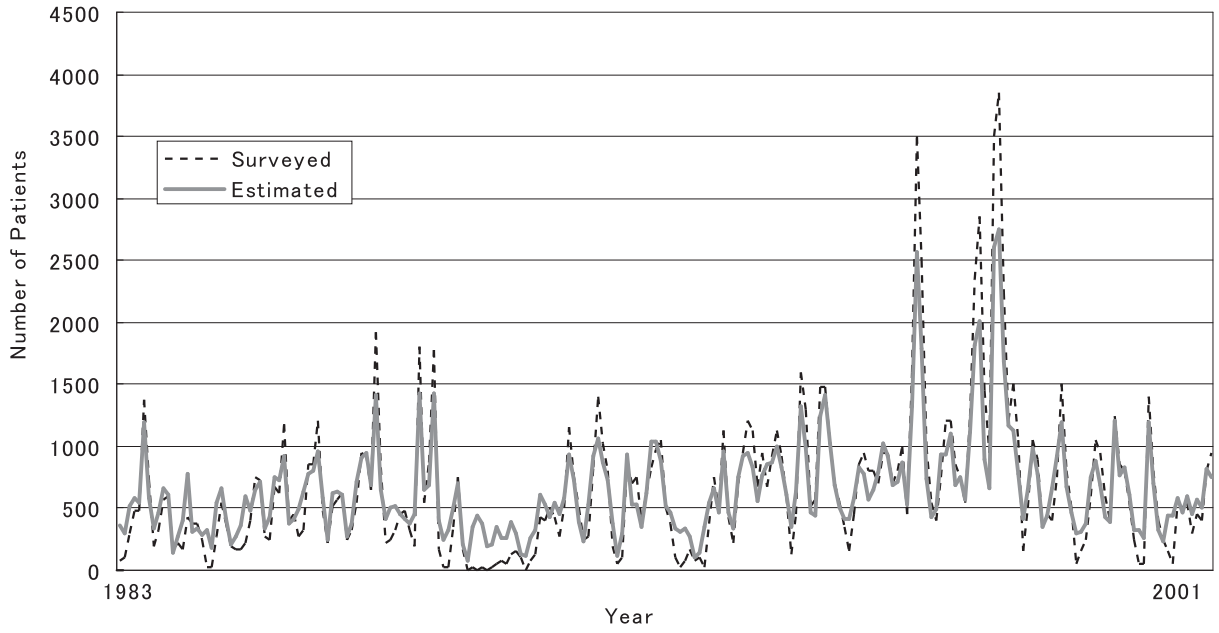

Fig. 4. Comparison between the surveyed and estimated patient number.

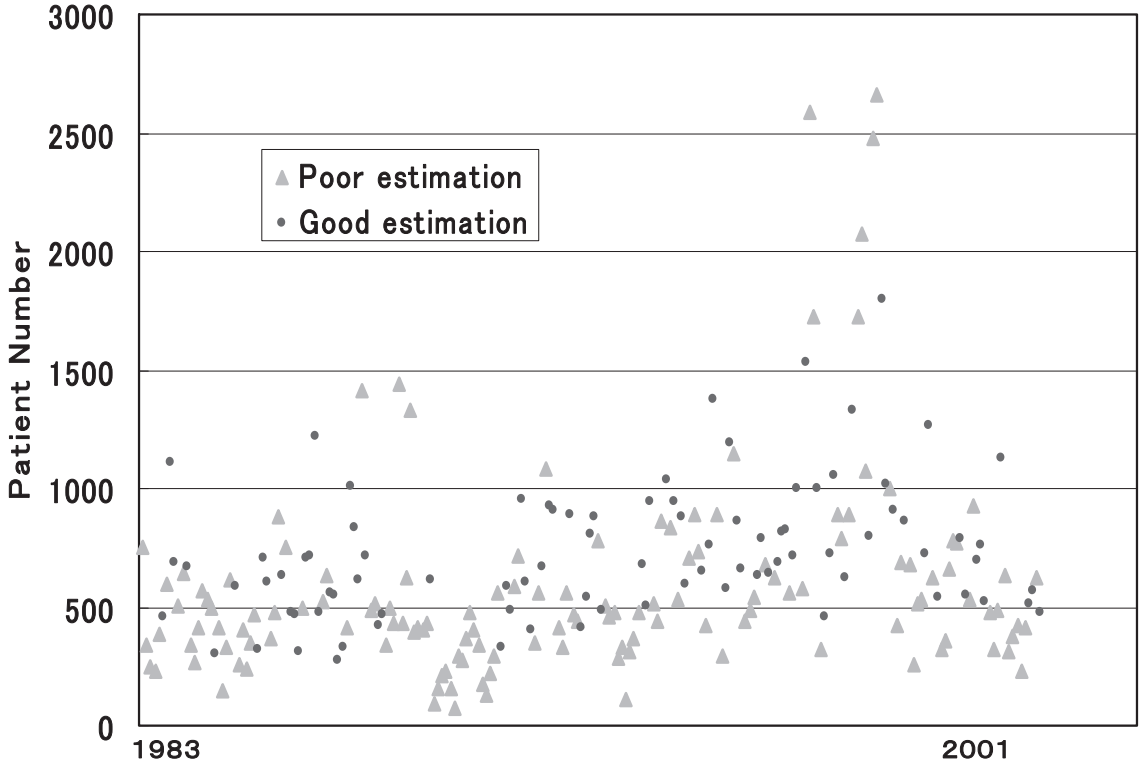

Fig. 5. Relationship between good and poor estimation and the number of the cholera patient under 10 years old in Dhaka for years between 1983 and 2001. Good and poor estimations are defined in the text.

these climatic changes and the start of cholera epidemic. It seems reasonable to speculate that the ecology of *V. cholerae* is under the direct influence of climate factors such as temperature and rain fall and that the change in the ecology of *V. cholerae* in turn induces epidemic cholera. The time lag as long as five months suggests the behavior of people such as drinking much water at high temperature is a less important factor among those mediate climate change and epidemic cholera. Further investigations are needed to elucidate how the climate change influences the ecology of cholera. These include proliferation of *V. cholerae* in the natural reservoir, genetic exchange between *V. cholerae* O1 and *V. cholerae* non-O1 to generate *V. cholerae* O1 strains loaded with virulence genes in full, and transmission of *V. cholerae* from the natural reservoir to a human community. They will make clear the role of the climate factors in stimulation of epidemic cholera. If the climate data are recorded on the Bay of Bengal rather than in Dhaka City and if other parameters like duration of sunshine are also used for the analysis, our estimation might become more accurate.

In recent years, cholera outbreak has come to a particular public health problem in refugee camps or after natural disaster rather than endemic areas, because the case fatality rates sharply increase in emergent situations. It is important to try to forecast the outbreak of infectious diseases in an emergent situation like Sumatran earthquake after which WHO alerted the possibility of cholera outbreak. Early warning system is also useful in the area where cholera is endemic. If we can estimate the size of an epidemic, it will allow medicare officials and stuffs to prepare for it. In Fig.2, we found large peaks in 1997 and 1998. Before the above regression analysis, we considered these extraordinary large outbreaks are due to abrupt devastation of sanitary conditions after floods and are difficult to predict. But as shown in Fig.4, the size of these extraordinary epidemics could also be estimated quite accurately by only 3 climate parameters in advance. Our analytical method may also be applied to the prediction of the epidemics of other contagious diseases, which show seasonal variations.

According to C. T. Codeço, epidemic is driven by extrinsic and intrinsic factors (20). Other researchers reported the involvement of food in the epidemiology of cholera (21-23). Immunity and nutrition are important intrinsic factors. These factors probably influence the number of patients. It is conceivable that the nutrition and the immunity of the children are affected by some seasonal factors; the people's life and diet in developing countries are probably directly influenced by the seasonal change although we do not have any evidence to prove it. Although economical, climatological, biological and epidemiological factors should be equally evaluated to determine the exact role of climate in epidemic cholera, we found that climate alone plays a major role in the epidemic. To support that our early warning system is valid, it is important to study the association between these climatic changes and emergence of epidemic O1 strains in the natural environment. Toxigenic O1 strains are hardly detected in the environmental waters during the non-epidemic season. It is proposed that toxigenic O1 strains may be generated by transfer of virulence genes, *ctx* and *tcp*, from non-O1 strains to O1 strains.

Conclusion

Our analysis could suggest strong correlation between climate factors, temperature and rail fall in particular, and epidemic cholera in Dhaka, Bangladesh. The climatic information allows us to estimate fairly accurately the number of cholera patients under 10 year old three moths ahead. Assuming that cholera epidemic can be predicted three moths ahead, studies on prevention of epidemic cholera would be needed in the future. We are currently preparing for the study to improve the efficacy of cholera vaccine for the children in Bangladesh.

Acknowledgments

We would like to thank Dr. A.S.G. Faruque, Mr. M. A. Malek and Dr. Y. Wagatsuma (ICDDR, B) for their excellent assistance in collection of the data in Dhaka, and S. Ishimura (Assoc. Prof., Laboratory of Mathematics, School of Dental Medicine, Tsurumi University) for his excellent suggestion for the statistical analysis. This study was supported by a research grant from

Waksman Foundation of Japan. This study was done in collaboration with Taiichi Hayashi (Assoc. Prof., Meteorological and Coastal Hazards Section, Disaster Prevention Research Institute, Kyoto University) and Fumiko Matsuda (Graduate student, Graduate School of Medicine, Kyoto University).

References

(1) Colwell, R. R. 1996. Global climate and infectious disease: The cholera paradigm. Science **274**: 2025−2031.

(2) Salazar-Lindo, E., Pinell-Salles, P., Maruy, A., and Chea-Woo, E. 1997. El Niño and diarrhea and dehydration in Lima, Peru. Lancet **350**: 1597−1598.

(3) Checkley, W., Epstein, L., Gilman, R. H., Figueroa, D., Cama, R. I., and Patz, J. A. 2000. Effects of El Niño and ambient temperature on hospital admissions for diarrhoeal diseases in Peruvian children. Lancet **355**: 442−450.

(4) Speelmon, E. C., Checkley, W., Gilman, R. H., Patz, J., Calderon, M., and Manga, S. 2000. Cholera incidence and El Niño-related higher ambient temperature. JAMA **283**: 3072−3074.

(5) Pascual, M., Rodó, X., Ellner, S. P., Colwell, R., and Bouma, M. J. 2000. Cholera dynamics and El Niño-Southern Oscillation. Science **289**: 1766−1769.

(6) Lobitz, B., Beck, L., Huq, A., Wood, B., Fuchs, G., Faruque, A. S. G., and Colwell, R. 2000. Climate and infectious disease: Use of remote sensing for detection of *Vibrio cholerae* by indirect measurement. Proc. Natl. Acad. Sci. **97**: 1438−1443.

(7) Bouma, M. J., and Pascual, M. 2001. Seasonal and interannual cycles of endemic cholera in Bengal 1891-1940 in relation to climate and geography. Hydrobiologia **460**: 147−156.

(8) Pascual, M., Bouma, M. J., and Dobson, A. P. 2002. Cholera and climate: revisiting the quantitative evidence. Microbes Infect. **4**: 237−245.

(9) Rodó, X., Pascual, M., Fuchs, G., and Faruque, A. S. G.. 2002. ENSO and cholera: A nonstationary link related to climate change? Proc. Natl. Acad. Sci. **99**: 12901−12906.

(10) Huq, A., West, P. A., Small, E. B., Huq, M. I., and Colwell, R. R. 1984. Influence of water temperature, salinity, and pH on survival and growth of toxigenic *Vibrio cholerae* serovar O1 associated with live copepods in laboratory microcosms. Appl. Environ. Microbiol. **48**: 420−424.

(11) Epstein, P. R. 1993. Algal blooms in the spread and persistence of cholera. Biosystems **31**: 209−221.

(12) Islam, M. S., Drasar, B. S., and Sack, R. B. 1994. Probable role of blue-green algae in maintaining endemicity and seasonality of cholera in Bangladesh: a hypothesis. J. Diarrhoeal Dis. Res. **12**: 245−256.

(13) Madico, G., Checkley, W., Gilman, R. H., Bravo, N., Cabrera, L., Calderon, M., and Ceballos, A. 1996. Active surveillance for *Vibrio cholerae* O1 and vibriophages in sewage water as a potential tool to predict cholera outbreaks. J. Clin. Microbiol. **34**: 2968−2972.

(14) Franco, A. A., Fix, A. D., Prada, A., Paredes, E., Palomino, J. C., Wright, A. C., Johnson, J. A., McCarter, R., Guerra, H., and Morris, J. G., Jr. 1997. Cholera in Lima, Peru, correlates with prior isolation of *Vibrio cholerae* from the environment. Am. J. Epidemiol. **146**: 1067−1075.

(15) Louis, V. R., Russek-Cohen, E., Choopun, N., Louis, V. R., Russek-Cohen, E., Choopun, N., Rivera, I. N., Gangle, B., Jiang, S. C., Rubin, A., Patz, J. A., Huq, A., and Colwell, R. R. 2003. Predictability of *Vibrio cholerae* in Chesapeake Bay. Appl. Environ. Microbiol. **69**: 2773−2785.

(16) Wachsmuth, I. K., Blake, P. A., and Olsvik . 1994. *Vibrio cholerae* and cholera: molecular to global perspectives. ASM Press.

(17) Colwell, R., and Huq, A. 2001. Marine ecosystems and cholera. Hydrobiologia **460**: 141−145.

(18) Kovats, R. S., Bouma, M. J., Hajat, S., Worrall, E., and Haines, A. 2003. El Niño and health. Lancet **362**: 1481−1489.

(19) ICDDR, B. 2002. Health and Science Bulletin; **1**: 13.

(20) Codeço, C. T., 2001. Endemic and epidemic dynamics of cholera: the role of the aquatic reservoir. BMC Infect. Dis. **1**:1.

(21) St. Louis, S. T., Porter, J. D., Helal A, Drame, K., Hargrett-Bean, N., Wells, J. G., and Tauxe, R. V. 1990. Epidemic cholera in West Africa: The role of food handling and high-risk foods. Am. J. Epidemiol. **131**: 719−728.
(22) Albert, M. J., Neira, M., and Motarjemi, Y. 1997. The role of food in the epidemiology of cholera. Wld. Hlth. Statist. Quart. **50**: 111−117.
(23) Rabbani, G. H., and Greenough, W. B. 1999. Food as a vehicle of transmission of cholera. J. Diarrhoeal Dis. Res. **17**: 1−9.